Baryon resonance spectroscopy in a unitary isobar model

by

Mir Shahab Aldin Razavi Hessabi

(Under the Direction of Kanzo Nakayama)

Abstract

In an effort to analyze the baryon spectrum in low and medium energies a unitary isobar model (UIM) is proposed. To build the proposed model, we first exhibit the full complex structure of the meson-baryon reaction amplitude in coupled channels approach. By doing so, the reaction amplitude is expressed in a form that may be viewed as the generalization of the well-known Watson's theorem in photoproduction. Furthermore, the reaction amplitude is decomposed into the so-called pole and non-pole parts, corresponding basically to the resonant and background contributions. This allowed us to construct a UIM in which unitarity is maintained automatically. As the first application of the proposed UIM, we performed simultaneous analyses of the reactions $\pi N \to \pi N$, $\pi N \to \eta N$, $\pi N \to \omega N$, and $\gamma N \to \omega N$. In total our model required 8 isospin $T = 1/2$ and 4 isospin $T = 3/2$ resonances to describe the πN elastic scattering. We found a significant contribution from $N(1520)\frac{3}{2}^-$, $N(1700)\frac{3}{2}^-$, and $N(1680)\frac{5}{2}^+$ to both pion and photon-induced ω production. Besides those 3 resonances we saw a large contribution from $N(1675)\frac{5}{2}^-$ in $\gamma N \to \omega N$ reaction. In $\pi N \to \eta N$ reaction apart from the well known dominant contribution of the $N(1535)\frac{1}{2}^-$ for low energies, we also found a significant contribution of the $N(1680)\frac{5}{2}^+$.

Index words: Baryon spectroscopy, T-matrix phase structure, unitary isobar model.

Baryon resonance spectroscopy in a unitary isobar model

by

Mir Shahab Aldin Razavi Hessabi

B. Sc., Shahid Beheshti University, 2006

M. Sc., University of Tehran, 2007

M. Sc., University of Georgia, 2009

A Dissertation Submitted to the Graduate

Faculty of The University of Georgia in Partial

Fulfillment of the

Requirements for the Degree

Doctor of Philosophy

Athens, Georgia

2019

Baryon resonance spectroscopy in a unitary isobar model

by

Mir Shahab Aldin Razavi Hessabi

Major Professor: Kanzo Nakayama

Committee: Michael Bachmann
Michael Geller

Electronic Version Approved:

Ron Walcott
Interim Dean of the Graduate School
The University of Georgia
December 2019

Dedication

I would like to dedicate this work to those whose dreams do not turn to reality; not due to the lack of dedication on their part, but merely as a result of their socioeconomic status. And to those whose futures are mandated to them as a result of their place of birth. To the day that arbitrary lines on the map will no longer define one's worth.

Acknowledgments

Above all, I would like to thank my parents, my father and mother, Mahmood Razavi and Leyla Sanei Moghadam, for their sacrifices and continued support through out my life. I also like to thank my sisters Seterah, Zohreh, and Zhinoos Razavi whose support made my journey to United States and the completion of my PhD possible.

I would also like to show my gratitude toward my PhD advisor, Professor Kanzo Nakayama, for his relentless support, guidance, and instruction which made my research possible. I would like to thank my committee members, Professor Michael Bachmann and Professor Michael Geller, who accepted and took the time to be part of this work.

Table of Contents

List of Figures

List of Tables

Chapter 1

Introduction

> "The miracle is that the universe created a part of itself, to study itself, and that this part in studying itself finds the rest of the universe in its own natural inner realities."
>
> John C. Lilly

Quantum Chromodynamics (QCD), a non-Abelian gauge theory, is the theory of strong force that describes the interactions of colored quarks and gluons based on a $\mathrm{SU}(3)_c$ symmetry group. The QCD Lagrangian is given by

$$\mathcal{L}_{QCD} = \sum_q \bar{\psi}_{q,a}(i\gamma^\mu \partial_\mu \delta_{ab} - g_s \gamma^\mu t^C_{ab} \mathcal{A}^C_\mu - m_q \delta_{ab})\psi_{q,b} - \frac{1}{4} G^A_{\mu\nu} G^{A\ \mu\nu} \ , \tag{1.1}$$

where $\psi_{q,a}$ is the quark-field spinor of flavor q, color charge a, and mass of m_q. The color index a runs from 1 to $N_c = 3$ indexing the three elements of a color triplet. This color triplet transforms under the fundamental representation of $\mathrm{SU}(3)_c$.

The $\mathcal{A}^C_\mu$ represents the gluon field of type C with C running from 1 to $N_c^2 - 1 = 8$. The gluon fields, $\mathcal{A}^C_\mu$, belong to the adjoint representation of the $\mathrm{SU}(3)_c$ group, and t^C_{ab} are the generators of that group. The field tensor $G^A_{\mu\nu}$ is given by

$$G^A_{\mu\nu} = \partial_\mu \mathcal{A}^A_\nu - \partial_\nu \mathcal{A}^A_\mu - g_s f_{ABC} \mathcal{A}^B_\mu \mathcal{A}^C_\nu \qquad \left[t^A, t^B\right] = i f_{ABC} t^C \ , \tag{1.2}$$

where f_{ABC} are the structure constants of the $\mathrm{SU}(3)_c$ group.

The QCD coupling constant g_s, or $\alpha_s = \frac{g_s^2}{4\pi}$, is a function of exchange energy, figure (1.1); this energy dependence not only results in asymptotic freedom of quarks at high-energies, but also at low energies results in the *confinement* of quarks and gluons inside color-neutral hadrons. Although the underlying QCD Lagrangian eq. (1.1) and the implied asymptotic freedom (106; 59) are well established, our understanding of the confinement property of QCD is not yet complete. The major objective of Hadron Physics is to understand the confinement phenomenon. For this the study of hadron spectroscopy is imperative.

To access the baryon spectrum, over the past few decades many facilities across the world have been accumulating observables in light-meson production reactions. Most data on πN elastic and inelastic scattering was collected in 1960s and 1970s. In recent years, facilities such as Jefferson Lab in the United States, the MAinz MIcrotron (MAMI), the GRenoble Anneau Accelerateur Laser (GRAAL), the ELectron Stretcher Accelerator (ELSA) in Eroupe, and the 8 GeV Super Photon Ring (SPring-8) in Japan have been collecting cross section and polarization observables in light-meson photo- and electro-production reactions.

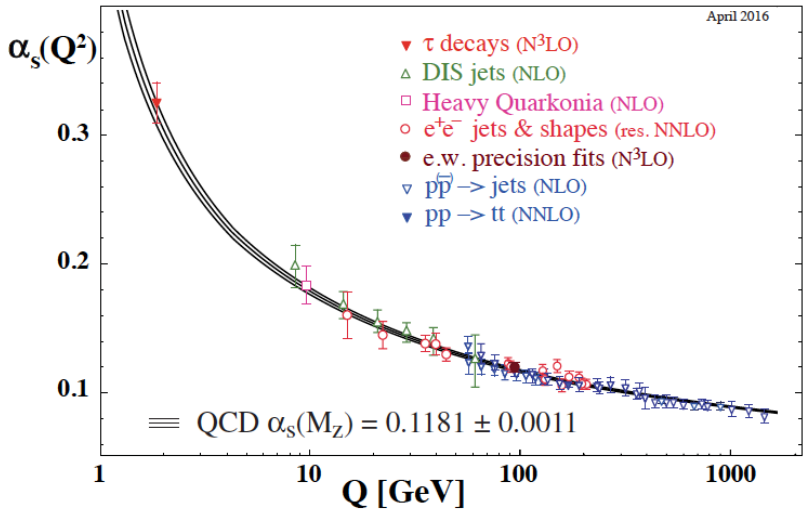

Figure 1.1: A summary of α_s measurements as a function of energy scale Q. Figure from PDG19.

These observables are being collected for a variety of different final states such as πN, $\pi\pi N$, ηN, $\eta' N$, ωN, $K\Sigma$, $K\Lambda$, etc. Analyzing such a large experimental data set in order to extract information on the baryon resonances requires a reaction theory capable of quantitatively describing these meson-baryon reaction processes. In the next section, we briefly overview some of the fundamental theories and phenomenological models used to extract and identify resonances.

1.1 Overview of theoretical models

One of the main goals of recent experiments at energies up to 2.5 $\sim$ 3 GeV is to study the baryon spectrum. Both these new experiments and the theoretical models bear on our search for and our understanding of baryon resonances. In the following we discuss some of theoretical models describing strong interactions in the non-perturbative regime.

1.1.1 Lattice QCD

An ab-initio approach to hadron physics is provided by Lattice QCD (LQCD) (142). In this approach, QCD is formulated on a 4-dimensional discrete Euclidean space-time lattice with no additional parameters or field variables resulting in a gauge invariant approach. LQCD retains the fundamental character of QCD. The discrete space-time lattice acts as a non-perturbative regularizer scheme and the lattice spacing, a, provides an ultraviolet cutoff rendering the quantum field theory finite. At the limit of $a \to 0$ the continuum theory is recovered.

The properties of both ground (89) and excited state (129; 50; 51) hadrons can be studied using LQCD calculations. Despite the success of LQCD in determining hadron resonance spectrum, a continuing problem for LQCD is an unphysical pion mass, around 300 MeV (104) as oppose to observed mass of 138 MeV, that enters in calculations.

1.1.2 Effective field theory

The assumption that high energy dynamics would not affect the dynamics of the low energy interactions give rise to one of the most powerful tools, effective field theories (EFT)s, in studying the non-perturbative regime of QCD. The free parameters of EFTs, also known as low energy constants (LEC), capture the omitted dynamics of the underlying theory at higher energies. The values of LECs can not be directly inferred from the underlying theory, instead they can be determined phenomenologically. As Weinberg stated (138) the goal is then to find the most generalized Lagrangian that preserves all the symmetries of the full theory but involves only the low energy degrees of freedom.

1.1.3 Chiral perturbation theory

At the "chiral limit", $m_q = 0$, the QCD Lagrangian exhibits *chiral* symmetry besides all the other obvious symmetries such as Lorentz invariance, $\mathrm{SU}(3)_c$ gauge invariance, etc. Considering that the masses of the three lightest quarks, u, d, and s, are not that far off from the

chiral limit, one can construct an effective field theory that invokes a perturbative expansion in the quark mass. Such an effective field theory is called Chiral perturbation theory (ChPT). In order to construct such a theory, we start by decomposing the quark field into its chiral components

$$= \frac{1}{2}(1-\gamma_5)\psi + \frac{1}{2}(1+\gamma_5)\psi = P_L\psi + P_R\psi = \psi_L + \psi_R, \tag{1.3}$$

where for simplicity we have suppressed the flavor and color indices.

Inserting Eq. (1.3) into Eq. (1.1) we have

$$\begin{aligned}
\mathcal{L}_{QCD} &= \mathcal{L}^0_{QCD} + \mathcal{L}^m_{QCD} + \dots \\
\mathcal{L}^0_{QCD} &= i\bar{\psi}_L \not{D}\psi_L + i\bar{\psi}_R \not{D}\psi_R - \frac{1}{4}G^A_{\mu\nu}G^{A\ \mu\nu} \\
\mathcal{L}^m_{QCD} &= \bar{\psi}_L \mathcal{M}\psi_R + \bar{\psi}_R \mathcal{M}^\dagger \psi_L,
\end{aligned} \tag{1.4}$$

where we introduced the covariant derivative $D = \partial_\mu + ig_s t\mathcal{A}_\mu$. Here ψ only collects the lightest quarks $\psi^T = (\psi_u, \psi_d, \psi_s)$ and $\mathcal{M} = \mathrm{diag}(m_u, m_d, m_s)$ is the quark mass matrix. The ellipse denotes the term for the higher mass quark, t, b, and c, Lagrangian and etc. $\mathcal{L}^0_{QCD}$ is invariant under the chiral flavor transformation $\mathrm{U}(3)_L \times \mathrm{U}(3)_R$ which can be rewritten as

$$\mathrm{U}(3)_L \times \mathrm{U}(3)_R = \mathrm{SU}(3)_L \times \mathrm{SU}(3)_R \times \mathrm{U}(1)_V \times \mathrm{U}(1)_A. \tag{1.5}$$

Here we introduced vector transformation $V = L + R$ and axial vector transformation $A = L - R$. The Noether current associated with each part of this symmetry group is realized in a different way. The $\mathrm{U}(1)_V$ current, the quark number, is a conserved current of the standard model. The $\mathrm{U}(1)_A$ current is broken by quantum effects. And finally the currents associated with chiral symmetry group $\mathrm{SU}(3)_L \times \mathrm{SU}(3)_R$ is explicitly broken by the quark masses, but this should be a small effect.

In nature, the Chiral symmetry is realized in the Goldstone mode and as a consequence "Goldstone bosons" appear. The 8 lightest pseudoscalar hadrons namely $\pi^\pm$, π^0, $K^\pm$, K^0, $\bar{K}^0$, and η are indeed the Goldstone bosons. At energies well below 1 GeV, these bosons are the only relevant degrees of freedom but a general formalism based on ChPT requires to

include baryons as well. Such a formalism can include the ground state baryons in form of matter fields, a review of ChPT involving one or more nucleons can be found in Ref. (52; 25).

Chiral Lagrangian can be used in a variety of different approaches. For example, in Unitarized Chiral Perturbation Theory (UChPT) one iterates a scattering kernel derived from Chiral Lagrangian in a Bethe-Salpeter equation. Then Baryon resonances can be described in S-waves. UChPT gives a complementary picture of these low-lying resonances (99; 87).

1.1.4 Quark model

In early 60s, Gell-Mann and, independently, George Zweig developed a model (55; 149) which successfully organized the large number of lighter hadrons into a meson octet, a baryon octet, and a baryon decuplet; Figure (1.2) shows these multiplets. At the time, Gell-Mann predicted the existence of Ω^- to complete the spin-3/2 baryon decuplet. Later, Ω^- was experimentally observed in 1964 (19). Based on the underlying *flavor SU(3)* or the *Eightfold Way* of quark model, the constituent quarks of the lighter hadrons are of three flavors, up (u), down (d), and strange (s). Although these 3 quark flavors were initially successful in describing the properties of lighter hadrons, the discovery of new hadrons suggested the existence of 3 additional heavy flavors, charm (c), bottom (b), and top (t).

Despite the success of quark model in organizing hadrons and predicting their quantum numbers, unfortunately it can not account for the mass discrepancy between the hadron's valence quarks' combined masses and the observed mass of the hadron. For example the lightest meson, the pion π, has a mass of ≈ 135 MeV which is almost 14 times the mass of its valence quarks. This difference in mass is contained in the quark-gluon 'soup' inside the hadron. At low and medium energy scattering experiments, this internal structure of hadrons is inaccessible to probe and one needs a non-perturbative description of the strong interaction to study such scatterings. It happens that within this energy range a rich spectrum of excited states, resonances, have been observed.

Understanding the excitation spectrum of hadrons is an essential part of a universal description of the non-perturbative regime of QCD. Quark model predictions of lighter resonances are in good agreement with experimental observations but when it comes to the higher mass resonances the evidence for such predictions is missing, as such this problem has been referred to as "missing resonance problem" (79). Partially this problem arises from the fact that not all resonances have a genuine three-quark structure. For example the quark model prediction for the mass of the first positive parity nucleon resonance, the Roper resonance $N(1440)$ $1/2^+$, lies above the mass of the first negative parity resonance but experimental observation revealed otherwise. This led to the interpretation that the Roper resonance is generated dynamically from the meson-baryon interaction instead. Such observations combined with the fact that there are no active quark models concerned with the decay width of resonances make more fundamental approaches the more attractive choice in hadron spectroscopy.

1.1.5 Dynamical couple channel

Dynamical couple channel (DCC) approaches are valuable tools in extracting broad resonances that are close in energy. These robust reaction theories are ideal specially at energies above the first inelastic threshold where different reaction channels become available and the coupling between them becomes more important. DCCs make use of effective Lagrangians to define their scattering kernel V; these kernels include meson exchange in t-channel and baryon exchange via u-channel. Resonances are explicitly contained in s-diagrams but they can also be dynamically generated. Dynamical generation of resonances is important in perceiving the nature of different resonances such as the Roper resonance. In a recent paper (29), Burkert and Roberts highlight the 5 decade effort in understanding the Roper resonance. They shed light on a coherent picture connecting the Roper resonance with the nucleon's first radial excitation.

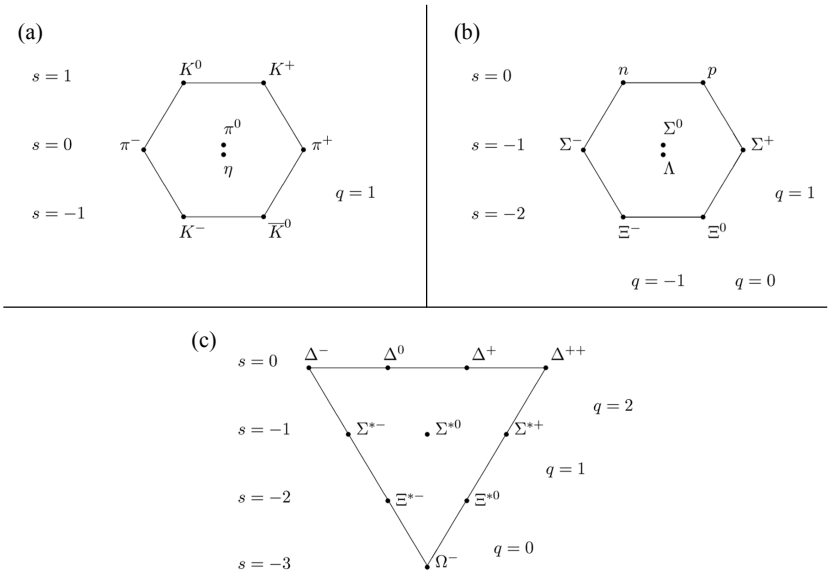

Figure 1.2: (a) Meson octet, (b) Baryon octet, (c) Baryon decuplet.

DCC approaches guarantee unitarity via Lippmann-Schwinger equation and by employing the full two body propagator in solving this equation, DCC approaches ensure analyticity of the scattering amplitude as well. Analytic continuation of the amplitude provides the opportunity to characterize baryon resonances by the poles and residues of S-matrix on second Riemann sheet with less ambiguity (than the usual Breit-Wigner parametrization) and model dependency.

Within the framework of DCC, multiple reactions can simultaneously be analyzed making DCC approaches very well suited to shed light on the "missing resonances problem" since resonances might couple to multiple channels.

1.1.6 K-matrix

Another approach to analyze and extract resonances from scattering data is K-matrix. Similarly in this method one solves Lippmann-Schwinger equation with the difference that the real part of the two body propagator is omitted. Even though the unitarity is still preserved since the imaginary part of the propagator is present, neglecting the real part of the two body propagator results in the loss of analyticity. This approximation means simplifying Lippmann-Schwinger equation by reducing the integral equations to a set of algebraic ones. This reduction is achieved by ignoring the real part of the two-body propagator. Furthermore ignoring the real part of two body propagator means only on shell intermediate states are taken into account which reduces the contribution from multiple scattering processes. Consequently this method is not capable of generating resonances dynamically and the lack of analyticity renders pole extraction impossible. The technical simplicity and flexibility of K-matrix approach makes it an efficient method to reproduce a large set of experimental data.

Some of the prominent groups such as Bonn-Gatchina (7), Gießen (121), Kent State University (123), GWU/SAID (143) rely on K-matrix approach and their variants for their analysis.

1.1.7 Isobar model

Since many resonances are packed within a small energy region with overlapping and large widths, studying their properties usually requires a large set of experimental data and a very robust method based on a coupled-channel approach. As a results such analysis can be very computationally expensive. Isobar models overcome that problem by decomposing the reaction amplitude into a resonance and a background contribution, corresponding to the pole and non-pole parts of the T-matrix amplitude. The simplicity of isobar models arises from the parametrization of the background by some smooth functions of energy and parametrization of the resonance amplitude by Breit-Wigner forms. Despite their simplicity

they can capture many properties of the resonances. This simplicity usually comes at the cost of violating the unitarity. Many efforts have been made to recover unitarity (14; 44; 42; 82; 21; 97; 18; 56; 91; 35; 1) by imposing unitary conditions separately on resonance and background contribution; this results in a rather involved constraint, specially on the resonance amplitude. For example, the Mainz group recently has introduced a constant complex phase to each of their resonance amplitudes in their etaMAID isobar model (132). It should be noted that, in principle, the complex phase is an energy-dependent function containing proper threshold behaviors.

1.2 Unitary Isobar model

Among the theoretical models mentioned above, DCCs are the most suited for identifying and extracting resonances states in the low energy region due to first the broad and overlapping nature of these states and second the coupling of resonances to multiple channels. The cost of such a robust method is its computational inefficiency. In order to capture the robustness of DCC without its computation cost, we proposed a couple channel approach in which we explicitly expose the full complex phase structure of the pole and non-pole parts of the reaction amplitude. This complex phase structure captures the channel opening dynamics, allowing us to maintain unitarity and analyticity for different levels of approximation. In chapter 2 we give a detailed explanation of this proposed model.

Chapter 2

Complex phase structure of the meson-baryon $\boldsymbol{T}$-matrix[1][2]

[1]Accepted by Physical Review D. Reprinted here with the permission of publisher.
[2]Shahab Razavi and K. Nakayama.

Abstract: The full complex phase structure of the meson-baryon reaction amplitude in coupled channels approach is investigated, including also the photon-baryon channel. The result may be viewed as a generalization of the well-known Watson's theorem. Furthermore, the complex phase structure is exhibited for the pole and non-pole parts of the reaction amplitude in such a way that it will serve as a convenient common starting point for constructing models with different levels of approximation, in particular, for building isobar models where the basic properties of the S-matrix can be maintained. Such models should be useful, especially, in coupled multichannel calculations, where a large amount of experimental data are considered in resonance analyses, a situation encountered in modern baryon spectroscopy. In particular, it is shown that the unitarity of the pole part of the T-matrix arises automatically from the dressing mechanism inherent in the basic scattering equation. This implies that no separate conditions are required for making this part of the resonance amplitude unitary as it has been done in some of the existing isobar models.

2.1 Introduction

Baryon spectroscopy is an important part of the study of non-perturbative regime of QCD. So far, most of the known baryon resonances have been identified in πN scattering experiments. With recent progresses in this field, it is clear that a reliable resonance identification and extraction of its properties from experimental spectra requires a consistent analysis of many independent reaction processes. Coupled channels approach is the tool of choice for this task. Indeed, reaction theories based on coupled channels approach have been developed at various degrees of sophistication. Nowadays, such analyses in baryon spectroscopy involve coupled multichannel calculations analyzing a large amount of experimental data in various meson production channels. These data are being accumulated at major facilities world wide, especially, in photoproduction reactions. The most sophisticated coupled channels approach is that of Dynamical Coupled Channels (DCC) developed over many years (90; 68; 69; 67; 71; 72; 73; 74; 47; 48; 66; 111; 112; 110; 113). These calculations are quite involved and

it is customary to make some sort of approximations in order to keep such calculations numerically more manageable. A common such approximation is the K-matrix approach and its variations employed by some of the resonance analyses groups (9; 10; 6; 5; 7; 8; 122; 120; 30; 121; 88; 123; 144; 23; 58; 12; 143; 135; 118). A nice feature of the K-matrix approach is that it reduces the original scattering equation to an algebraic equation while preserving unitarity of the S-matrix. This feature enables incorporating a large amount of experimental data in coupled multichannel analyses.

A particular variation of the K-matrix approach is the so-called isobar models, where the reaction amplitude is decomposed into a resonance and a background contribution. Basically, they should correspond to the pole and non-pole parts of the T-matrix amplitude. The background amplitude is usually parametrized by some smooth functions of energy while the resonance amplitude is parametrized by Breit-Wigner forms. Isobar models are practical and very economical in performing numerically demanding calculations, and are often used in resonance analyses based on coupled channels calculations and also dealing with a large amount of experimental data. Despite being simple, isobar models still capture many interesting properties of the resonances. One issue that arises in these models is that unitarity is usually violated. There are many efforts to unitarize isobar models (1; 35; 92; 57; 17; 98; 22; 83; 43; 45; 131; 14). There, the resonance and the background amplitudes are unitarized separately and independently. This leads to a quite involved constraint on the resonance amplitude in particular. One of the unitary isobar models used intensively in the analyses of both the photo- and electro-production reactions is that of Mainz group (43; 45; 131; 130). In their approach, the unitarization of the background amplitude is done by solving the scattering equation for that amplitude. For the resonance pole amplitude, based on Ref. (98), it introduces complex resonance coupling constants which are constrained by imposing the unitarity condition independent from the background amplitude. Recently the Mainz group has updated its etaMAID isobar model (132) by introducing a constant complex phase to each of their resonance amplitudes. Note that, in principle, the complex phase is

an energy-dependent function containing proper threshold behaviors. Complex phases in the resonance coupling constants have been also introduced in the study of hadronic reactions (see, e.g., Ref. (84)).

In the present work, we exhibit the full complex phase structure of the meson-baryon T-matrix reaction amplitude in coupled channels approach. To this end, we first expose the complex phase structure of the full reaction amplitude written in terms of the K-matrix and the so-called *generalized* Watson's factor. The result may be considered as a generalization of the well-known Watson's theorem in photoproduction (137). This helps us to expose, in a second step, the full complex phase structure of the pole and non-pole parts of the reaction amplitude which serves as a common staring point for introducing approximations to the reaction amplitude with varying degrees of sophistication. The resulting form of the reaction amplitude is such that the fundamental properties of the S-matrix, such as unitarity and/or analyticity, can be maintained straightforwardly in different approximations. In particular, we show how the unitarity of the pole part of the T-matrix arises automatically from the dressing mechanism inherent in the basic T-matrix equation, and that, no separate conditions are required for making this part of the resonance amplitude unitary as it has been done in some of the existing isobar models.

This paper is organized as follows. In Sec. 2.2, we introduce the notation used throughout this work for the sake of conciseness. In Sec. 2.3, we derive the full phase structure of the meson-baryon reaction amplitude which is essentially a generalization of the Watson's theorem. Based on this, the complex phase structure of the pole and non-pole parts of the reaction amplitude is derived in Sec. 2.4. In Sec. 2.5, the phase structure of the photoproduction amplitude in one-photon approximation is derived. In Sec. 2.6, possible levels of approximation to the full reaction amplitude are briefly discussed. A summary is given in Sec. 2.7. For completeness, the phase-shift parametrizations of the T- and K-matrices as well as of the generalized Watson's factor are given in Appendix A. Since the decomposition of the T-matrix into the pole and non-pole parts plays a central role in the present

work, this decomposition is derived in Appendix B for both the meson-baryon and photoproduction reaction processes. Appendix C contains the explicit form of the dressed resonance propagator in the case of the two resonance coupling.

2.2 Notation

Before starting the derivation of the complex phase structure of the meson-baryon reaction amplitude, a remark on the notation used in the present work is in order.

The two-body reaction amplitude T obeys, in general, the Lippmann-Schwinger-type scattering equation (also referred to as the T-matrix equation)

$$T = V + VGT \ , \tag{2.1}$$

where V denotes the driving potential kernel, irreducible with respect to the "two-particle cut" (116), and G stands for the two-body propagator. Note that the above equation is an integral equation for operators in abstract space.

In momentum space, and in the coupled channels approach, the above equation becomes [3]

$$\begin{aligned} T_{\nu'\nu}(\vec{q}\,', \vec{q}; E) &= V_{\nu'\nu}(\vec{q}\,', \vec{q}) \\ &+ \sum_{\lambda} \int d^3q'' V_{\nu'\lambda}(\vec{q}\,', \vec{q}\,'') G_{\lambda}(\vec{q}\,''^2, E) T_{\lambda\nu}(\vec{q}\,'', \vec{q}; E) \ . \end{aligned} \tag{2.2}$$

Here, $\vec{q}\,'$, $\vec{q}$, and $\vec{q}\,''$, denote the final, initial and intermediate two-particle relative momenta, respectively. E stands for the total energy of the system. The indices ν', ν, and λ stand for the final, initial and intermediate two-particle channels.

[3] The relativistic generalization of the scattering equation given by Eq. (2.2) - the so called Bethe-Salpeter equation (116) - involving a four-dimensional momentum integration, may be reduced to a three-dimensional integral equation of the form given by Eq. (2.2) in such a way to maintain Lorentz covariance and elastic unitarity of the original reaction amplitude (34). This means that Lorentz covariance can be also maintained in three-dimensional scattering equations, along with the other basic properties of the S-matrix, such as unitarity and analyticity.

The reaction amplitude given by Eq. (2.2) can be expanded in partial-waves as

$$\begin{aligned}
&\langle S'M_{S'}|T_{\nu'\nu}(\vec{q}\,',\vec{q};E)|SM_S\rangle = \\
&= \sum i^{L-L'}(S'M_{S'}L'M_{L'}|JM_J)(SM_SLM_L|JM_J) \\
&\qquad \times T^{JIS'S}_{\nu'\nu L'L}(q',q;E)Y_{L'M_{L'}}(\hat{q}')Y^*_{LM_L}(\hat{q})\hat{P}_I \ , \qquad (2.3)
\end{aligned}$$

where S, L, and J denote the spin, orbital angular momentum and total angular momentum, respectively of the two-body initial state, while M_S, M_L and M_J stand for the corresponding projection quantum numbers. The primed quantities refer to the corresponding quantum numbers of the final two-body state. $\hat{P}_I$ stands for the isospin projection operator which projects the two-body state onto the total isospin state I. $Y_{lm_l}(\hat{p})$ stands for the usual spherical harmonic function. Here, the argument $\hat{p}$ is a short-hand notation for the polar (θ) and azimuthal (ϕ) angles, i.e., $\hat{p} = (\theta_p, \phi_p)$. The geometrical factor $(j_1m_1j_2m_2|j_3m_3)$ is the usual $SU(2)$ Clebsch-Gordan coefficient. The summation in the above equation is over all the quantum numbers appearing on the right-hand side and not specified on the left-hand side of the equation.

The partial-wave amplitude $T^{JIS'S}_{\nu'\nu L'L}(q',q;E)$ in Eq. (2.3) can be extracted by inverting that equation. We have

$$\begin{aligned}
&T^{JIS'S}_{\nu'\nu L'L}(q',q;E) = \sum i^{L'-L}\left(\frac{8\pi^2}{2J+1}\right)\left(\frac{2L+1}{4\pi}\right)^{\frac{1}{2}} \\
&\times (S'M_{S'}L'M_{L'}|JM_J)(SM_SL0|JM_J)\ \hat{P}_I \\
&\times \int_{-1}^{+1} d(\cos\theta_{q'})\langle S'M_{S'}|T_{\nu'\nu}(\vec{q}\,',\vec{q};E)|SM_S\rangle \\
&\qquad \times Y^*_{L'M_{L'}}(\theta_{q'},0) \ , \qquad (2.4)
\end{aligned}$$

where, without loss of generality, the initial relative momentum $\vec{q}$ is chosen along the $+z$-axis and the final relative momentum $\vec{q}\,'$ in the x-z plane. Similarly to Eq. (2.3), the summation in the above equation is over all the quantum numbers appearing on the right-hand side and not specified on the left-hand side of the equation.

Inserting Eq. (2.3) into (2.2), yields the scattering equation for the partial-wave amplitude

$$T^{JIS'S}_{\nu'\nu\,L'L}(q',q;E) = V^{JIS'S}_{\nu'\nu\,L'L}(q',q) + \sum_{S'',L'',\lambda}\int_0^\infty dq''q''^2 V^{JIS'S''}_{\nu'\lambda\,L'L''}(q',q'') \times G_\lambda(q''^2,E)T^{JIS''S}_{\lambda\nu\,L''L}(q'',q;E)\ . \tag{2.5}$$

In the present work, we use the notation

$$T_{\alpha'\alpha} = V_{\alpha'\alpha} + \sum_\beta V_{\alpha'\beta}G_\beta T_{\beta\alpha} \tag{2.6}$$

to denote either Eq. (2.2) or (2.5) for the sake of conciseness. Accordingly, if the above equation is to represent Eq. (2.2), the indices α', α and β in the above equation stand for the two-particle channel of the final, initial and intermediate states, respectively, and the summation over β is to be understood as the summation over the intermediate two-particle channels. On the other hand, if the above equation is to represent Eq. (2.5), then, the indices α', α and β specify, in addition to the two-particle channel of the final, initial and intermediate states, respectively, also the corresponding two-body partial-wave states. Note also that the reference to the two-particle relative momentum is completely suppressed in the present notation, including its integration over the intermediate states.

The notation explained above is used throughout the present paper. In particular, the main result of this work, given by Eqs. (2.66, 2.69), can be interpreted as given either in plane-wave or in partial-wave basis.

2.3 Phase structure of the two-body T-matrix amplitude

To expose the phase structure of the two-body reaction amplitude, it is convenient to express the T-matrix in terms of the K-matrix. We start with the T-matrix scattering equation

$$T = V + TGV = V + VGT\ , \tag{2.7}$$

where the two-body propagator G can, in general, be decomposed into the real and imaginary parts

$$G = G^R - iG^I \ . \tag{2.8}$$

In fact, the propagator involving stable particles is of the form ($\epsilon \to 0$)

$$G = \frac{1}{E - H_0 + i\epsilon} = \mathcal{P}\frac{1}{E - H_0} - i\pi\delta(E - H_0) \ , \tag{2.9}$$

with $\mathcal{P}$ standing for the principal value part, while the propagator involving unstable particles is of the form (90; 47) (Π = finite)

$$\begin{aligned} G &= \frac{1}{E - h_0 - \Pi} \\ &= \frac{E - H_0}{(E - H_0)^2 + \Pi^{I\,2}} - i\frac{\Pi^I}{(E - H_0)^2 + \Pi^{I\,2}} \ , \end{aligned} \tag{2.10}$$

where h_0 denotes the unperturbed Hamiltonian involving the bare unstable particle and Π is the self-energy of that unstable particle. $H_0 \equiv h_0 + \Pi^R$, with $\Pi = \Pi^R - i\Pi^I$.

Inserting Eq. (2.8) into Eq. (2.7), we have (16)

$$T = K - iTG^IK = K - iKG^IT \ , \tag{2.11}$$

with the K-matrix (K) given by

$$K = V + VG^RK = V + KG^RV \tag{2.12}$$

which is Hermitian if the driving potential V is Hermitian.

For stable particles, using Eq. (2.9), Eq. (2.11) becomes

$$T(E) = K(E) - i\pi T(E)\delta(E - H_0)K(E) \ , \tag{2.13}$$

which is the familiar equation for the T-matrix in terms of the K-matrix. Note that, for unstable particles propagation (cf. Eq, (2.10)), the imaginary part of G – for which there is no δ-function in energy – leads to a momentum loop integration over the intermediate state.

Equation (2.7) – and consequently all the subsequent equations – represents actually coupled equations in two-particle channels. Explicitly, for Eqs. (2.11,2.12), we have (using the corresponding first equalities)

$$T_{\alpha'\alpha} = K_{\alpha'\alpha} - i\sum_{\beta} T_{\alpha'\beta} G^I_\beta K_{\beta\alpha} \ ,$$
$$K_{\alpha'\alpha} = V_{\alpha'\alpha} + \sum_{\beta} K_{\alpha'\beta} G^R_\beta V_{\beta\alpha} \ , \tag{2.14}$$

where the subscripts stand for the two-particle channels, i.e., α' denotes the final two-particle channel and α, the initial two-particle channel. β denotes the intermediate two-particle channel and it is summed over all the channels (including the stable- and unstable-particles propagations) to account for the possible couplings of the initial and final states to all other channels. Note that, as explained in Sec. 2.2, the equations in (2.14) may be interpreted as given either in plane-wave or in partial-wave basis. For the latter, the indices α', α and β specify also the partial-wave states, in addition to the two-particle channels. Note also that the reference to the two-particle relative momentum is completely suppressed in the present notation, including the momentum-loop integration over the intermediate states.

Usually, the integral equation for T in Eq. (2.14) is solved to yield

$$T_{\alpha'\alpha} = \sum_{\beta} K_{\alpha'\beta} \left[\frac{1}{1+iG^I K}\right]_{\beta\alpha} \ . \tag{2.15}$$

In the present work, however, we solve that equation as follows. First, we write it as

$$\sum_{\beta\neq\alpha'} T_{\alpha'\beta}(\delta_{\beta\alpha} + iG^I_\beta K_{\beta\alpha}) = (1 - iT_{\alpha'\alpha'}G^I_{\alpha'})K_{\alpha'\alpha}$$
$$\sum_{\beta\neq\alpha'} T_{\alpha'\beta} D_{\beta\alpha} = N_{\alpha'} K_{\alpha'\alpha} \ , \tag{2.16}$$

where we have defined

$$D_{\beta'\beta} \equiv \delta_{\beta'\beta} + iG^I_{\beta'} K_{\beta'\beta} \ , \qquad (\beta', \beta \neq \alpha')$$
$$N_{\alpha'} \equiv 1 - iT_{\alpha'\alpha'} G^I_{\alpha'} \ . \tag{2.17}$$

Next, we multiply Eq. (2.16) throughout from the right by the inverse matrix of D to get

$$T_{\alpha'\alpha} = N_{\alpha'} \sum_{\beta' \neq \alpha'} K_{\alpha'\beta'} D^{-1}_{\beta'\alpha} \ . \tag{2.18}$$

Finally, we insert the above result back into the equation for T in (2.14) to arrive at

$$\begin{aligned} T_{\alpha'\alpha} &= N_{\alpha'} \Big[K_{\alpha'\alpha} - i \sum_{\beta,\beta' \neq \alpha'} K_{\alpha'\beta'} \left(D^{-1}\right)_{\beta'\beta} G^I_\beta K_{\beta\alpha} \Big] \\ &= N_{\alpha'} \hat{K}_{\alpha'\alpha} \ . \end{aligned} \tag{2.19}$$

The last equality in Eq. (2.19) defines $\hat{K}$ to be

$$\hat{K}_{\alpha'\alpha} \equiv K_{\alpha'\alpha} - i \sum_{\beta,\beta' \neq \alpha'} K_{\alpha'\beta'} \left(D^{-1}\right)_{\beta'\beta} G^I_\beta K_{\beta\alpha} \ , \tag{2.20}$$

which – unlike the K-matrix – is, in general, a complex quantity. Note that below the first inelastic threshold, $\hat{K} = K$. Also, note that the explicit dependence on the channel α' in the intermediate state is absent in $\hat{K}_{\alpha'\alpha}$. This dependence is contained implicitly in the K-matrices, K_{ij}.

Inserting Eq. (2.19) into the definition of $N_{\alpha'}$ in Eq. (2.17), yields

$$N_{\alpha'} = 1 - i T_{\alpha'\alpha'} G^I_{\alpha'} = \frac{1}{1 + i \hat{K}_{\alpha'\alpha'} G^I_{\alpha'}} \ . \tag{2.21}$$

Starting from the second equality in Eq. (2.11), it is straightforward to show that the T-matrix can be also expressed as

$$T_{\alpha'\alpha} = \hat{\bar{K}}_{\alpha'\alpha} \bar{N}_\alpha \ , \tag{2.22}$$

where

$$\begin{aligned} \bar{N}_\alpha &\equiv 1 - i G^I_\alpha T_{\alpha\alpha} = \frac{1}{1 + i G^I_\alpha \hat{K}_{\alpha\alpha}} \ , \\ \bar{D}_{\beta'\beta} &\equiv \delta_{\beta'\beta} + i K_{\beta'\beta} G^I_\beta \ , \qquad (\beta', \beta \neq \alpha) \\ \hat{\bar{K}}_{\alpha'\alpha} &\equiv K_{\alpha'\alpha} - i \sum_{\beta,\beta' \neq \alpha} K_{\alpha'\beta'} G^I_{\beta'} \left(\bar{D}^{-1}\right)_{\beta'\beta} K_{\beta\alpha} \ . \end{aligned} \tag{2.23}$$

Equation (2.19) or (2.22) is the desired result: we have exhibited the full phase structure of the T-matrix which is non-trivial in general due to the phase structure of $\hat{K}_{\alpha'\alpha}$, introduced by the terms involving G^I_βs in Eq. (2.20) or (2.23). For on-shell $\hat{K}_{\alpha\alpha}$, its phase structure can be expressed simply in terms of the phase-shift and inelasticity of the elastic scattering T-matrix as shown in Appendix A.

Note also that Eq. (2.19) or (2.22) is completely general and holds for fully off-shell T-matrix. Hereafter, we refer to the factors $N_{\alpha'}$ and $\bar{N}_\alpha$ defined in Eqs. (2.17,2.23) as the *generalized* Watson's factors. For completeness, we show how Watson's theorem emerges from these equations in the following Sec. 2.3.1, when the initial channel α corresponds to the photon-baryon channel.

If we wish, combining Eqs. (2.19,2.22), the T-matrix can be expressed in a symmetric form

$$T_{\alpha'\alpha} = \frac{1}{2}\left(N_{\alpha'}\hat{K}_{\alpha'\alpha} + \hat{\bar{K}}_{\alpha'\alpha}\bar{N}_\alpha\right) \ . \tag{2.24}$$

2.3.1 Two-channel case and Watson's theorem

Confining now to the case of two channels problem, $\hat{K}_{\alpha'\alpha}$ in Eq. (2.20) simplifies and Eq. (2.19) takes the form

$$T_{\alpha'\alpha} = N_{\alpha'}\left[K_{\alpha'\alpha} - iK_{\alpha'\beta}\bar{N}_{K\beta}G^I_\beta K_{\beta\alpha}\right] \ , \quad (\beta \neq \alpha') \tag{2.25}$$

with

$$\bar{N}_{K\alpha} \equiv \frac{1}{1 + iG^I_\alpha K_{\alpha\alpha}} \ . \tag{2.26}$$

For a transition reaction, where $\alpha' \neq \alpha$, Eq. (2.25) further reduces to

$$T_{\alpha'\alpha} = N_{\alpha'}K_{\alpha'\alpha}\bar{N}_{K\alpha} \ . \tag{2.27}$$

If the two channels considered involve only stable particles, then, in partial-wave basis, Eqs. (2.25,2.27) are simple algebraic equations, where $G^I_\beta \to \rho_\beta$ after the momentum loop integration with ρ_β denoting the phase-space density. Moreover, if the on-shell T-matrix and

the on-shell K-matrix can be parametrized in terms of phase-shifts and inelasticities as given in Appendix A, we obtain from Eq. (2.27),

$$T_{\alpha'\alpha} = \left\{ \frac{1}{2} \left(\eta_{\alpha'} e^{i2\delta_{\alpha'}} + 1 \right) \right\} K_{\alpha'\alpha} \left(e^{i\delta_\alpha} \cos\delta_\alpha \right) \ , \tag{2.28}$$

for the transition amplitude ($\alpha' \neq \alpha$). Here, we have made use of Eqs. (A.4,A.5).

Equation (2.28) reveals the phase structure of the T-matrix amplitude explicitly in terms of the phase-shifts for the transition amplitude in the case of a two-channel problem. It is the analog of the well-known Watson's theorem for photoproduction (137) in the case of two-body hadronic reactions. The phase of the reaction amplitude is determined by both the on-shell initial and final state interactions through the Watson's factors $\bar{N}_{K\alpha}$ and $N_{\alpha'}$, respectively. Note that, in Eq. (2.28), the effect of the channel openings is lumped entirely into the final state interaction factor. We remind that, from Eq. (2.12), if V is Hermitian, so is K and, together with time reversal invariance, $K_{\alpha'\alpha}$ is either pure real or pure imaginary.

If we start with the T-matrix in the form given by Eq. (2.22), instead of Eq. (2.19) as we have done above, we obtain an equivalent alternative form for the transition amplitude ($\alpha' \neq \alpha$),

$$T_{\alpha'\alpha} = N_{\alpha'} K_{\alpha'\alpha} \bar{N}_\alpha \ , \tag{2.29}$$

with

$$N_{K\alpha} \equiv \frac{1}{1 + iK_{\alpha\alpha} G^I_\alpha} \ . \tag{2.30}$$

In terms of the phase-shift parametrization, Eq. (2.29) becomes

$$T_{\alpha'\alpha} = \left(e^{i\delta_{\alpha'}} \cos\delta_{\alpha'} \right) K_{\alpha'\alpha} \left\{ \frac{1}{2} \left(\eta_\alpha e^{i2\delta_\alpha} + 1 \right) \right\} \ . \tag{2.31}$$

In contrast to Eq. (2.28), where the effect of the channel openings is lumped into the final state interaction factor, here, this effect is lumped into the initial state interaction factor.

It should be mentioned that, strictly speaking, the two channels consideration of the meson-baryon reaction processes applies only to πN charge-exchange scatterings, such as $\pi^0 p \to \pi^+ n$. This is due to the fact that the lightest meson-baryon channel, apart from πN,

is the ηN channel which is already above the $\pi\pi N$ threshold, leading to the presence of an inelastic channel even when the isospin symmetry breaking of the strong interaction is ignored.

In the case of meson photoproduction, Eq. (2.27) becomes ($\alpha' \neq \alpha = \gamma$)

$$T_{\alpha'\gamma} = N_{\alpha'} K_{\alpha'\gamma} \bar{N}_{K\gamma} \ , \tag{2.32}$$

where $\bar{N}_{K\gamma} = 1/(1 + iG^I_\gamma K_{\gamma\gamma})$ is the Watson's factor due to the γN initial state interaction. In the one-photon approximation, due to the weakness of the electromagnetic interaction, the Watson's factor $N_{K\gamma}$ approaches unit since we may set $K_{\gamma\gamma}$ appearing in $N_{K\gamma}$ to zero. Likewise, for the two-channel case, where one of the channels is the photon-baryon channel, $N_{\alpha'} = N_{K\alpha'}$ in one-photon approximation. Equation (2.32), then, becomes

$$T_{\alpha'\gamma} = N_{K\alpha'} K_{\alpha'\gamma} = \left(e^{i\delta_{\alpha'}} \cos\delta_{\alpha'}\right) K_{\alpha'\gamma} \ , \tag{2.33}$$

which is the usual form of Watson's theorem for photoproduction (137). Equation (2.29) yields the same result as above. Note that Watson's theorem is a direct consequence of unitarity and time reversal invariance of the S-matrix, in addition to the one-photon approximation assumption. Also, as is well known, in practice, ignoring the isospin symmetry breaking of the hadronic interactions, Watson's theorem applies to pion photoproduction below $\pi\pi N$ threshold.

2.4 Phase structure of the pole and non-pole meson-baryon T-matrix

In this section we exhibit the phase structure of the T-matrix in terms of the pole (T^P) and non-pole ($X \equiv T^{NP}$) parts.

First, we recall that the full T-matrix given by Eq. (2.7) can be decomposed as (see, Appendix B)

$$\begin{aligned} T &= V + VGT \\ &\equiv T^P + X \ , \end{aligned} \tag{2.34}$$

where

$$X = U + UGX \ , \tag{2.35}$$

with $U \equiv V^{NP} \equiv V - V^P$ and

$$V^P = \sum_r |F_{0r}\rangle S_{0r} \langle F_{0r}| \ , \tag{2.36}$$

where $|F_{0r}\rangle$ and $S_{0r}^{-1} = E - m_{0r}$ denote the bare meson-baryon vertex and bare baryon propagator, respectively. The summation is over the resonances specified by index r.

The pole part of the T-matrix in Eq. (2.34) is (following the ket and bra notation used in Ref. (61; 62))

$$T^P = \sum_{r'r} |F_{r'}\rangle S_{r'r} \langle F_r| \ , \tag{2.37}$$

where the dressed vertices read

$$\begin{aligned} |F\rangle_{r'} &\equiv (1 + XG) \, |F_{0r'}\rangle \ , \\ \langle F|_r &\equiv \langle F_{0r}| \, (1 + GX) \ , \end{aligned} \tag{2.38}$$

and the dressed baryon propagator, $S_{r'r}$,

$$S_{r'r}^{-1} = S_{0r}^{-1} \delta_{r'r} - \Sigma_{r'r} \tag{2.39}$$

with the self-energy

$$\Sigma_{r'r} \equiv \langle F_{0r'}|G|F_r\rangle \ . \tag{2.40}$$

Note that the dressed baryon propagator in Eq. (2.39) couples resonances, so it is a matrix propagator in resonance space. It's structure is shown explicitly in Appendix C for the case of a two-resonance coupling since, in practice, this is the maximum number of resonance couplings in most of the cases.

Second, since the structures of the T- and K-matrix scattering equations are the same (cf. Eqs. (2.7,2.12)), it is straightforward to decompose the K-matrix into the pole (K^P) and non-pole ($W \equiv K^{NP}$) parts

$$\begin{aligned} K &= V + VG^R K \\ &\equiv K^P + W \ , \end{aligned} \tag{2.41}$$

where

$$W = U + UG^R W \ , \tag{2.42}$$

and

$$K^P = \sum_{r'r} |F_{Kr'}\rangle S_{Kr'r} \langle F_{Kr}| \ . \tag{2.43}$$

Here, the dressed vertices are given by

$$\begin{aligned} |F_{Kr'}\rangle &\equiv \left(1 + WG^R\right) |F_{0r'}\rangle \ , \\ \langle F_{Kr}| &\equiv \langle F_{0r}| \left(1 + G^R W\right) \ , \end{aligned} \tag{2.44}$$

and the dressed baryon propagator by

$$S^{-1}_{Kr'r} = S^{-1}_{0r} \delta_{r'r} - \Sigma_{Kr'r} \ , \tag{2.45}$$

with the self-energy

$$\Sigma_{Kr'r} = \langle F_{0r'}|G^R|F_{Kr}\rangle \ . \tag{2.46}$$

Third, since the T-matrix can be expressed in terms of the K-matrix as given by Eq. (2.11), which exhibits the same integral-equation structure as Eq. (2.7), except for the appearance of the imaginary part of the meson-baryon propagator $-iG^I$ instead of the full propagator G, it is straightforward to express the pole and non-pole T-matrices (cf. Eqs.(2.34,2.35,2.37,2.38,2.39,2.40)) in terms of the K-matrix (cf. Eqs.(2.41,2.42,2.43,2.44,2.45,2.46)). Then, the non-pole T-matrix $X(\equiv T^{NP})$ given by Eq. (2.35) becomes

$$X = W - iXG^I W = W - iWG^I X \ . \tag{2.47}$$

The pole part (T^P) is given by Eq. (2.37) with

$$\begin{aligned} |F_{r'}\rangle &\equiv (1 - iXG^I)|F_{Kr'}\rangle \ , \\ \langle F_r| &\equiv \langle F_{Kr}|(1 - iG^I X) \ , \end{aligned} \tag{2.48}$$

and the dressed propagator $S_{r'r}$ expressed as

$$S^{-1}_{r'r} = S^{-1}_{Kr'r} - \hat{\Sigma}_{r'r} \tag{2.49}$$

where the self-energy $\hat{\Sigma}$ is

$$\hat{\Sigma}_{r'r} \equiv -i\langle F_{Kr'}|G^I|F_r\rangle \ . \tag{2.50}$$

Writing the meson-baryon channel indices explicitly, we have, for Eq. (2.42),

$$W_{\alpha'\alpha} = U_{\alpha'\alpha} + \sum_\beta W_{\alpha'\beta} G^R_\beta U_{\beta\alpha} \ . \tag{2.51}$$

For Eq. (2.47), we have,

$$\begin{aligned} X_{\alpha'\alpha} &= W_{\alpha'\alpha} - i\sum_\beta X_{\alpha'\beta} G^I_\beta W_{\beta\alpha} \\ &= W_{\alpha'\alpha} - i\sum_\beta W_{\alpha'\beta} G^I_\beta X_{\beta\alpha} \ , \end{aligned} \tag{2.52}$$

which can be solved to yield (from the first equality)

$$X_{\alpha'\alpha} = N^X_{\alpha'} \hat{W}_{\alpha'\alpha} \ , \tag{2.53}$$

with

$$\hat{W}_{\alpha'\alpha} \equiv W_{\alpha'\alpha} - i\sum_{\beta,\beta'\neq\alpha'} W_{\alpha'\beta'} \left((D^X)^{-1}\right)_{\beta'\beta} G^I_\beta W_{\beta\alpha} \ , \tag{2.54}$$

and

$$\begin{aligned} D^X_{\beta'\beta} &\equiv \delta_{\beta'\beta} + iG^I_{\beta'} W_{\beta'\beta} \ , \\ N^X_{\alpha'} &\equiv 1 - iX_{\alpha'\alpha'} G^I_{\alpha'} = \frac{1}{1 + i\hat{W}_{\alpha'\alpha'} G^I_{\alpha'}} \ . \end{aligned} \tag{2.55}$$

From the second equality in Eq. (2.52), it is also immediate that $X_{\alpha'\alpha}$ can be expressed as

$$X_{\alpha'\alpha} = \hat{\bar{W}}_{\alpha'\alpha} \bar{N}^X_\alpha \ , \tag{2.56}$$

with

$$\hat{\bar{W}}_{\alpha'\alpha} \equiv W_{\alpha'\alpha} - i\sum_{\beta,\beta'\neq\alpha} W_{\alpha'\beta'} G^I_{\beta'} \left((\bar{D}^X)^{-1}\right)_{\beta'\beta} W_{\beta\alpha} \ , \tag{2.57}$$

and

$$\bar{D}^X_{\beta'\beta} \equiv \delta_{\beta'\beta} + iW_{\beta'\beta}G^I_\beta \ ,$$
$$\bar{N}^X_\alpha \equiv 1 - iG^I_\alpha X_{\alpha\alpha} = \frac{1}{1 + iG^I_\alpha \hat{\bar{W}}_{\alpha\alpha}} \ . \tag{2.58}$$

Note that in the case the particles in channel α are stable ($G^I_\alpha \to \rho_\alpha$), $\bar{N}^X_\alpha = N^X_\alpha$.

In the following, to exhibit the phase structure of the pole T-matrix, T^P, we make use of the dressed vertices and propagator as given by Eqs. (2.48,2.49,2.50). Writing the meson-baryon channel indices explicitly, Eq. (2.37) becomes

$$T^P_{\alpha'\alpha} = \sum_{r'r} |F_{r'}\rangle_{\alpha'} S_{r'r} \langle F_r|_\alpha \ . \tag{2.59}$$

The dressed meson-baryon vertex $|F_{r'}\rangle$ (cf. Eq. (2.48)) becomes

$$|F_{r'}\rangle_{\alpha'} \equiv |F_{Kr'}\rangle_{\alpha'} - i\sum_\beta X_{\alpha'\beta} G^I_\beta |F_{Kr'}\rangle_\beta$$
$$= N^X_{\alpha'} |\hat{F}_{Kr'}\rangle_{\alpha'} \ , \tag{2.60}$$

where

$$|\hat{F}_{Kr'}\rangle_{\alpha'} \equiv |F_{Kr'}\rangle_{\alpha'} - i\sum_{\beta\neq\alpha'} \hat{W}_{\alpha'\beta} G^I_\beta |F_{Kr'}\rangle_\beta \ . \tag{2.61}$$

To arrive at the last equality in Eq. (2.60), Eqs. (2.55,2.53) have been used.

Analogously,

$$\langle F_r|_\alpha \equiv \langle \hat{F}_{Kr}|_\alpha \bar{N}^X_\alpha \ , \tag{2.62}$$

where

$$\langle \hat{F}_{Kr}|_\alpha \equiv \langle F_{Kr}|_\alpha - i\sum_{\beta\neq\alpha} \langle F_{Kr}|_\beta G^I_\beta \hat{\bar{W}}_{\beta\alpha} \ . \tag{2.63}$$

The self-energy given by Eq. (2.50) reads

$$\hat{\Sigma}_{r'r} = -i\sum_\beta \langle F_{Kr'}|_\beta G^I_\beta |F_r\rangle_\beta$$
$$= -i\sum_\beta \langle F_{Kr'}|_\beta G^I_\beta N^X_\beta |\hat{F}_{Kr}\rangle_\beta \ . \tag{2.64}$$

Then, inserting the above result into Eq. (2.49), we have for the full propagator,

$$S^{-1}_{r'r} = S^{-1}_{Kr'r} + i \sum_{\beta} \langle F_{Kr'}|_\beta G^I_\beta N^X_\beta |\hat{F}_{Kr}\rangle_\beta \ . \tag{2.65}$$

Finally, making use of Eq. (2.45) and inserting Eqs. (2.60,2.62,2.65) into Eq. (2.59), and combining with Eq. (2.53), we arrive at the result we are seeking

$$\begin{aligned} T_{\alpha'\alpha} &= T^P_{\alpha'\alpha} + X_{\alpha'\alpha} \\ &= \sum_{r'r} \left\{ N^X_{\alpha'} |\hat{F}_{Kr'}\rangle_{\alpha'} \left(\frac{1}{(E-m_0)I - \Sigma_K + i\sum_\beta \langle F_K|_\beta G^I_\beta N^X_\beta |\hat{F}_K\rangle_\beta} \right)_{r'r} \langle \hat{F}_{Kr}|_\alpha \bar{N}^X_\alpha \right\} + N^X_{\alpha'} \hat{W}_{\alpha'\alpha} \ . \end{aligned} \tag{2.66}$$

where I stands for the identity matrix in resonance space. Σ_K is given by Eq. (2.46).

The above equation exhibits the full phase structure of the T-matrix amplitude in terms of the pole and non-pole parts. First of all, we note that the phase structure of the T-matrix is determined by the branch points introduced in the amplitude due to the opening of the meson-baryon channels. This is controlled by the availability of the phase space for a given meson-baryon channel β encoded in the imaginary part of the corresponding meson-baryon propagator G^I_β. This quantity appears implicitly in many places in Eq. (2.66) and, consequently, makes the phase structure of the T-matrix highly non-trivial in general. Note that the Watson's factor N^X and all the quantities with "hat" in Eq. (2.66) involve G^I [cf. Eqs. (2.53,2.55,2.57,2.58,2.61,2.63)]. All other terms appearing in Eq. (2.66) are real quantities and do not involve G^I. We also recall that the dressed vertex $|\hat{F}_K\rangle(\langle\hat{F}_K|)$, as well as the Watson's factor $N^X(\bar{N}^X)$, are all expressed in terms of the quantity $\hat{W}(\hat{\bar{W}})$ (cf. Eqs. (2.55,2.58,2.61,2.63)). The latter quantity is the non-pole T-matrix apart from the Watson's factor N^X (cf. Eqs. (2.53,2.56)). This means that the dynamical effects on the phase structure are determine by the non-pole part of the T-matrix (up to the corresponding Watson's factor), and that there is an intimate relationship between the phase structure of the pole and non-pole parts of the T-matrix amplitude.

In the following, we discuss the elastic scattering below the first inelastic threshold where the phase structure of the T-matrix amplitude becomes much simpler. Here, we ignore the resonance couplings for simplicity. We also assume a stable meson-baryon channel α and consider the phase-shift parametrization of the on-shell non-pole T-matrix such that $N_\alpha^X = \bar{N}_\alpha^X = e^{\delta_\alpha^X} \cos\delta_\alpha^X$, where δ_α^X stands for the phase-shift of the non-pole T-matrix ($X \equiv T^{NP}$). Then, in partial-wave basis, Eq. (2.66) reduces to

$$T_{\alpha\alpha} = \sum_r \left\{ e^{i\delta_\alpha^X} g_{\alpha r} \frac{1}{E - M_r + i\frac{\Gamma_r}{2}} g_{\alpha r} e^{i\delta_\alpha^X} \right\} + e^{i\delta_\alpha^X} \tilde{W}_{\alpha\alpha} \ , \tag{2.67}$$

where we have introduced the (suggestive) notations

$$\begin{aligned} g_{\alpha r} &\equiv \cos\delta_\alpha^X \, |F_K\rangle_{\alpha,r} \ , \\ \Gamma_r &\equiv 2\rho_\alpha \, g_{\alpha r}^2 \ , \\ M_r &\equiv m_{0r} + \Sigma_{Krr} + \tan\delta_\alpha^X \, \frac{\Gamma_r}{2} \ , \\ \tilde{W}_{\alpha\alpha} &\equiv \cos\delta_\alpha^X W_{\alpha\alpha} \ . \end{aligned} \tag{2.68}$$

Equation (2.67) exhibits, explicitly, the full phase structure of the elastic T-matrix amplitude below the first inelastic threshold. Apart from the phase $e^{i\delta_\alpha^X}$ arising from the Watson's factors in the dressed vertices and propagator, there is also the same phase factor arising from the Watson's factor in the non-pole part of the amplitude. Note that the last term in Eq. (2.67) is simply the statement of Watson's theorem for the non-pole T-matrix X. Recall that W is the non-pole part of the K-matrix and, as such, it is Hermitian if the non-pole driving potential $U \equiv V^{NP}$ is.

Equation (2.66) is the main result of this section. It serves as a convenient starting point for approximations one can make with varying degrees of sophistication. In particular, it allows to keep track on the basic properties of the S-matrix in these approximations. Indeed, Eq. (2.66) is being used by us in the construction of an isobar model in which unitarity is automatically satisfied.

2.5 Phase Structure of the Photoproduction amplitude

As shown explicitly in Appendix B, the gauge-invariant photoproduction amplitude in one-photon approximation also admits a decomposition into the pole and non-pole parts. Thus, we must be able to exhibit the complex phase structure of this amplitude in terms of the corresponding pole and non-pole amplitudes, analogous to what has been done for the meson-baryon T-matrix amplitude in the previous section. [4] Indeed, the meson photoproduction amplitude can be obtained by simply considering the photon-baryon channel as an additional channel in the coupled channels T-matrix equation of Eq. (2.34), i.e., all the results of the previous sections apply to photoproduction as well. In terms of the coupled channels formulation of the previous sections, the one-photon approximation means to ignore the photon-baryon channel in the intermediate states, i.e, this channel appears only as the initial state. Then, Eq. (2.66) leads to

$$\begin{aligned} M^{\mu}_{\alpha'\gamma} &= M^{P\,\mu}_{\alpha'\gamma} + X^{\mu}_{\alpha'\gamma} \\ &= \sum_{r'r} \left\{ N^X_{\alpha'} |\hat{F}_{Kr'}\rangle_{\alpha'} \left(\frac{1}{(E-m_0)I - \Sigma_K + i\sum_\beta \langle F_K|_\beta G^I_\beta N^X_\beta |\hat{F}_K\rangle_\beta} \right)_{r'r} \langle \hat{F}^{\mu}_{Kr}|_\gamma \right\} + N^X_{\alpha'} \hat{W}^{\mu}_{\alpha'\gamma} \ , \end{aligned} \tag{2.69}$$

where the initial meson-baryon channel α has been replaced by the photon-baryon channel γ which appears only in the initial state. In particular, note that the Watson's factor $\bar{N}^X_\gamma = 1/(1+iG^I_\gamma \hat{\bar{W}}^{\mu}_{\gamma\gamma}) \to 1$ in one-photon approximation. The superscript μ stands for the Lorentz index of the photon polarization.

[4] Note that, to preserve gauge invariance of the decomposed photoproducton amplitude into the pole and non-pole parts, we need to consider what to take for the non-pole driving potential $U^{\mu}(\equiv V^{NP\,\mu})$ and for the bare photon coupling $\langle F^{\mu}_{0r}|$. They enter in the definition of W^{μ} and $\langle F^{\mu}_{Kr}|$ in Eqs. (2.71,2.73), respectively. For example, in the field theoretic approach of Appendix B, the bare coupling $\langle F^{\mu}_{0r}|$ gets renormalized as given by Eq. (B.17). And the driving potential U^{μ} contains additional terms compared to the usual u- and t-channel Feynman diagrams (cf. Eq. (B.20)). These observations should be kept in mind when constructing (gauge-invariant) photoproduction amplitude in the present approach.

The quantity $\hat{W}^{\mu}_{\alpha'\gamma}$ in Eq. (2.69) follows from Eq. (2.54). Explicitly, we have

$$\hat{W}^{\mu}_{\alpha'\gamma} \equiv W^{\mu}_{\alpha'\gamma} - i \sum_{\beta,\beta' \neq \alpha'} W_{\alpha'\beta'} \left(\left(D^X \right)^{-1} \right)_{\beta'\beta} G^I_{\beta} W^{\mu}_{\beta\gamma} \ . \tag{2.70}$$

where, from Eq. (2.51),

$$W^{\mu}_{\alpha'\gamma} = U^{\mu}_{\alpha'\gamma} + \sum_{\beta} W_{\alpha'\beta} G^R_{\beta} U^{\mu}_{\beta\gamma} \ . \tag{2.71}$$

Note that the summations over the channels in the above two equations, and all the subsequent equations in this section, exclude the photon-baryon channel in the intermediate states, i.e., $\beta, \beta' \neq \gamma$ due to the one-photon approximation. This is to be understood for the remainder of this paper.

The dressed photon vertex $\langle \hat{F}^{\mu}_{Kr}|_{\gamma}$ in Eq. (2.69) follows from Eq. (2.63):

$$\langle \hat{F}^{\mu}_{Kr}|_{\gamma} \equiv \langle F^{\mu}_{Kr}|_{\gamma} - i \sum_{\beta} \langle F_{Kr}|_{\beta} G^I_{\beta} \hat{\bar{W}}^{\mu}_{\beta\gamma} \ , \tag{2.72}$$

where, from Eq. (2.44),

$$\begin{aligned} \langle F^{\mu}_{Kr}|_{\gamma} &\equiv \langle F^{\mu}_{0r}|_{\gamma} + \sum_{\beta} \langle F_{0r}|_{\beta} G^R_{\beta} W^{\mu}_{\beta\gamma} \\ &= \langle F^{\mu}_{0r}|_{\gamma} + \sum_{\beta} \langle F_{Kr}|_{\beta} G^R_{\beta} U^{\mu}_{\beta\gamma} \ , \end{aligned} \tag{2.73}$$

and, from Eq. (2.57),

$$\hat{\bar{W}}^{\mu}_{\alpha'\gamma} \equiv W^{\mu}_{\alpha'\gamma} - i \sum_{\beta,\beta'} W_{\alpha'\beta'} G^I_{\beta'} \left(\left(\bar{D}^X \right)^{-1} \right)_{\beta'\beta} W^{\mu}_{\beta\gamma} \ . \tag{2.74}$$

It is straightforward to show that Eq. (2.69) reduces (as it should) to Watson's theorem for photoproduction below the first inelastic threshold (137). To this end, we realize that the first term on the right-hand side of Eq. (2.69) is the pole part of the photoproduction amplitude given by Eq. (B.23) as shown in Appendix B. This equation, in turn, can be recast in terms of the pole and non-pole K-matrices (cf. Eq. (2.76)) as $M^{P\mu} = N^X K^{P\mu} - iT^P G^I (K^{P\mu} + W^{\mu})$ through the substitutions $G \to -iG^I$, $V^{P\mu} \to K^{P\mu}$ and $V^{NP\mu} \to K^{NP\mu}$ ($\equiv W^{\mu}$). Then,

below the first inelastic threshold, we have

$$
\begin{aligned}
M^{\mu}_{\alpha'\gamma} &= \sum_{r'r} \left\{ N^X_{\alpha'} |F_{Kr'}\rangle_{\alpha'} \left(\frac{1}{(E-m_0)I - \Sigma_K + i\langle F_K|_{\alpha'} G^I_{\alpha'} N^X_{\alpha'} |F_K\rangle_{\alpha'}} \right)_{r'r} \langle \hat{F}^{\mu}_{Kr}|_{\gamma} \right\} + N^X_{\alpha'} W^{\mu}_{\alpha'\gamma} \\
&= N^X_{\alpha'} K^{P\,\mu}_{\alpha'\gamma} - i T^P_{\alpha'\alpha'} G^I_{\alpha'} \left(K^{P\,\mu}_{\alpha'\gamma} + W^{\mu}_{\alpha'\gamma} \right) + N^X_{\alpha'} W^{\mu}_{\alpha'\gamma} \\
&= \left(N^X_{\alpha'} - i T^P_{\alpha'\alpha'} G^I_{\alpha'} \right) \left(K^{P\,\mu}_{\alpha'\gamma} + W^{\mu}_{\alpha'\gamma} \right) = \left(1 - i T_{\alpha'\alpha'} G^I_{\alpha'} \right) K^{\mu}_{\alpha'\gamma} = N_{\alpha'} K^{\mu}_{\alpha'\gamma} \\
&= e^{\delta_{\alpha'}} \cos\delta_{\alpha'} K^{\mu}_{\alpha'\gamma} \ , \qquad (2.75)
\end{aligned}
$$

where we have also made use of Eqs. (2.70,2.72) and of Eq. (2.41) for photoproduction, i.e.,

$$K^{\mu}_{\alpha'\gamma} = K^{P\,\mu}_{\alpha'\gamma} + W^{\mu}_{\alpha'\gamma} \qquad (2.76)$$

with $W^{\mu}_{\alpha'\gamma}$ given by Eq. (2.71) and

$$K^{P\,\mu}_{\alpha'\gamma} = \sum_{r'r} |F_{Kr'}\rangle_{\alpha'} S_{Kr'r} \langle F^{\mu}_{Kr}|_{\gamma} \ . \qquad (2.77)$$

Recall that $K^{\mu}_{\alpha'\gamma}$ is Hermitian if the driving term $V^{\mu}_{\alpha'\gamma}$ in Eq. (2.41) is.

Equation (2.69) is the main result of this section. Together with Eq. (2.66) of the previous section, they may be used as the starting points in the construction of unitary isobar models. This is done in the following sections.

Before leaving this section, a remark is in order. It is straightforward to show that if we use the form of the non-pole T-matrix given by Eq. (2.53) for photoproduction,

$$X^{\mu}_{\alpha'\gamma} = N^X_{\alpha'} \hat{W}^{\mu}_{\alpha'\gamma} \ , \qquad (2.78)$$

instead of that given by Eq. (2.56), the full dressed photoproduction vertex $\langle F^{\mu}_r|_{\gamma}$ can be expressed in the form (cf. Eq. (2.48))

$$
\begin{aligned}
\langle F^{\mu}_r|_{\gamma} &\equiv \langle F^{\mu}_{Kr}|_{\gamma} - i \sum_{\beta} \langle F_{Kr}|_{\beta} G^I_{\beta} X^{\mu}_{\beta\gamma} \\
&= \langle F^{\mu}_{Kr}|_{\gamma} - i \sum_{\beta} \langle F_{Kr}|_{\beta} G^I_{\beta} N^X_{\beta} \hat{W}^{\mu}_{\beta\gamma} \ , \qquad (2.79)
\end{aligned}
$$

instead of that form given by Eq. (2.62). Thus, one can replace the photon vertex $\langle F_r^\mu|_\gamma = \langle \hat{F}_{Kr}^\mu|_\gamma N_\gamma^X = \langle \hat{F}_{Kr}^\mu|_\gamma$ appearing in Eq. (2.69) by the form given in the above equation. Which of the two forms to use depends on what one wants to do. In the full calculation, where the channel couplings are fully taken into account, the form given by Eq. (2.79) would be preferable numerically, for it involves $\hat{W}_{\beta\gamma}^\mu$ which requires the matrix inversion of the same D^X that enters in the calculation of the final state hadronic interaction part. In contrast, $\langle F_r^\mu|_\gamma = \langle \hat{F}_{Kr}^\mu|_\gamma$ involves $\hat{\bar{W}}_{\beta\gamma}^\mu$ that requires an independent matrix inversion of $\bar{D}^X$ from that for the final hadronic interaction. In an approximate calculation, however, as discussed in the following sections, the form $\langle F_r^\mu|_\gamma = \langle \hat{F}_{Kr}^\mu|_\gamma$ may be more suitable.

2.6 Possible approximations

The basic result of Sec. 2.4 given by Eq. (2.66) and of Sec. 2.5 given by Eq. (2.69) provide a convenient starting point for possible approximations one can make with different levels of sophistications. In Eq. (2.66), the three basic ingredients for possible approximations are the non-pole K-matrix amplitude $W(\equiv K^{NP})$ as given by the integral equation (2.51), the dressed K-matrix resonance vertex $|F_{Kr'}\rangle$ ($\langle F_{Kr}|$) given by Eq. (2.44) and the K-matrix self-energy $\Sigma_{Kr'r}$ given by Eq. (2.46). These involve an integration over the loop momentum through the real part of the meson-baryon propagator G_β^R. Note that all the ingredients, the Watson's factor N^X, the dressed K-matrix vertex as well as the K-matrix self-energy, entering in Eq. (2.66) are expressed in terms of W. W enters the K-matrix self-energy through the dressed K-matrix vertex. The different approximations one makes on the basic three ingredients just mentioned may be classified into few broad categories:

a) *Unitary and Analytic Isobar Model* (UAIM) : In this approach, the driving non-pole term U in Eq. (2.51) is approximated by a phenomenological separable potential (see, e.g., Ref. (94)) whose form allows to solve the integral equation for W in Eq. (2.51) analytically. The bare vertex $|F_{0r'}\rangle$($\langle F_{0r}|$) is obtained either from a microscopic Lagrangian or simply parametrized phenomenologically. Then, the momentum-loop integration in

Eq. (2.44) is carried out analytically to obtain $|F_{Kr'}\rangle(\langle F_{Kr}|)$. $\Sigma_{Kr'r}$ is obtained as given by Eq. (2.46), also by performing the momentum loop integration analytically. This model maintains unitarity and analyticity; the latter, by keeping explicitly both the real and imaginary parts of the meson-baryon propagator. Of course, the adopted separable potential should be analytic. Note that the contribution due to the real part of the meson-baryon propagator may lead to pole structures in the resulting reaction amplitude in the complex-energy plane that would correspond to dynamically generated resonances (70; 100; 28).

b) *Unitary Isobar Model* (UIM) : Here, W and $|F_{Kr'}\rangle(\langle F_{Kr}|)$ are directly parametrized in a completely phenomenological or semi-phenomenological manner, thereby avoiding to solve the integral equation for W and the momentum-loop integration for $|F_{Kr'}\rangle(\langle F_{Kr}|)$. Here, the self-energy $\Sigma_{Kr'r}$ (cf. Eq. (2.46)) is also simply parametrized. In this model, the analyticity of the original reaction amplitude is lost, because the momentum-loop integrations involving the real part of the meson-baryon propagator in Eqs. (2.44,2.46,2.51) are not performed. In general, ignoring the contributions arising from the real part of the meson-baryon propagator violates analyticity, since the dispersion relation condition due to analyticity between the real and imaginary parts of the reaction amplitude (119) will no longer be satisfied.

2.7 Summary

We have exposed the full complex phase structure of the meson-baryon T-matrix reaction amplitude in the coupled channels framework. By exhibiting the complex phase structure of the pole and non-pole parts of the T-matrix, we have achieved to express the reaction amplitude in a form which suitably serves as a starting point for making approximations of varying degrees of sophistication. In particular, it allows for approximations where the basic properties of the S-matrix, namely, unitarity and analyticity, can be maintained automatically. Recall that in earlier works (98; 43; 45; 131) unitarity of the reaction amplitude in isobar

models is implemented by imposing the unitarity condition on the resonance amplitude (pole amplitude T^P), separately from the unitarity condition on the background amplitude (non-pole amplitude $X(\equiv T^{NP})$). In the present work no such additional condition is required. Here, the unitarity of T^P arises automatically from the dressing mechanism inherent in the basic scattering equation (Eq. (2.7)). In the case of photoproduction, gauge invariance can be satisfied as well. Furthermore, we have shown how the analog in meson-baryon reaction of the well-known Watson's theorem in photoproduction emerges in the present formulation.

Finally, we mention that calculations based on a coupled channels unitary isobar model as described briefly in Sec. 2.6 will be reported shortly.

2.8 ACKNOWLEDGMENTS

The authors thank Helmut Haberzettl for sharing his private note on the resonance coupling propagator.

Chapter 3

Pion and photon-induced reactions

In recent years, the interest in studying photoproduction of vector mesons, such as ω, ρ, and ϕ, has been growing. The production of these vector mesons is particularly interesting since they carry the same quantum numbers, $J^{PC} = 1^{--}$, as the incoming photons and therefore, they are expected to play an important role in photoproduction. At very high energies, $E_\gamma > 20$ GeV, the photoporuction of vector mesons can be successfully described as a diffractive process; photons convert to vector meson, which then scatters off the proton by exchange of Pomerons (40; 41). Pomerons are virtual colorless objects that carry the same quantum numbers, $J^{PC} = 0^{++}$, as the vacuum. However, at intermediate energies, $E_\gamma < 5$ GeV, Pomeron exchange alone is no longer sufficient to describe the existing data for ω photoproduction, and the authors of Ref. (126) suggested that the exchange of π and f_2-meson become the dominant contribution. At energies below 3 GeV, N^* states strongly contribute to the production of ω.

The interest, in general, in heavier meson production is not only directed toward the non-strangeness sector, and an intense effort has been directed toward the search for hyperon resonances with strangeness quantum number $S = -1$ via $K\Lambda$ and $K\Sigma$ photoproduction. Furthermore, most known baryon states were discovered in elastic πN scattering (79). The heavier meson productions are of main interest due to the opportunity they provide to search for new baryon resonances that might have not been detected before because of their weak coupling to πN final state (12).

In this effort, we have studied 4 reaction channels, $\pi N \to \pi N$, $\pi N \to \eta N$, $\pi N \to \omega N$, and $\gamma N \to \omega N$, among which the production of ω-meson was of particular interest. Considering

the 782.6 MeV mass of ω, these reactions provide a means of probing the possible missing resonances in 2 GeV mass region, a region of resonance energy much less explored than at lower mass resonance region. Besides, being an iso-scalar meson, ω-meson production provides an "isospin filter", guaranteeing no Δ^* with $T = 3/2$ contribution, which simplifies the already complex task of resonance extraction. The available data for pion-induced ω production is sparse and of low precision, hence, the inclusion of high-statistics measurements for photon-induced ω production is highly valuable in this analysis.

The amplitude for ω photoproduction off the proton is represented by $2 \times 2 \times 2 \times 3 = 24$ complex numbers, 2 spin states of target nucleon, 2 spin states of the photon beam, 2 spin states of recoil nucleon, and 3 spin states of ω. By the virtue of parity conservation, out of these 24 complex amplitudes, only 12 complex amplitudes or 24 real numbers are independent. This means, in order to achieve a "complete experiment" (105) one needs 23 carefully chosen observables to be measured to fix the amplitude up to an overall arbitrary phase. This is a challenging task and many collaborations are working toward collecting as many of these observables as possible.

Earlier this year, first measurements of the double-polarization observables F, P, and H in ω photo-production were reported (115). Besides these newly measured observables, various collaborations reported cross section measurements (20; 139; 141; 127), spin-density matrix elements (SDMEs) (139; 141), the beam asymmetry Σ (114; 3; 77; 136; 33), double polarization observables E (49; 4) and G(49), and target asymmetry T (114) in this reaction.

Several attempts have been made to extract resonant contributions from ω photo-production in the past, but they produced conflicting results (39; 3; 140; 96; 145; 101; 145; 134; 103; 122; 146; 95; 117; 15; 148). Using a quark model approach with an effective Lagrangian developed in (148; 147), Zhao (145) found $N(1720)\frac{3}{2}^+$ and $N(1680)\frac{5}{2}^+$ have the dominant contribution. Oh et al. (96) used the quark model by Capstick and Roberts (31; 32) and reported that the dominant contributions are from a "missing" $N(1910)\frac{3}{2}^+$ state (i.e., a state predicted by the constituent quark model but not observed experimentally) and

a $N(2080)\frac{3}{2}^-$ state. Titov and Lee (134) showed the dominant resonant contribution comes from $N(1680)\frac{5}{2}^+$, while the next large contribution arises from $N(1520)\frac{3}{2}^-$, $N(1650)\frac{1}{2}^-$, and $N(1720)\frac{3}{2}^+$. In their calculation, they fixed the resonance couplings from the helicity amplitudes with vector meson dominance assumption. Meanwhile Denisenko et al. (39), within the the Bonn-Gatchina (BnGa) coupled channels partial-wave analysis, considered the contribution of 12 N^* states, along with their branching ratios, and determined the dominant contribution near threshold was found to be from P_{13} partial-wave, which was primarily identified with the sub-threshold $N(1720)\frac{3}{2}^+$ resonance. In (140), Williams et al., within a partial-wave model, described differential cross section and spin density matrix elements with a reasonable accuracy. They identified the dominant resonance states are $N(1680)\frac{5}{2}^+$ and $N(1700)\frac{3}{2}^-$ near threshold, as well as the $N(2190)\frac{7}{2}^-$ at higher energies. Analyzing only the cross-section data, the Giessen group (103) found the ωN photo-production is dominated by large $N(1710)\frac{1}{2}^+$ and $N(1900)\frac{3}{2}^+$ contributions. In a later analysis, with the inclusion of the low-precision polarization data from SAPHIR, they found a strong contribution from the $N(1675)\frac{5}{2}^-$ and $N(1680)\frac{5}{2}^+$, while the effects of $N(1520)\frac{3}{2}^-$ and $N(1950)\frac{3}{2}^-$ states were of minor importance. Within the frame work of constituent quark model approach, the numerical calculation done by Zhao et al. (147; 148) showed that the resonance coupling of $N(2000)\frac{5}{2}^+$ was larger than other resonances.

Most of these analyses only included cross section data and some of the older polarization data with limited precision. Incorporating the new high precision polarization data in the analysis imposes more stringent constraints on the model used, in particular, on the resonance content. In this work, we included, in our analysis, all the cross section and polarization data currently available.

This chapter is organized as follows. We present in Sec. 3.1 a brief description of the unitary isobar model used in this work. In Sec. 3.2 the details of the database and fitting techniques, together with the description of the observables achieved in the various reaction channels is presented. In particular, we discuss the dominant contribution from partial-wave

and resonance contributions in each reaction channel considered. Some technical details are presented in appendices D and E.

3.1 Unitary Isobar Model

We construct our unitarized effective isobar model based on the results obtained in the previous chapter. Our starting pint is the final form of the T-matrix amplitude, Eq. (2.66), derived in previous chapter

$$\begin{aligned} T_{\alpha'\alpha} &= T^P_{\alpha'\alpha} + X_{\alpha'\alpha} \\ &= \sum_{r'r} \left\{ N^X_{\alpha'} |\hat{F}_K\rangle_{\alpha',r'} \left(\frac{1}{(E-m_0)I - \Sigma_K + i\sum_\beta \langle F_K|_\beta G^I_\beta N^X_\beta |\hat{F}_K\rangle_\beta} \right)_{r'r} \langle \hat{F}_K|_{\alpha,r} \bar{N}^X_\alpha \right\} + N^X_{\alpha'} \hat{W}_{\alpha'\alpha} \ . \end{aligned}$$

Time reversal invariance in conjunction with hermiticity implies that the driving potential U and consequently W should be be either pure real or pure imaginary. We start by parametrizing W in Eq. (2.42) as a separable function of the modulus of the outgoing, $q'_{\alpha'} \equiv |\vec{q'}_{\alpha'}|$, and incoming, $q_\alpha \equiv |\vec{q}_\alpha|$, meson-baryon three-momenta.

$$W_{\alpha'\alpha}(q'_{\alpha'}, q_\alpha) = \bar{h}_{\alpha'}(q'_{\alpha'}) h_\alpha(q_\alpha) \ , \tag{3.1}$$

where h is appropriately chosen to be a polynomial with respect to q_α

$$\begin{aligned} \bar{h}_{\alpha'}(q'_{\alpha'}) &= \Gamma_{\alpha'} \sum_{j=j_{min}}^{j_{max}} \bar{a}_{j\,\alpha'} \left(\frac{q'_{\alpha'}}{\Lambda} \right)^{(L_{\alpha'}+j)} e^{-\lambda_{j\,\alpha'} \left(\frac{q'_{\alpha'}}{\Lambda} \right)^2} \ , \\ h_\alpha(q_\alpha) &= \Gamma_\alpha \sum_{j=j_{min}}^{j_{max}} a_{j\,\alpha} \left(\frac{q_\alpha}{\Lambda} \right)^{(L_\alpha+j)} e^{-\lambda_{j\,\alpha} \left(\frac{q_\alpha}{\Lambda} \right)^2} \ , \end{aligned} \tag{3.2}$$

where $\Gamma_{\alpha'}$ (Γ_α) is equal to i ($-i$) when the α' (α) channel has even parity, and is equal to 1 when the parity of channel α' (α) is even. The overall sign of $\Gamma_{\alpha'} \times \Gamma_\alpha$, for $\alpha = \alpha'$, is chosen by the fit to experimental data. $a_{j\,\alpha}$ ($\bar{a}_{j\,\alpha'}$) and $\lambda_{j\,\alpha}$ are real constant fit parameters and Λ is a hadronic scale parameter which may be chosen to be $\Lambda \sim 1$ GeV.

Second, the dressed resonance vertex $|F_K\rangle_r (\langle F_K|_r)$ is parametrized as a pure real or pure imaginary function of the relative meson-baryon momentum involved at that vertex.

Explicitly,

$$|F_K(q'_{\alpha'})\rangle_{\alpha' r'} = \Gamma_{\alpha'}\ \bar{g}_{\alpha' r'}\ \left(\frac{q'_{\alpha'}}{\Lambda}\right)^{L'_\alpha}\ F_{\alpha' r'}(p_r^2)\ ,$$
$$\langle F_K(q_\alpha)|_{\alpha r} = \Gamma_\alpha\ g_{\alpha r}\ \left(\frac{q_\alpha}{\Lambda}\right)^{L_\alpha}\ F_{\alpha r}(p_r^2)\ , \tag{3.3}$$

with $\bar{g}_{\alpha' r'}$, $g_{\alpha r}$, and $F_{\alpha r}(p_r^2)$ denoting the coupling constants and off-shell form factor, respectively. They are to be adjusted to fit the data. p_r^2 stands for the four-momentum squared of the off-shell baryon r at the three-point vertex. q_α stands for the meson-nucleon relative (three-) momentum in the channel α and L_α, the corresponding relative orbital angular momentum. The off-shell form factor in the above equation is, in turn, parametrized as

$$F_{\alpha r}(p_r^2) = \left(\frac{n\Lambda_{\alpha r}^4}{n\Lambda_{\alpha r}^4 + (p_r^2 - m_{0r}^2)^2}\right)^n\ . \tag{3.4}$$

As mentioned in Sec. 2.3, the momentum integration involving the imaginary part of the meson-baryon propagator G_β^I for stable particles (cf. Eq. (2.9)) can be carried out trivially such that

$$G_\beta^I = \pi\delta(E - H_{0\,\beta})$$
$$\rightarrow \rho_\beta = \pi q_\beta \frac{\varepsilon_\beta \omega_\beta}{\varepsilon_\beta + \omega_\beta}\Theta(E - m_{B_\beta} - m_{M_\beta})\ , \tag{3.5}$$

with $\varepsilon_\beta \equiv \sqrt{q_\beta^2 + m_{B_\beta}^2}$ and $\omega_\beta \equiv \sqrt{q_\beta^2 + m_{M_\beta}^2}$ denoting the on-shell energies of the the baryon and meson, respectively, in the channel β. m_{B_β} (m_{M_β}) stands for the mass of the baryon B_β (meson M_β), specified by the channel index β. q_β is the on-shell relative momentum of the particles determined by $E = \varepsilon_\beta + \omega_\beta$. The last factor, $\Theta(E - m_{B_\beta} - m_{M_\beta})$, is a step function ($\Theta(x) = 0$ if $x \leq 0$ and 1, if $x > 0$) indicating that below the β channel threshold, ρ_β vanishes identically.

Note that the 'collapse' of the momentum integration involving G_β^I for stable particles in channel β, turns the T-matrix equation in Eq. (2.66) into an algebraic equation with respect to momentum variables. This is, however, not the case for G_β^I associated with the unstable particle channels (cf. Eq. (2.10)), where the momentum integration is present. The

meson-baryon propagator G_β for these channels are more involved (81), (47). In the present application, to reduce computational complexity, we will make an additional approximation to reduce the integral equations involving unstable channel propagators to algebraic ones. To achieve this, we start with equations involving the momentum integration of G^I_β for an unstable channel β.

$$I_{\alpha'\beta\alpha}(p'_{\alpha'}, p_\alpha) \equiv \int_0^\infty p''^2 dp''\ O^{(1)}_{\alpha'\beta}(p'_{\alpha'}, p'')\ G^I_\beta(E, p'')\ O^{(2)}_{\beta\alpha}(p'', p_\alpha)\ .$$

Here $O^{(1)}$ and $O^{(2)}$ stand for any of the quantities that multiply G^I from the left and from the right and are under the momentum integral. We approximate this integral with

$$I_{\alpha'\beta\alpha}(p'_{\alpha'}, p_\alpha) \to \mathcal{O}^{(2)}_{\alpha'\beta}(p'_{\alpha'}, p_\beta)\ \mathcal{G}^I_\beta(E)\ \mathcal{O}^{(1)}_{\beta\alpha}(p_\beta, p_\alpha)\ , \tag{3.6}$$

where

$$\begin{aligned}
\mathcal{G}^I_\beta(E) &\equiv \int_0^\infty p''^2 dp''\ f_\beta(p'') G^I_\beta(E, p'') f_\beta(p'')\ , \\
\mathcal{O}^{(2)}_{\alpha'\beta}(p'_{\alpha'}, p_\beta) &\equiv O^{(2)}_{\alpha'\beta}(p'_{\alpha'}, p_\beta) f^{-1}_\beta(p_\beta)\ , \\
\mathcal{O}^{(1)}_{\beta\alpha}(p_\beta, p_\alpha) &\equiv f^{-1}_\beta(p_\beta) O^{(1)}_{\beta\alpha}(p_\beta, p_\alpha)\ ,
\end{aligned} \tag{3.7}$$

with

$$f_\beta(p_\beta) \equiv (p_\beta)^{L_\beta}\, e^{-\bar{\lambda}_\beta \left(\frac{p_\beta}{\Lambda}\right)^2}\ . \tag{3.8}$$

The parameter $\bar{\lambda}_\beta$ in the above equation is chosen to be some averaged value of $\lambda_{j\,\beta}$ appearing in Eq. (3.2). p_β stands for the on-shell meson-baryon relative momentum in the channel β.

With the approximation given by Eq. (3.6), Eq. (2.66) becomes an algebraic equation in momentum space even when unstable particle channels are present. Together with the parametrizations of the non-pole part and dressed resonance vertex (cf. Eqs. (3.9,3.2,3.3,3.4)), it defines our UIM. Of course, Eq. (2.66) is still a matrix equation in meson-baryon channel space.

Analogously, for the photoproduction amplitude, we parametrize $W^\mu_{\alpha'\gamma}$ appearing in Eq. (2.71) as follows

$$W^{\mu}_{\alpha'\gamma}(q'_{\alpha'}, q_\gamma) = \bar{h}_{\alpha'}(q'_{\alpha'}) h^{\mu}_{\gamma}(q_\gamma) \ , \tag{3.9}$$

where $\bar{h}$ is parameterized exactly as in Eq. (3.2) while h^μ is chosen to be a polynomial with respect to c.m. energy $E = \sqrt{q_\gamma^2 + m_N^2} + q_\gamma$

$$h^{\mu}_{\gamma}(E) = \Gamma_\gamma \sum_j g^{\mu}_j \left(\frac{E - E_s}{m_N} \right)^{L_\gamma + j} e^{-\lambda_\gamma (E - E_s)} \ , \tag{3.10}$$

where g^μ_j and λ_γ are fit parameters, with E_s being a suitable expansion point equal to the hadronic channel threshold, e.g. $E_s = m_N + m_\omega$ in the case of ω photo-production. Respectively the dressed photon vertex $\langle F^\mu_{Kr}|_\gamma$ in Eq. (2.73) is parametrized as follows

$$\langle F^{\mu}_{Kr}(E)|_\gamma = \Gamma_\gamma \ g^{\mu}_r \left(\frac{E - E_s}{m_N} \right)^{L_\gamma} e^{-\lambda_\gamma (E - E_s)} \ , \tag{3.11}$$

where $g_{\mu\, r}$ and λ_μ are fit parameters.

3.2 Results

3.2.1 Database and fit parameters

In this analysis, we consider 4 reaction channels, $\pi N \to \pi N$, $\pi N \to \eta N$, $\pi N \to \omega N$, and $\gamma N \to \omega N$. The results of our fit together with the included experimental data are displayed in figures 3.1 to 3.14(a). Some of the data sets that differ by only a few MeV in C.M. energy are depicted in the same panel.

To extract resonance masses and widths, we determined the values of our UIM's free parameters, coupling constants a_α and g_α in Eqs. (3.9, 3.2, 3.3, 3.4, 3.8, 3.10, 3.11) and the effective resonance masses, $M_R \equiv m_0 I - \Sigma_K$ in Eqs. (2.66), by optimizing χ^2 using MINUIT on UGA Linux High Performance Computing (HPC) cluster called Sapelo2. Since the fitting procedure is not very sensitive to the exact values of the cut off parameters in Eqs. (3.3, 3.8, 3.10, 3.11) as long as they are set to a reasonable value; as such, we set the cut of parameters to 1 for all channels except for πN which is set to 1.5. We started our fitting procedure by fitting the coupling constants to SAID partial-wave solution (143) for πN elastic scattering.

Starting the fit by finding the coupling constants to reproduce SAID partial-waves guarantee a good initial value for those couplings since each partial-wave can be fitted independently while capturing the dynamics of $\pi N \to \pi N$ reaction. We then included 3 inelastic reactions $\pi N \to \eta N$, $\pi N \to \omega N$, and $\gamma N \to \omega N$ at a later stage.

The combined study of these reactions provide us with a means to probe the resonance states in the 2 GeV mass region, referred to as the third resonance region. The inclusion of ω-meson photoproduction is of particular importance in probing the possible missing states in the third resonance region which may couple to ωN channel and not to πN channel. Besides the πN, ηN, ωN, and γN channels that are constrained by experimental data, we also included σN, ρN, and $\pi\Delta$ channels which effectively account for the $\pi\pi N$ intermediate state.

3.2.2 Reactions

3.2.3 $\pi N \to \pi N$

We included the energy dependent partial-wave WI08 solution of SAID group (143) as an input in our calculation. We considered partial waves up to H wave both for isospin 1/2 and 3/2. The results of our calculation for the partial-waves are displayed in Figs. 3.1 and 3.2. The points displayed in these figures, however, show the single energy (energy independent) solutions of Ref. (143).

The resonances required in our calculation to fit the partial-waves S_{11} to F_{15} matched those reported in GWU/SAID SP06 solution (12) plus one extra D_{13} state, $N(1700)\frac{3}{2}^-$, which was mainly added to the our analysis to describe other reactions. However this was not the case for higher partial-waves, F_{17} to H_{19}. We could describe the WI08 solution (143) with a good agreement without the need to include any resonances explicitly for those partial-waves. We have tabulated all these resonances and their respective mass and total width in Table 3.1.

N Baryons	Status	Mass	Γ_{tot}	Δ Baryons	Status	Mass	Γ_{tot}
$N(1535)\frac{1}{2}^-$	****	1539 ± 1	135 ± 5	$\Delta(1620)\frac{1}{2}^-$	****	1608 ± 2	140 ± 5
$N(1650)\frac{1}{2}^-$	****	1693 ± 3	99 ± 8	$\Delta(1232)\frac{3}{2}^+$	****	1229 ± 3	99 ± 8
$N(1440)\frac{1}{2}^+$	****	1446 ± 5	183 ± 3	$\Delta(1905)\frac{5}{2}^+$	****	1907 ± 1	169 ± 8
$N(1720)\frac{3}{2}^+$	****	1704 ± 8	320 ± 17	$\Delta(1950)\frac{7}{2}^+$	****	1950 ± 1	170 ± 7
$N(1520)\frac{3}{2}^-$	****	1508 ± 2	104 ± 7				
$N(1700)\frac{3}{2}^-$	***	1720 ± 3	259 ± 6				
$N(1675)\frac{5}{2}^-$	****	1669 ± 2	151 ± 11				
$N(1680)\frac{5}{2}^+$	****	1684 ± 6	109 ± 4				

Table 3.1: List of isospin $T = 1/2$ and $T = 3/2$ resonances and their extracted masses and widths.

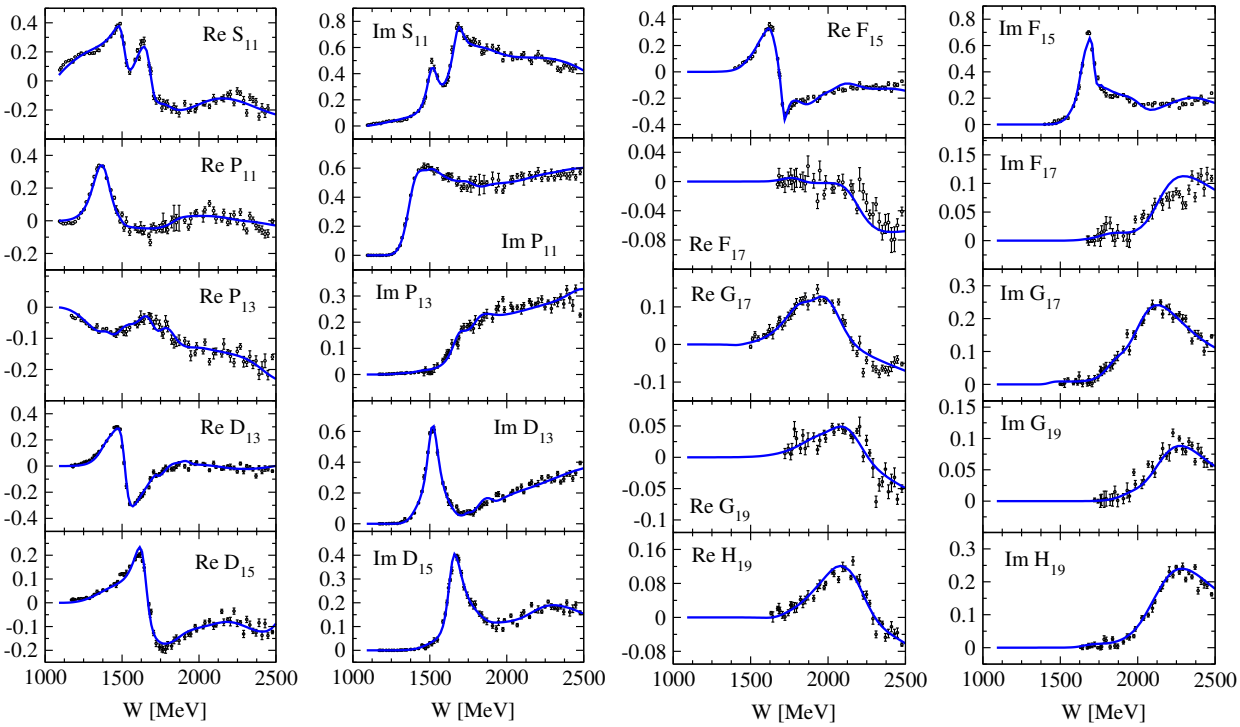

Figure 3.1: Reaction $\pi N \to \pi N$ isospin, $T = 1/2$, $S-$ to $H-$ waves. points: GWU/SAID partial-wave analysis (single-energy solution) from Ref (143).

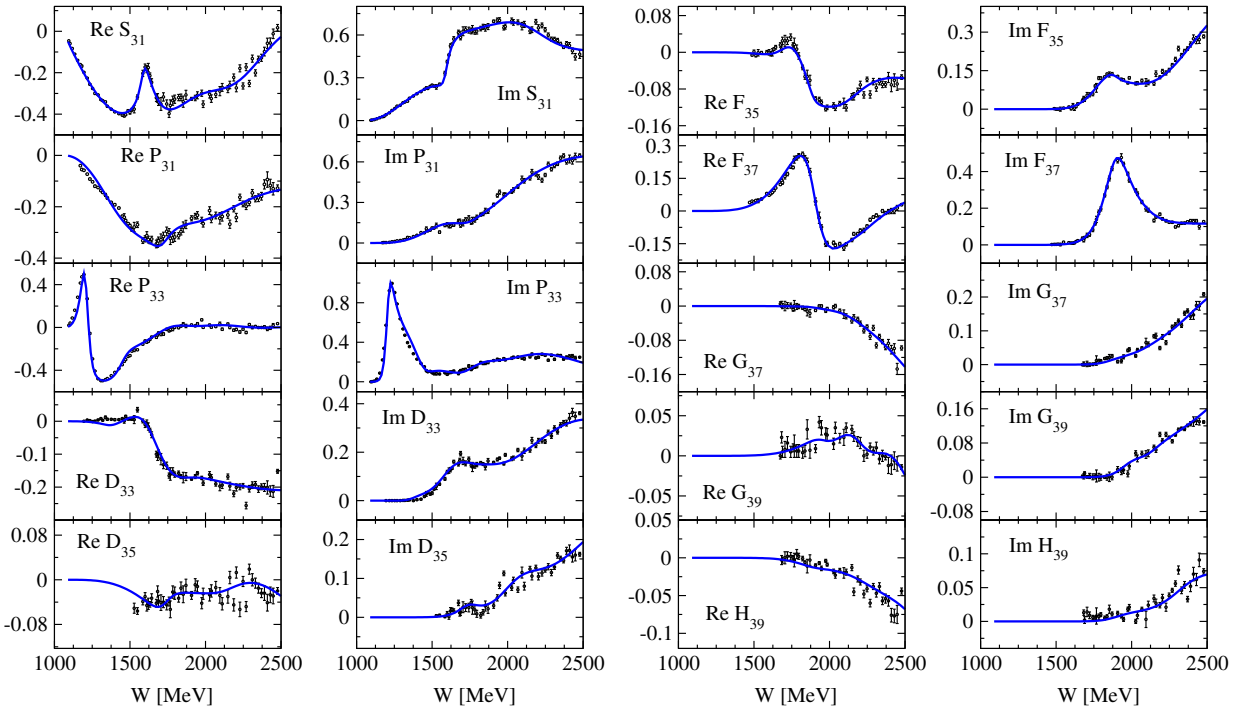

Figure 3.2: Reaction $\pi N \to \pi N$, isospin $T = 3/2$, $S-$ to $H-$ waves. points: GWU/SAID partial-wave analysis (single-energy solution) from Ref (143).

For isospin $T = 3/2$ waves, our model required only the inclusion of 4, 4 star, resonances; a list of which is tabulated in Table 3.1.

We should point out that in describing the second S_{11} resonance peak at $w = 1650$ MeV, our model shifted the mass of $N(1650)\frac{1}{2}^-$ to a much higher value of 1693 MeV and a width of 99 MeV. Despite this higher mass our results, qualitatively, are in very good agreement with the SAID single energy solution as it can be seen in Fig. 3.1.

3.2.4 $\pi N \to \eta N$

The experimental data for $\pi N \to \eta N$ reaction was mostly measured between 1960s and 1980s. These observables exhibit many inconsistencies among each other, as such, Clajus et al. (128) scrutinized these inconsistencies and published their detailed analysis of different experiments and the quality of the corresponding data. GWU/SAID group (11) and (125)

also provided their ηN data selection analysis. Rönchen et al. (111) have done a detailed analysis of all the available data and provided their systematical error assignment to different experimental data which in this work we took advantage of. It is worth mentioning that the differential cross section data from Brown et al. (27) is highly questionable at low energies but at higher energies the data can be used if the beam momenta are lowered by 4% and an additional 10% systematic error is added to data as mentioned in (111). In general due the inconsistencies and unreliability of differential cross section data for $\pi N \to \eta N$ reaction, this data was entered our fit with a very low weight. For total cross section we included the data that GWU/SAID analysis (11; 12) deemed reliable. Note that we did not include the total cross section data in our fitting process.

The differential cross section results from our calculation alongside the experiential data are shown in Fig. 3.3. As it can be seen the overall agreement between our calculation and the experimental data is good.

The total cross section prediction from our calculation is shown in Fig. 3.4(a). In order to display the influence of each partial-wave we have included a partial-wave decomposition of total cross section in Fig. 3.4(b). As it can be seen the first peak in total cross section is mostly due to S_{11} contribution, specifically $N(1535)\frac{1}{2}^-$, to this reaction. Meanwhile, $N(1680)\frac{5}{2}^+$ is responsible for the second peak measured in total cross section. Besides the dominant contribution from $N(1535)\frac{1}{2}^-$ and $N(1680)\frac{5}{2}^+$, we have also noticed a minor contribution from $N(1440)\frac{1}{2}^+$, $N(1650)\frac{1}{2}^-$, and $N(1700)\frac{3}{2}^-$ states.

3.2.5 $\pi N \to \omega N$

In a series of bubble and drift chamber experiments (26; 76; 75) the cross section of the $\pi N \to \omega N$ reaction was measured. Over the years these data resisted a consistent theoretical description which were mainly caused by too large Born contributions (78). Consequently these diagrams were either suppressed by very soft formfactors (133) or completely neglected (107; 86). Due to these findings, a discussion was motivated in the literature over the methods

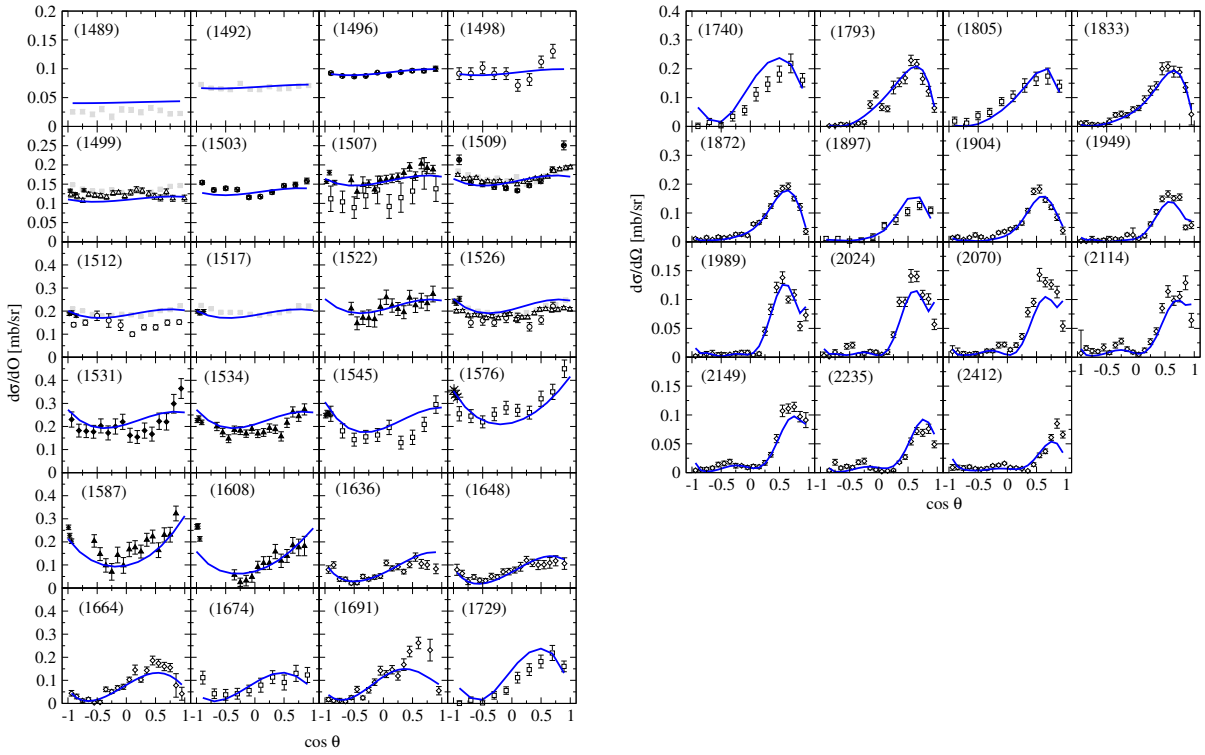

Figure 3.3: Differential cross section for the reaction $\pi N \to \eta N$. Data: filled squares from Ref. (108); filled circles from Ref. (24); empty circles from Ref. (93); empty triangles up from Ref. (80); stars from Ref. (37); filled triangles up from Ref. (38); empty squares from Ref. (109); filled diamonds from Ref. (54); empty diamonds from Ref. (27).

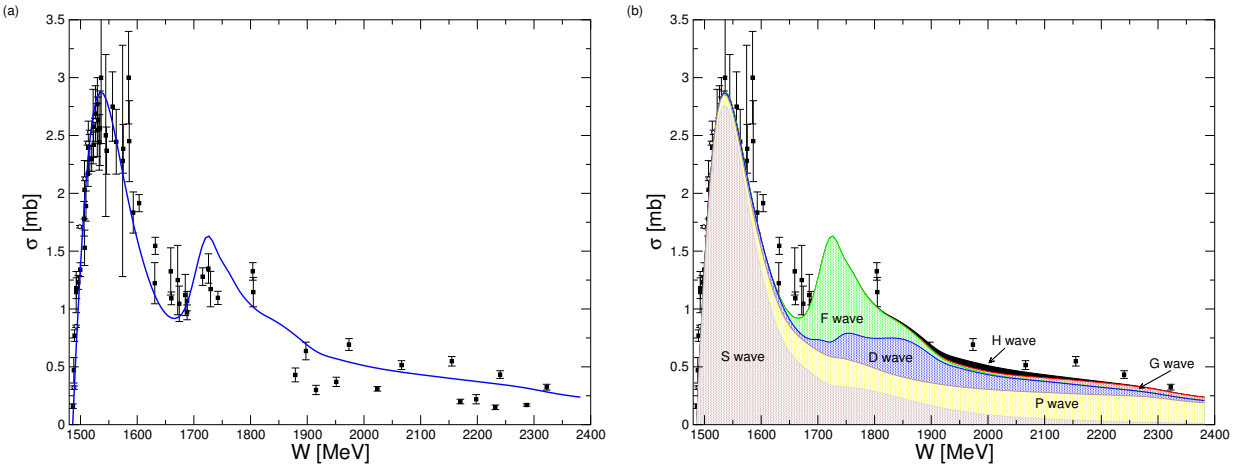

Figure 3.4: Total cross section and partial-wave decomposition of total cross section for the reaction $\pi N \to \eta N$. Data: filled squares indicate experiments accepted by the GWU/SAID group (13); empty circles from Ref. (108).

used by the experimentalists to extract the two-body cross section (63) and readjustment of the published $\pi^- p \to \omega n$ cross section data were performed (124; 133).

The experimentalists used an unusual method to cover the full range of the ω spectral function (102; 64). Conventionally, to insure that all pion triples with invariant masses around m_ω are taken into account to successfully cover the ω spectral function with a width of 8 MeV, one needs to perform an integration over at least one kinematical variable. The authors of (26; 76; 75) fixed the outgoing neutron laboratory momentum and angle and integrated over the incoming pion momentum, instead of fixing the incoming pion momentum and integrating out the invariant mass of the pion triples directly. Despite these controversies over the validity of the experimental data, here we assumed the experimental data is correct as it was originally published but we entered these data with a lower weight in our analysis.

Due to the lack of any differential cross section data above 2.0 GeV, we included the total cross section data for this reaction as well as the available differential cross section data at lower energies in our fit. The results of our calculation for the differential cross section and total cross section are presented in figures 3.5 and 3.6(a) respectively.

At and near the threshold, two resonances $N(1680)\frac{5}{2}^+$ and $N(1700)\frac{3}{2}^-$ play the most important role in describing the hadronic production of ω meson; their role can be seen in the dominance of F and D waves, respectively, in the partial-wave decomposition of total cross section shown in figure 3.6(b). $N(1440)\frac{1}{2}^+$ and $N(1520)\frac{3}{2}^-$ also play a minor role in this reaction as well. The photoproduction of ω is dominated by$N(1520)\frac{3}{2}^-$ and $N(1700)\frac{3}{2}^-$ and, even though, these two states play an important role in $\pi N \to \omega N$ their significance in this reaction is subdued.

3.2.6 $\gamma N \to \omega N$

Different groups (SAPHIR, CLAS, A2 and CBELSA/TAPS) have reported differential cross section and single and double spin polarization experimental data for $\gamma p \to \omega p$ reaction. Although these data sets have been measured with high precision, some of the measured

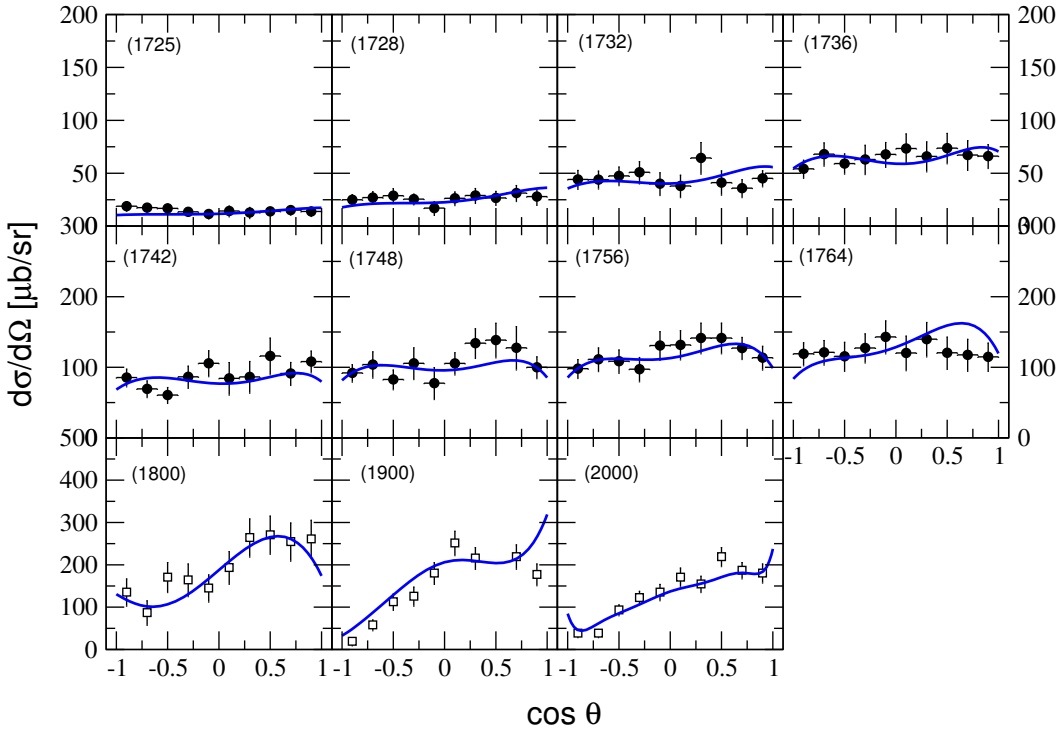

Figure 3.5: Differential cross section for the reaction $\pi N \to \omega N$. Data from Refs. (75; 76; 36).

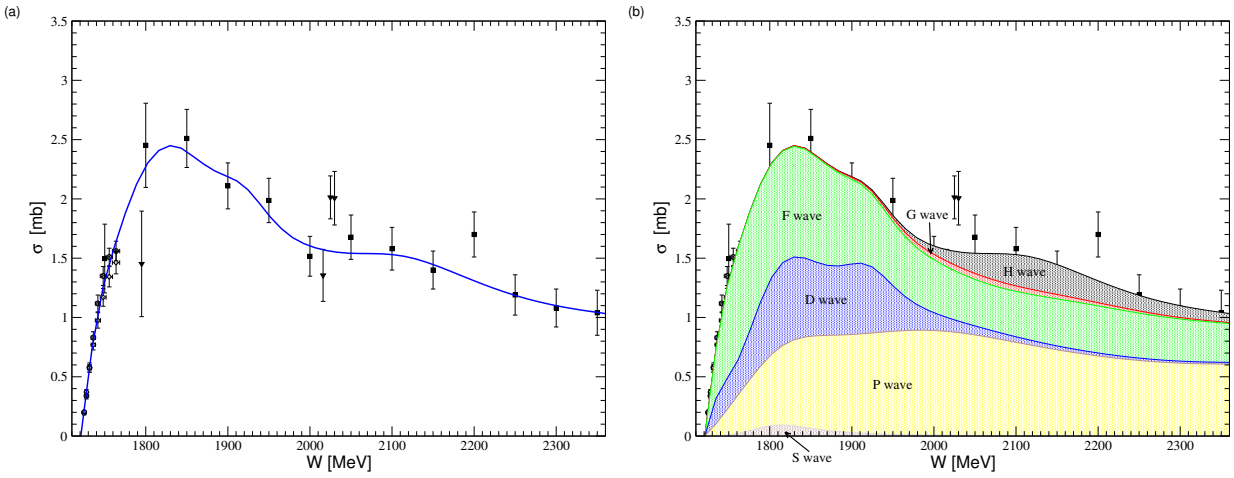

Figure 3.6: Total cross section and partial-wave decomposition of total cross section for the reaction $\pi N \to \omega N$. Data: triangles down from Ref. (65), squares from Ref. (36), and circles from Ref. (75).

observables by different groups show inconsistencies. The cross section data from SAPHIR, CLAS, and A2 collaborations are in good agreement with each other overall, but near the threshold there are some noticeable inconsistencies. Despite a considerable effort to find the source of these inconsistencies, in particular, between the CBELSA/TAPS and CLAS Collaborations, no clear reason for the nature of these inconsistencies have been found (141). Ideally, we should prune the data using statistical methods, but since at the moment a full statistical analysis of the data is not feasible, we chose to include CLAS data, differential cross section, SDMEs data, Σ, T, E, and recently reported P, F, and H in our analysis as the input. Due to the sparse differential cross section data near forward and backward angles specially at energies near the threshold, we also included A2 total cross section data to further constrain our fit parameters at energies close to the threshold.

Considering the inconsistencies between the A2 and CLAS data near the threshold and the contribution from many resonances, we could not achieve an accurate agreement between our calculation and the data at energies near the threshold. The differential cross section measurements from A2 are systematically smaller than those of CLAS from the threshold up to 1820 MeV. This meant our model, besides a significant contribution from D_{13} wave, required a stronger S-wave to describe the CLAS data. The effect of this S-wave contribution, caused by the $N(1535)\frac{1}{2}^-$ resonance, opening was also seen in ηN cross section results. We have considered the contribution from other resonances such as $N(1710)\frac{1}{2}^+$, $N(1875)\frac{3}{2}^-$, $N(1895)\frac{1}{2}^-$, and $N(1900)\frac{3}{2}^+$ but they didn't help much to provide the required enhancement in question. We have also considered the effects of ω meson width via a folding mechanism and, also, the effect of energy bin spans reported by experimentalists by an averaging method. Although, taking into account those effects reduced our underestimation of these observables, it did not completely eliminate it.

On the other hand, if we instead considered the A2 cross section data, at lower energies stronger S-wave contribution is required.

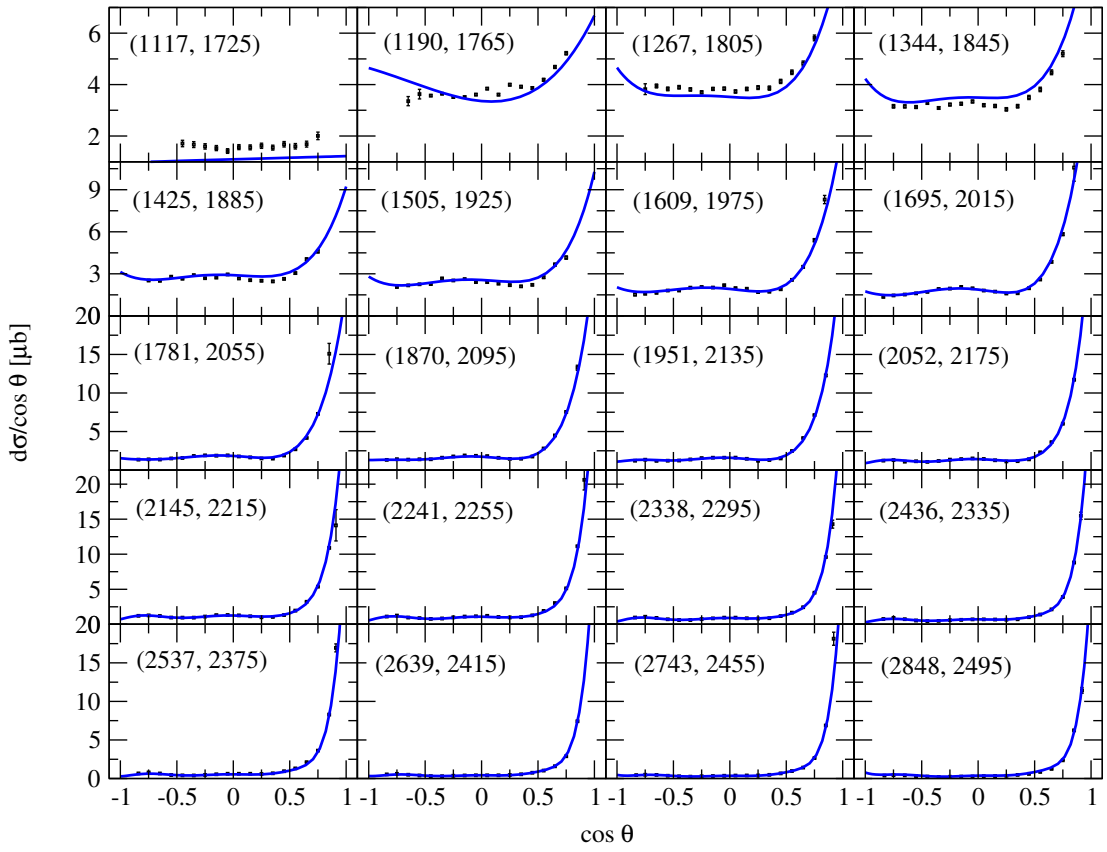

Figure 3.7: Differential cross section for the reaction $\gamma N \to \omega N$. Data was taken from CLAS collaboration Ref. (139).

The partial-wave decomposition of $\gamma N \to \omega N$ reaction is shown in Fig. 3.14(b). We found a significant contribution from P_{13}, D_{13}, D_{15}, and F_{15} while other partial-waves have a smaller contribution. At the threshold the D_{13} has the most significant contribution and S_{11} has the second largest contribution.

We found a significant contribution from $N(1520)\frac{3}{2}^-$, $N(1700)\frac{3}{2}^-$, $N(1675)\frac{5}{2}^-$, and $N(1680)\frac{5}{2}^+$ in the photoproduction of ω off proton. The inclusion of $N(1535)\frac{1}{2}^-$ is also important specially near the threshold. $N(1650)\frac{1}{2}^-$ and $N(1720)\frac{3}{2}^+$ play less of a role compared to other resonances in this reaction.

We also checked whether the inclusion of several heavier resonances, namely $N(2040)\frac{3}{2}^+$, $N(2060)\frac{5}{2}^-$, $N(2120)\frac{3}{2}^-$, $N(2190)\frac{7}{2}^-$, and $N(2250)\frac{9}{2}^-$, would improve the results but we could not obtain any significant improvement in our description of ω meson production.

3.3 Summary

Following the proposed approximation for constructing a Unitary Isobar Model (UIM) after exposing the complex phase structure of T-matrix in previous chapter, we proposed a UIM by directly parameterizing W and dressed vertices $|F_K\rangle$ and $\langle F_K|$ in a completely phenomenological manner. Subsequently, we performed an analysis of ω meson production in πN and γN reactions within proposed model. We have also included η production in πN reaction and πN elastic scattering. We have investigated the contribution of several resonance states with masses up to 2250 MeV to these reactions. To fix the phenomenological resonance couplings, a coupled-channel calculation has been carried out for final states $(\gamma/\pi)N \to \pi N$, ηN, and ωN. All the hadronic channels, πN, ηN, and ωN, plus $\pi\pi N$ which is parametrized by σN, ρN, and $\pi\Delta$ were considered as intermediate states. Due to the weakness of the electromagnetic interaction, we carried the photoproduction amplitude in one-photon approximation. The resonance and background amplitude contribution couplings are constrained by experimental reaction data for energies from the pion threshold up to 2.5 GeV. The extracted widths and masses for resonances are in good agreement with PDG.

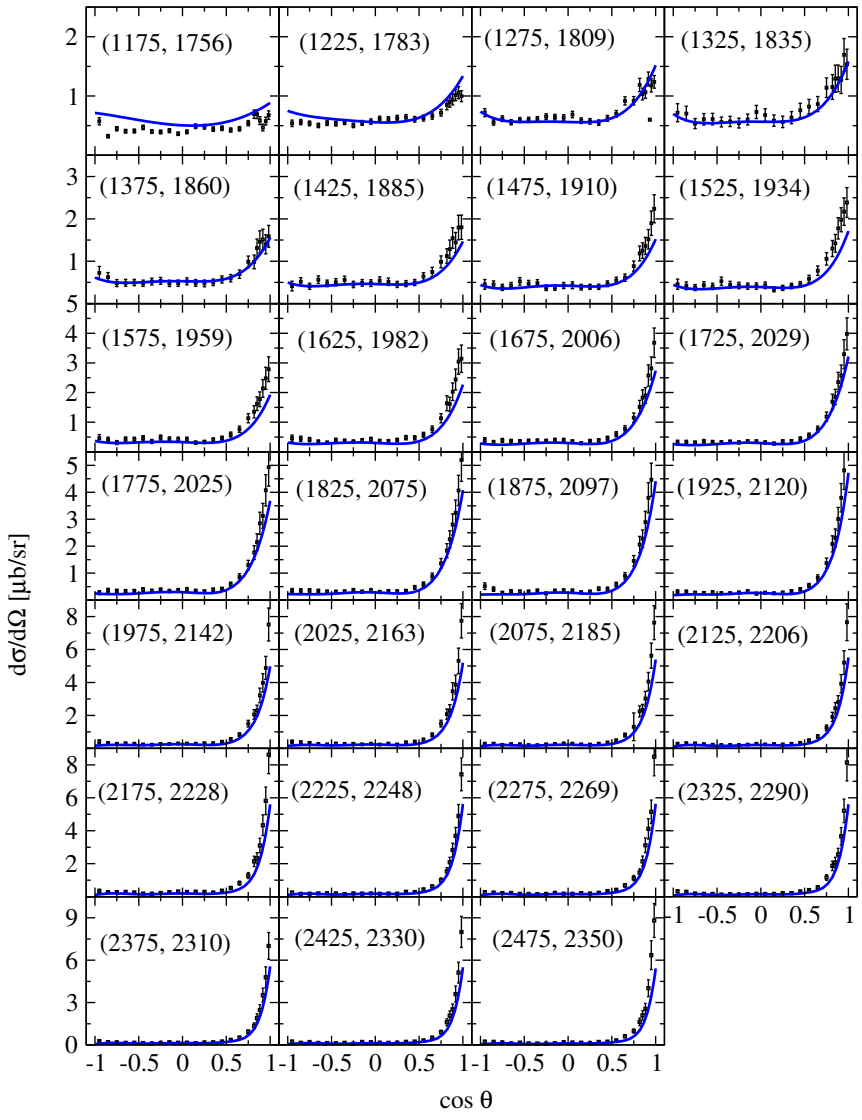

Figure 3.8: Differential cross section for the reaction $\gamma N \rightarrow \omega N$. Data was taken from CBELSA/TAPS collaboration Ref. (141).

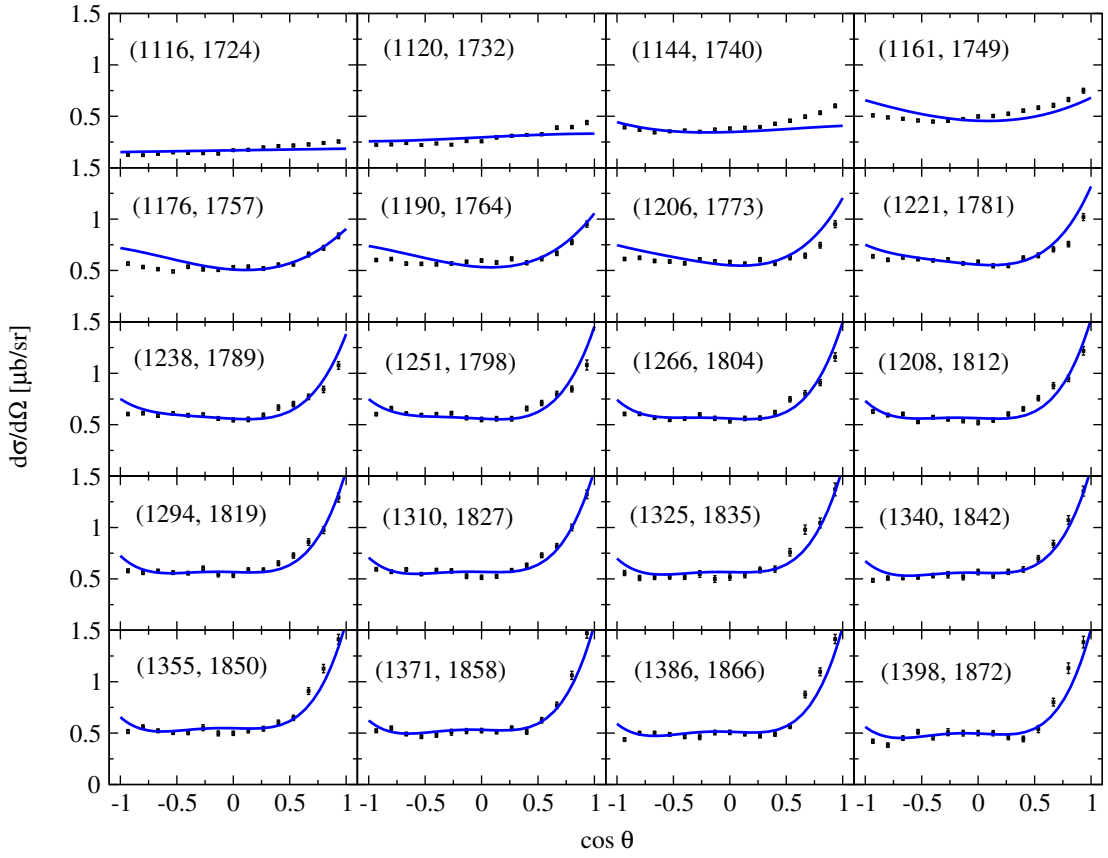

Figure 3.9: Differential cross section for the reaction $\gamma N \to \omega N$. Data from A2 collaboration at MAMI (127).

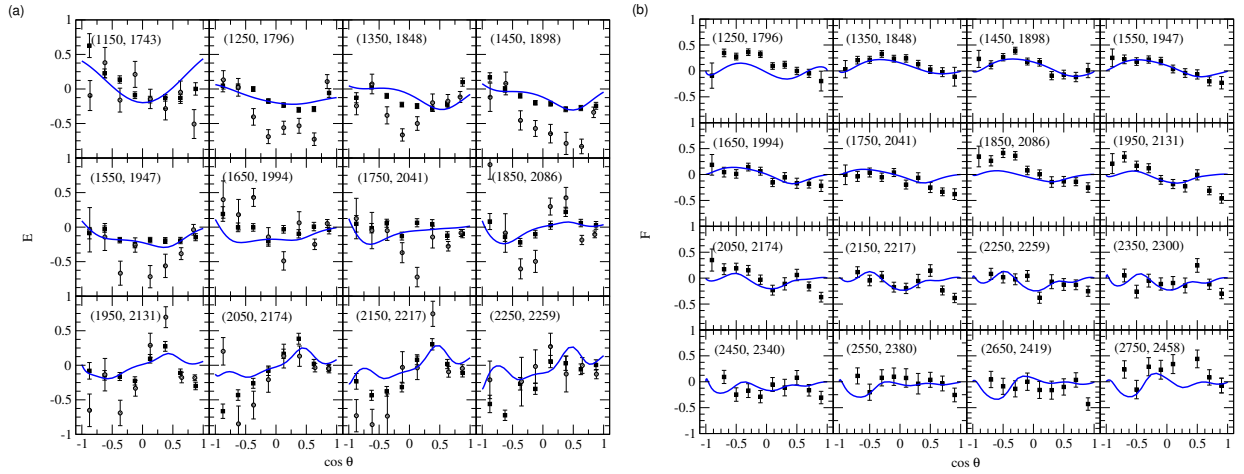

Figure 3.10: (a) Beam target helicity asymmetries E for the reaction $\gamma N \to \omega N$. Data displayed with squares is taken from CLAS collaboration Ref. (4), and those shown with circles are from CBELSA/TAPS Collaboration Ref. (39). (b) Beam target helicity asymmetries F for the reaction $\gamma N \to \omega N$. Data from CLAS collaboration Ref. (115).

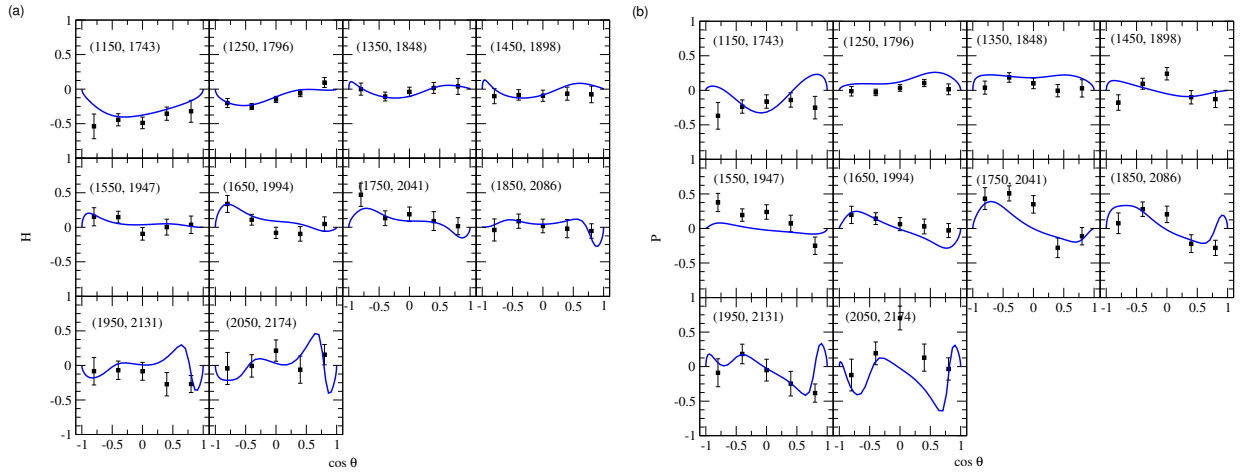

Figure 3.11: (a) Beam target helicity asymmetries H for the reaction $\gamma N \to \omega N$. Data from CLAS collaboration Ref. (115). (b) Recoil polarization asymmetry P for the reaction $\gamma N \to \omega N$. Data from CLAS collaboration Ref. (115).

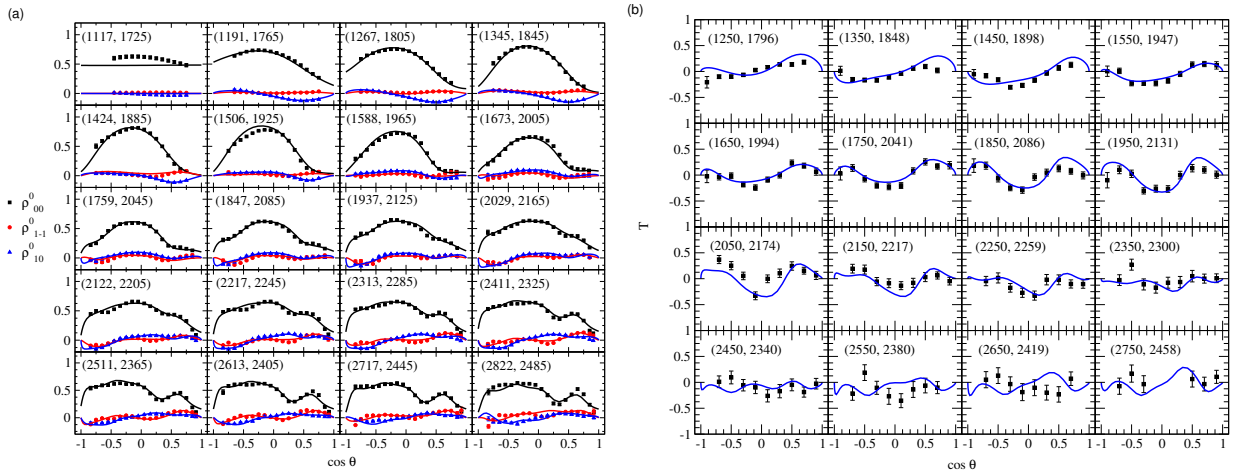

Figure 3.12: (a) Spin Density Matrix Elements in the Adair frame for the reaction $\gamma N \to \omega N$ as a function of $\cos\theta$. Data from CLAS collaboration Ref. (139). (b) Target asymmetry T for the reaction $\gamma N \to \omega N$. Data from CLAS Collaboration Ref. (114).

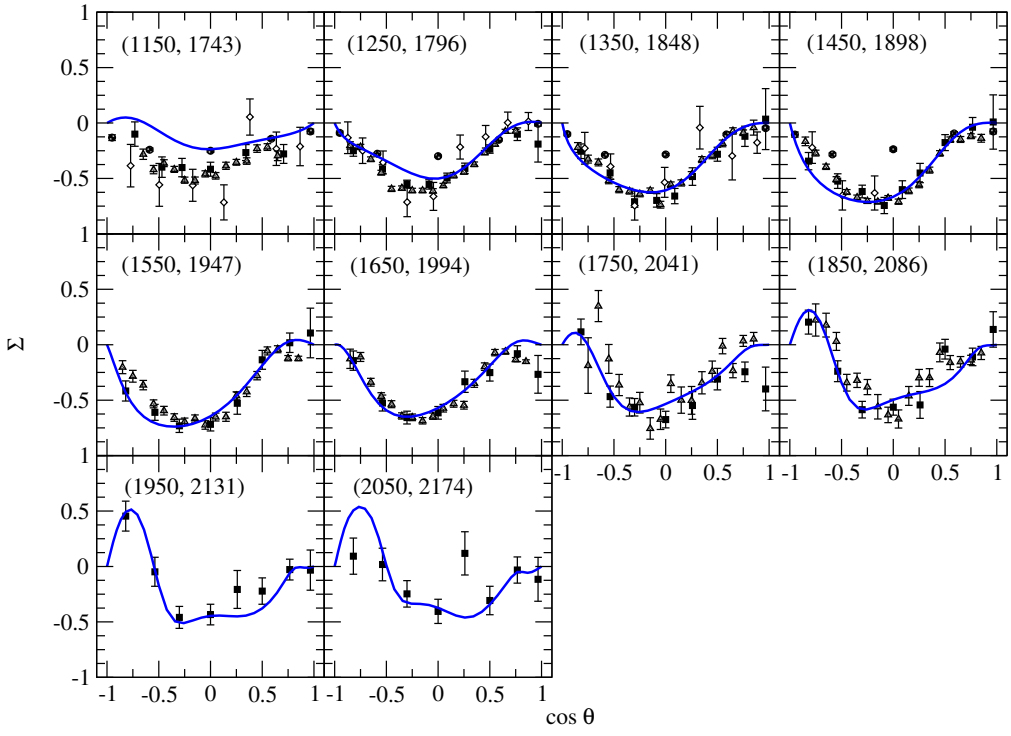

Figure 3.13: Beam asymmetry Σ for the reaction $\gamma N \to \omega N$. Data displayed with triangles up is from CLAS collaboration Ref.(33), diamonds from CBELSA/TAPS collaboration Ref. (39), circles from GRAAL Collaboration Ref. (136), and squares from CLAS Collaboration Ref. (114).

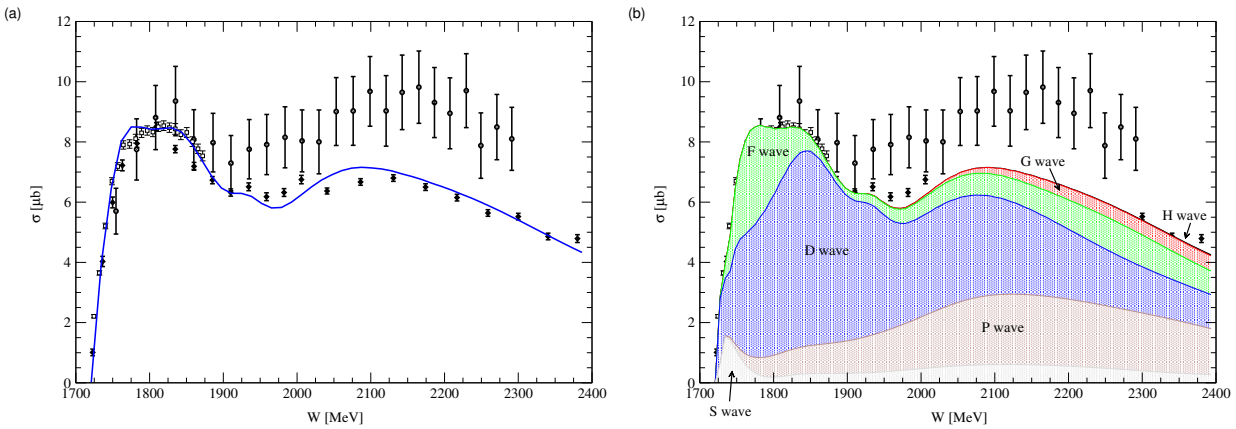

Figure 3.14: Total cross section and partial-wave decomposition of total cross section for the reaction $\gamma N \to \omega N$. Data displayed with empty squares is from A2 collaboration at MAMI Ref. (127), partially filled circles from CBELSA/TAPS collaboration Ref. (141), and black diamonds from SAPHIR collaboration Ref. (20).

Our calculation shows the available data of the reaction channels studied can be satisfactorily described by the 8 identified resonances in this work. It is worth mentioning that although we have tried our best to look at a variety of combinations of resonances available in this region, it was not feasible to consider all combinations. Perhaps taking advantage of statistical methods, e.g. the least absolute shrinkage and selection operator (LASSO) (85), would be beneficial in identifying, in a more statistically significant manner, contributing resonance states in the spectrum to these reaction channels. Inclusion of more reaction channels such as $\gamma N \to \eta N$ and $\gamma N \to \eta' N$ is required to further constrain the free parameters in our model.

Chapter 4

Summary and Outlook

There has been a multi decade effort to understand the QCD confinement and to this date studying color neutral hadrons is our best means in this quest. For this the study of a hadron spectroscopy is imperative and a robust and computationally efficient reaction theory is needed to extract relevant information from experimental data. Over the years, many theoretical models have been proposed to help us with extracting resonances information from experimental data. Dynamical coupled-channel models (DCC) can capture the coupling of different reaction channels and describe the complicated nature of overlapping and broad resonances at the high computational cost. On the other hand models such as K-matrix approaches are computationally efficient but lack the machinery to generate resonances dynamically and violate analyticity. Isobar models are based on coupled-channel approach and very effective in handling a large set of experimental data. In isobar models the reaction amplitude is decomposed into a resonance and a background contribution, corresponding to the pole and non-pole parts of the T-matrix amplitude. The simplicity of these models arises from the parametrization of the background with some smooth function of energy and parametrization of the resonance amplitude by Breit-Wigner forms. This simplicity usually comes at the cost of violating the unitarity.

In this work, we proposed a unitary isobar model (UIM) in which unitarity is maintained automatically. To build the proposed model, we have exposed the full complex phase structure of the meson-baryon T-matrix reaction amplitude in a coupled channels framework. This could be viewed as a generalization of the well-known Watson's theorem in photoproduction (137). Exposing the complex phase structure of the pole and non-pole parts of the T-matrix,

enable us to build computationally efficient and robust reaction amplitude by introducing approximations with varying degrees of sophistication while easily maintaining the fundamental properties of S-matrix, such as unitarity and/or analyticity. In particular, we show how the unitarity of the pole part of the T-matrix arises automatically from the dressing mechanism inherent in the basic T-matrix equation, and that, no separate conditions are required for making this part of the resonance amplitude unitary.

As the first application, we performed simultaneous analyses of the reactions $\pi N \to \pi N$, ηN , ωN, and $\gamma N \to \omega N$ within the framework of the proposed UIM. We identified the relevant resonances to achieve an overall good description of the observables. This description required 8 isospin $T = 1/2$ and 4 isospin $T = 3/2$ resonances.

An improvement of this work would be the approximation of the driving non-pole term U in Eq. (2.51) by a phenomenological separable potential (see, e.g., Ref. (94)) whose form allows to solve the integral equation for W in Eq. (2.51) analytically. The bare vertex $|F_0\rangle_{r'}$($\langle F_0|_r$) is obtained either from a microscopic Lagrangian or simply parametrized phenomenologically. Then, the momentum loop integration in Eq. (2.44) is carried out analytically to obtain $|F_K\rangle_{r'}$ ($\langle F_K|_r$). $\Sigma_{K\,r'r}$ is obtained as given by Eq. (2.46), also by performing the momentum loop integration analytically. This will results in a model that not only requires no separate conditions to preserve unitarity, but also it maintains analyticity, to the extent that the adopted separable potential is analytic.

We can also reduce the number of phenomenological parameters required in this analysis by approximating either the driving non-pole term U or the dressed non-pole, W, part of K-matrix by Feynman diagrams.

Appendix A

Phase-shift parametrization

In this appendix, we give the phase-shift parametrization of the Watson's factors N_α and $\bar{N}_\alpha$ defined in Eqs. (2.17,2.23) as well as of the on-shell $\hat{K}_{\alpha\alpha}$ defined in Eq. (2.20). Here, we confine ourselves to stable particles only and consider the channels whose on-shell elastic scattering T-matrix amplitude in partial-wave basis can be parametrize in terms of the phase-shift (δ_α) and inelasticity (η_α) as

$$\rho_\alpha T_{\alpha\alpha} = \frac{i}{2}\left(\eta_\alpha e^{i2\delta_\alpha} - 1\right) \ , \tag{A.1}$$

with ρ_α denoting the (phase-space) density of state in the channel specified by the index α. Then, inserting Eq. (A.1) into Eqs. (2.17,2.23), we have for the Watson factor, [1]

$$N_\alpha = \bar{N}_\alpha = 1 - i\rho_\alpha T_{\alpha\alpha} = \frac{1}{2}\left(\eta_\alpha e^{i2\delta_\alpha} + 1\right) \ . \tag{A.2}$$

Inserting the above two equations into Eq. (2.19), and solving for $\hat{K}_{\alpha\alpha}$, we obtain

$$\hat{K}_{\alpha\alpha} = -\frac{1}{\rho_\alpha}\ \frac{2\eta_\alpha \sin 2\delta_\alpha + i(1-\eta_\alpha^2)}{1+\eta_\alpha^2 + 2\eta_\alpha \cos 2\delta_\alpha} \ . \tag{A.3}$$

This result reveals a very simple phase structure of the on-shell $\hat{K}_{\alpha\alpha}$ in terms of the phase-shift and inelasticity of the elastic scattering T-matrix amplitude.

Below the inelastic threshold ($\eta_\alpha = 1$), Eq. (A.3) reduces to

$$\hat{K}_{\alpha\alpha} = K_{\alpha\alpha} = -\frac{\sin 2\delta_\alpha}{\rho_\alpha\,(1+\cos 2\delta_\alpha)} = -\frac{1}{\rho_\alpha}\tan\delta_\alpha \ , \tag{A.4}$$

and, as it should, one recovers the phase-shift parametrization of the on-shell K-matrix $K_{\alpha\alpha}$ (valid even above the inelastic threshold) which is a pure real quantity.

[1] Note that, for a stable particles channel β, $G^I_\beta = \pi\delta(E - H_{0\beta}) \to \rho_\beta$ after the momentum loop integration.

Inserting the phase-shift parametrization of the on-shell K-matrix into Eq. (2.26), yields

$$N_{K\,\alpha} = \bar{N}_{K\,\alpha} = e^{i\delta_\alpha} \cos\delta_\alpha \ . \tag{A.5}$$

In complete analogy to the phase-shift parametrization of the on-shell elastic T-matrix amplitude (cf. Eq. (A.1)), if we assume the corresponding phase-shift parametrization of the on-shell elastic non-pole T-matrix ($X \equiv T^{NP}$) in Eq. (2.35) to be

$$\rho_\alpha X_{\alpha\alpha} = \frac{i}{2}\left(\eta_\alpha^X e^{i2\delta_\alpha^X} - 1\right) \ , \tag{A.6}$$

then, the corresponding Watson's factors N_α^X and $\bar{N}_\alpha^X$ defined by Eqs. (2.55,2.58) become

$$N_\alpha^X = 1 - i\rho_\alpha X_{\alpha\alpha} = \frac{1}{2}\left(\eta_\alpha^X e^{i2\delta_\alpha^X} + 1\right) = \bar{N}_\alpha^X \ . \tag{A.7}$$

For the on-shell $\hat{W}_{\alpha\alpha}$, we obtain

$$\hat{W}_{\alpha\alpha} = -\frac{1}{\rho_\alpha}\ \frac{2\eta_\alpha^X \sin 2\delta_\alpha^X + i(1-\eta_\alpha^{X\,2})}{1+\eta_\alpha^{X\,2} + 2\eta_\alpha^X \cos 2\delta_\alpha^X} \ , \tag{A.8}$$

and below the inelastic threshold ($\eta_\alpha^X = 1$), it reduces to

$$\hat{W}_{\alpha\alpha} = W_{\alpha\alpha} = -\frac{\sin 2\delta_\alpha^X}{\rho_\alpha\,(1+\cos 2\delta_\alpha^X)} = -\frac{1}{\rho_\alpha}\tan\delta_\alpha^X \ . \tag{A.9}$$

Appendix B

Pole and non-pole decomposition of the T-matrix reaction amplitude

Although the pole and non-pole decomposition of the meson-baryon T-matrix reaction amplitude is widely used in the literature (see, e.g., (2; 90)), due to its central role in the present work, its derivation is provided in this Appendix. We will also decompose the photoproduction amplitude starting from the gauge-invariant amplitude obtained from the field theoretic considerations (61). In this Appendix, the reference to two-particle channels are suppressed for the sake of not overloading with unessential notations in the derivation.

B.1 Meson-baryon T-matrix reaction amplitude

The meson-baryon T-matrix obeys the Lippmann-Schwiger-type scattering equation

$$T = V + VGT \ . \tag{B.1}$$

It can be recast into the form

$$T = T^P + T^{NP} \ , \tag{B.2}$$

with

$$T^{NP} = V^{NP} + V^{NP}GT^{NP} \ , \tag{B.3}$$

where V^{NP} stands for one-nucleon irreducible potential (the non-pole part of V), i.e.,

$$V^{NP} = V - V^P \ , \tag{B.4}$$

with the one-nucleon reducible potential V^P (the pole part of V) given by

$$V^P = \sum_r |F_{0r}\rangle S_{0r} \langle F_{0r}| \ . \tag{B.5}$$

In the above equation, $|F_{0r}\rangle$ denotes the bare vertex and S_{0r}, the bare baryon propagator for a given bare resonance r, including the nucleon ($r = N$).

Below, we show how the pole T-matrix, T^P, in Eq. (B.2) can be expressed in a compact form. For this purpose, let us start from Eqs. (B.1,B.2,B.3,B.4) to express T^P as

$$\begin{aligned} T^P &= \left(1 + T^{NP}G\right) V^P + T^P G V \\ T^P(1 - GV) &= \left(1 + T^{NP}G\right) V^P \\ T^P &= \left(1 + T^{NP}G\right) V^P (1 - GV)^{-1} \\ &= \left(1 + T^{NP}G\right) V^P (1 + GT) \\ &= \left(1 + T^{NP}G\right) V^P \left[\left(1 + GT^{NP}\right) + GT^P\right] \ . \end{aligned} \tag{B.6}$$

Inserting Eq. (B.5) into Eq. (B.6), we have

$$T^P = \sum_r \left\{ |F_r\rangle S_{0r} \langle F_r| + |F_r\rangle S_{0r} \langle F_{0r}| G T^P \right\} \ , \tag{B.7}$$

with the dressed vertex defined as

$$\begin{aligned} |F_r\rangle &\equiv \left(1 + T^{NP}G\right) |F_{0r}\rangle \ , \\ \langle F_r| &\equiv \langle F_{0r}| \left(1 + GT^{NP}\right) \ , \end{aligned} \tag{B.8}$$

Multiplication of Eq. (B.7) by $\langle F_{0r'}|G$ from the left gives

$$\begin{aligned} \langle F_{0r'}|GT^P &= \sum_r \left\{ \Sigma_{r'r} S_{0r} \langle F_r| + \Sigma_{r'r} S_{0r} \langle F_{0r}| G T^P \right\} \\ \sum_r \Sigma_{r'r} S_{0r} \ \langle F_r| &= \sum_r \left(S_{0r}^{-1} \delta_{r'r} - \Sigma_{r'r} \right) S_{0r} \langle F_{0r}| G T^P \ , \end{aligned} \tag{B.9}$$

where the last equality is a simple rearrangement of the first equality together with the introduction of the self-energy matrix

$$\Sigma_{r'r} \equiv \langle F_{0r'}|G|F_r\rangle \ . \tag{B.10}$$

Defining the dressed propagator matrix

$$S^{-1}_{r'r} \equiv S^{-1}_{0r}\delta_{r'r} - \Sigma_{r'r} \ , \tag{B.11}$$

we have, from Eq. (B.9),

$$\begin{aligned} \sum_{r'r} S_{kr'}\Sigma_{r'r}S_{0r}\langle F_r| &= \sum_{r'r} S_{kr'}S^{-1}_{r'r}S_{0r}\langle F_{0r}|GT^P \\ &= S_{0k}\langle F_{0k}|GT^P \ . \end{aligned} \tag{B.12}$$

Inserting the above result back into Eq. (B.7), we have

$$\begin{aligned} T^P &= \sum_r \Big\{ |F_r\rangle S_{0r}\langle F_r| + |F_r\rangle \sum_{r'l} S_{rl}\Sigma_{lr'}S_{0r'}\langle F_{r'}| \Big\} \\ &= \sum_{rr'} |F_r\rangle \Big\{ \delta_{rr'}S_{0r'} \\ &\qquad + \sum_l S_{rl}\left(S^{-1}_{0l}\delta_{lr'} - S^{-1}_{lr'}\right) S_{0r'} \Big\} \langle F_{r'}| \\ &= \sum_{rr'} |F_r\rangle S_{rr'}\langle F_{r'}| \ . \end{aligned} \tag{B.13}$$

B.2 Photoproduction reaction amplitude

Following the field theoretic approach of Haberzettl (61), the gauge-invariant photoproduction amplitude in the one-photon approximation can be expressed as

$$M^\mu = V^\mu + TGV^\mu, \tag{B.14}$$

with μ denoting the Lorentz index of the photon polarization and

$$V^\mu = \tilde{m}^\mu_s + M^\mu_u + M^\mu_t + m^\mu_{KR} + U^\mu G|F_N\rangle \ , \tag{B.15}$$

where U^μ stands for the exchange current which arises from the coupling of the photon to V^{NP}; m^μ_{KR} stands for the sum of the bare Kroll-Ruderman contact current arising from the direct coupling of the photon to the bare vertex $|F_{0r}\rangle$ appearing in Eq. (B.5); $M^\mu_x(x = u, t)$

denotes the x-channel (tree-level Feynman diagram) contribution and, $\tilde{m}_s^\mu$ stands for the s-channel bare current. The latter is given by

$$\tilde{m}_s^\mu = \sum_r |F_{0r}\rangle S_{0r} \langle \tilde{F}_{0r}^\mu| \ , \tag{B.16}$$

where $\langle \tilde{F}_{0r}^\mu|$ is defined as

$$\langle \tilde{F}_{0r}^\mu| \equiv \langle F_{0r}^\mu| + \bar{m}_{KRr}^\mu G|F_N\rangle \ , \tag{B.17}$$

with $\langle F_{0r}^\mu|$ denoting the bare $rN\gamma$ vertex and, $\bar{m}_{KRr}^\mu$, the bare Kroll-Ruderman term for a given resonance r in m_{KR}^μ with the meson leg reversed, i.e., $NM\gamma \to r$.

Now, analogous to Eq. (B.4), we decompose V^μ in Eq. (B.15) as

$$V^\mu = V^{P\mu} + V^{NP\mu} \ , \tag{B.18}$$

where

$$V^{P\mu} \equiv \tilde{m}_s^\mu = \sum_r |F_{0r}\rangle S_{0r} \langle \tilde{F}_{0r}^\mu| \ , \tag{B.19}$$

and

$$V^{NP\mu} \equiv M_u^\mu + M_t^\mu + m_{KR}^\mu + U^\mu G|F_N\rangle \ . \tag{B.20}$$

Inserting Eqs. (B.2,B.18) into Eq. (B.14), we have

$$\begin{aligned} M^\mu &= V^{P\mu} + V^{NP\mu} + (T^P + T^{NP})G(V^{P\mu} + V^{NP\mu}) \\ &= M^{P\mu} + M^{NP\mu} \ , \end{aligned} \tag{B.21}$$

where

$$M^{NP\mu} \equiv V^{NP\mu} + T^{NP} G V^{NP\mu} \ , \tag{B.22}$$

and

$$M^{P\mu} \equiv V^{P\mu} + T^{NP} G V^{P\mu} + T^P G(V^{P\mu} + V^{NP\mu}) \ . \tag{B.23}$$

Now, using Eqs. (B.8,B.19),

$$V^{P\mu} + T^{NP} G V^{P\mu} = \sum_r |F_r\rangle S_{0r} \langle \tilde{F}_{0r}^\mu| \ . \tag{B.24}$$

Similarly, using Eqs. (B.10,B.13,B.19),

$$\begin{aligned} T^P G \quad (\quad V^{P\mu} + V^{NP\mu}) = & \\ = \quad & \sum_{rr'} |F_r\rangle S_{rr'} \Big[\langle F_{r'}| G \sum_l |F_{0l}\rangle S_{0l} \langle \tilde{F}^\mu_{0l}| \\ & \qquad + \langle F_{r'}| G V^{NP\mu} \Big] \\ = \quad & \sum_{rr'l} |F_r\rangle S_{rr'} \left[\Sigma_{r'l} S_{0l} \langle \tilde{F}^\mu_{0l}| + \delta_{r'l} \langle F_l| G V^{NP\mu} \right] \ . \end{aligned} \tag{B.25}$$

Inserting Eqs. (B.24,B.25) into Eq. (B.23), and with help of Eq. (B.11), we have

$$\begin{aligned} M^{P\mu} \quad = \quad & \sum_{rr'l} |F_r\rangle S_{rr'} \Big[(S)^{-1}_{r'l} S_{0l} \langle \tilde{F}^\mu_{0l}| + \Sigma_{r'l} S_{0l} \langle \tilde{F}^\mu_{0l}| \\ & \qquad + \delta_{r'l} \langle F_l| G V^{NP\mu} \Big] \\ = \quad & \sum_{rr'l} |F_r\rangle S_{rr'} \Big[\left\{ (S)^{-1}_{r'l} + \Sigma_{r'l} \right\} S_{0l} \langle \tilde{F}^\mu_{0l}| \\ & \qquad + \delta_{r'l} \langle F_l| G V^{NP\mu} \Big] \\ = \quad & \sum_{rr'} |F_r\rangle S_{rr'} \langle F^\mu_{r'}| \ , \end{aligned} \tag{B.26}$$

where, in the last equality above, we have introduced the dressed electromagnetic vertex

$$\begin{aligned} \langle F^\mu_{r'}| &\equiv \langle \tilde{F}^\mu_{0r'}| + \langle F_{r'}| G V^{NP\mu} \\ &= \langle \tilde{F}^\mu_{0r'}| + \langle F_{0r'}| G M^{NP\mu} \ . \end{aligned} \tag{B.27}$$

Appendix C

Two-resonance coupling

The resonance propagator appearing in the pole part of the T-matrix (cf. Eq. (2.66)) is, in general, a matrix in resonance space. In most of the cases, there is only one resonance for a given partial-wave state, in which case, the propagator reduces to a number. In other cases, such as in the πN S_{11} partial wave, there can be two resonances close to each other ($S_{11}(1535)$ and $S_{11}(1650)$) which causes a considerable resonance coupling effect. For the two-resonance case, the resonance propagator matrix S can be obtained explicitly. Following Ref. (60), we have,

$$S^{-1} = S_0^{-1} - \Sigma = \begin{pmatrix} E - m_{0\,1} - \Sigma_{11} & -\Sigma_{12} \\ -\Sigma_{21} & E - m_{0\,2} - \Sigma_{22} \end{pmatrix} \ , \tag{C.1}$$

and hence

$$\begin{aligned} S &= \left(\frac{1}{S_0^{-1} - \Sigma} \right) \\ &= \frac{1}{|D|} \begin{pmatrix} E - m_{0\,2} - \Sigma_{22} & \Sigma_{12} \\ \Sigma_{21} & E - m_{0\,1} - \Sigma_{11} \end{pmatrix} \ , \end{aligned} \tag{C.2}$$

where $|D|$ stands for the determinant of S^{-1},

$$|D| = (E - m_{0\,1} - \Sigma_{11})(E - m_{0\,2} - \Sigma_{22}) - \Sigma_{12}\Sigma_{21} \ . \tag{C.3}$$

Now, defining

$$\mu_i \equiv m_{0\,i} + \Sigma_{ii} \qquad \text{and} \qquad \mathrm{C}^2 \equiv \Sigma_{12}\Sigma_{21} \ , \tag{C.4}$$

the pole condition reads

$$|D| = (E - \mu_1)(E - \mu_2) - C^2 = 0 \ , \tag{C.5}$$

producing two solutions

$$E \quad \rightarrow \quad M_{\pm} = \frac{\mu_1 + \mu_2}{2} \pm \frac{1}{2}\sqrt{(\mu_1 - \mu_2)^2 + 4C^2} \; . \tag{C.6}$$

We then have

$$\begin{aligned} \frac{1}{|D|} &= \frac{1}{(E - M_-)(E - M_+)} \\ &= \frac{1}{(E - M_-) + (E - M_+)} \left[\frac{1}{E - M_-} + \frac{1}{E - M_+} \right] \\ &= \frac{1}{(E - \mu_1) + (E - \mu_2)} \left[\frac{1}{E - M_-} + \frac{1}{E - M_+} \right] \; , \end{aligned} \tag{C.7}$$

where the equality $M_- + M_+ = \mu_1 + \mu_2$ has been used.

Equation (C.7) allows to write the propagator in the form

$$S = \frac{R}{E - M_-} + \frac{R}{E - M_+} \; , \tag{C.8}$$

with the "residue" matrix R given by

$$R \equiv \begin{pmatrix} \frac{E-\mu_2}{d} & \frac{\Sigma_{12}}{d} \\ \frac{\Sigma_{21}}{d} & \frac{E-\mu_1}{d} \end{pmatrix} \; , \qquad \frac{1}{d} = \frac{1}{(E - \mu_1) + (E - \mu_2)} \; . \tag{C.9}$$

If the resonance coupling is small enough, i.e., $\Sigma_{12} \sim \Sigma_{21} \sim 0$, then $M_{\pm}$ and R reduce to

$$M_+ = \mu_1 \; , \qquad M_- = \mu_2 \; , \qquad \text{and} \qquad R = \begin{pmatrix} \frac{E-\mu_2}{d} & 0 \\ 0 & \frac{E-\mu_1}{d} \end{pmatrix} \; , \tag{C.10}$$

so that

$$S = \begin{pmatrix} \frac{1}{E-\mu_1} & 0 \\ 0 & \frac{1}{E-\mu_2} \end{pmatrix} \; , \tag{C.11}$$

as it should be.

Appendix D

Two body propagators

We begin with the explicit form of the propagator G_α for $\alpha = \sigma N$ channel. According to Refs. (46), (47), the σN propagator $G_{\alpha=\sigma N}$ given by Eq. (2.10) may be parametrized as

$$G_{\sigma N}(E,p) = \frac{1}{E - \sqrt{m_N^2 + p^2} - \sqrt{m_{0\ \sigma}^2 + p^2} - \Pi_\sigma(z_\sigma, p)} \ , \tag{D.1}$$

where $m_{0\ \sigma}$ and $\Pi_\sigma(z_\sigma, p)$ stand for the bare σ mass and σ self-energy, respectively. The latter is given by

$$\Pi_\sigma(z_\sigma, p) = \int_0^\infty q^2 dq \frac{\Gamma^2_{\sigma\pi\pi}(q,p)}{z_\sigma - 2\sqrt{m_\pi^2 + q^2} + i\epsilon} \ , \tag{D.2}$$

with

$$z_\sigma \equiv z_\sigma(E,p) \equiv E - \left(\sqrt{m_{0\ \sigma}^2 + p^2} - m_{0\ \sigma}\right) - \sqrt{m_N^2 + p^2} \tag{D.3}$$

and $\Gamma_{\sigma\pi\pi}(q,p)$ denoting the $\sigma\pi\pi$ vertex in the $\pi\pi$ partial-wave state with $l = 0$ and isospin $T = 0$. Here, we follow its definition as given in the PDG. It may be obtained from the Lagrangian density[1]

$$\mathcal{L}_{\sigma\pi\pi} = g_{\sigma\pi\pi} m_\pi \vec{\pi}(x).\vec{\pi}(x)\sigma(x) \ , \tag{D.4}$$

yielding (46)

[1]This form of the Lagrangian violates the chiral symmetry constraint at low energy. A form that satisfies the chiral constraint is $\mathcal{L}_{\sigma\pi\pi} = (g_{\sigma\pi\pi}/m_N)\partial^\mu\vec{\pi}(x).\partial_\mu\vec{\pi}(x)\sigma(x)$.

$$\Gamma_{\sigma\pi\pi}(q,p) = \frac{g_{\sigma\pi\pi}}{2\pi\left(\sqrt{m_{0\ \sigma}^2 + p^2}\right)^{\frac{1}{2}}}\sqrt{3}\left(\frac{m_\pi}{\sqrt{m_\pi^2+q^2}}\right)F_{\sigma\pi\pi}(q^2)\ . \tag{D.5}$$

In the above equation, the form factor of of the form $F_{\sigma\pi\pi}(q^2) = \Lambda_{\sigma\pi\pi}^2/(\Lambda_{\sigma\pi\pi}^2 + q^2)$ has been introduced in order to make the integral in Eq. (D.2) converge. The free parameters of the model given above for calculating the σ self-energy Π_σ in Eq. (D.2) are adjusted to reproduce the $\pi\pi$ phase-shift δ_{00} (46).

Analogously, the ρN propagator is obtained from the σN propagator given above by replacing all the quantities referring to the σ meson by the corresponding ones referring to the ρ meson. The $\rho\pi\pi$ vertex, $\Gamma_{\rho\pi\pi}$, in the $\pi\pi$ partial-wave state with $l = 1$ and isospin $T = 1$ may be obtained from the Lagrangian density

$$\mathcal{L}_{\rho\pi\pi} = -g_{\rho\pi\pi}(\partial^\mu\vec{\pi}(x)\times\vec{\pi}(x)).\vec{\rho}_\mu(x) \tag{D.6}$$

yielding (46)

$$\Gamma_{\rho\pi\pi}(q,p) = \frac{g_{\rho\pi\pi}}{2\pi\left(\sqrt{m_{0\ \rho}^2 + p^2}\right)^{\frac{1}{2}}}\frac{1}{\sqrt{3}}\left(\frac{q}{\sqrt{m_\pi^2+q^2}}\right)F_{\rho\pi\pi}(q^2)\ . \tag{D.7}$$

In the above equation, the form factor $F_{\rho\pi\pi}(q^2) = (\Lambda_{\rho\pi\pi}^2 + m_\rho^2)/(\Lambda_{\rho\pi\pi}^2 + 4(m_\pi^2+q^2))$ has been introduced. The parameters of the model are adjusted to reproduce the $\pi\pi$ phase-shift δ_{11} (46).

Similarly, the $\pi\Delta$ propagator is given by (46)

$$G_{\pi\Delta}(E,p) = \frac{1}{E - \sqrt{m_\pi^2+p^2} - \sqrt{m_{0\ \Delta}^2+p^2} - \Pi_\Delta(z_\Delta,p)}\ , \tag{D.8}$$

where $m_{0\ \Delta}$ and $\Pi_\Delta(z_\Delta,p)$ stand for the bare Δ mass and Δ self-energy, respectively. The latter is given by

$$\Pi_\Delta(z_\Delta,p) = \int_0^\infty q^2dq\frac{\Gamma_{\Delta N\pi}^2(q,p)}{z_\Delta - \sqrt{m_\pi^2+q^2} - \sqrt{m_N^2+q^2} + i\epsilon}\ , \tag{D.9}$$

with

$$z_\Delta \equiv z_\Delta(E,p) \equiv E - \left(\sqrt{m_{0\ \Delta}^2 + p^2} - m_{0\ \Delta}\right) - \sqrt{m_\pi^2 + p^2} \tag{D.10}$$

and $\Gamma_{\Delta N\pi}(q,p)$ denoting the $\Delta N\pi$ vertex in the πN partial-wave state with $l = 1$ and $T = 3/2$. It may be obtained from the Lagrangian

$$\mathcal{L}_{\Delta N\pi} = \frac{f_{\Delta N\pi}}{m_\pi} \bar{\Delta}^\mu(x) T^\dagger . \partial_\mu \vec{\pi}(x) N(x) + h.c.\ , \tag{D.11}$$

yielding (46)

$$\Gamma_{\Gamma N\pi}(q,p) = \frac{f_{\Delta N\pi}}{2\pi m_\pi} \frac{q}{\sqrt{6}} \left(\frac{\sqrt{m_N^2 + q^2} + m_N}{\sqrt{m_N^2 + q^2}\sqrt{m_\pi^2 + q^2}}\right)^{\frac{1}{2}} F_{\Delta N\pi}(q^2)\ . \tag{D.12}$$

In the above equation, the form factor of the form $F_{\Delta N\pi}(q^2) = (\Lambda_{\Delta N\pi}^4 + m_\Delta^4)/(\Lambda_{\Delta N\pi}^4 + (\sqrt{m_\pi^2 + q^2} + \sqrt{m_N^2 + q^2})^4)$ has been introduced. Here, the parameters of the model are adjusted to reproduce the πN phase-shift δ_{33} (46).

Appendix E

Observables

We start by connecting the dimensionless meson-baryon amplitude τ (143) to the partial wave amplitude T-matrix defined in Eq. (2.4),

$$\tau^{JIS'S}_{\nu'\nu\,L'L} = -\pi\sqrt{\rho_{\nu'}\rho_\nu}\; T^{JIS'S}_{\nu'\nu\,L'L},\;\; \rho_\nu = \frac{k_\nu E_\nu w_\nu}{W} \tag{E.1}$$

where W is the c.m. energy and k_ν, E_ν, and w_ν are on-shell three-momentum, baryon energy, and meson energy respectively of the initial or final meson-baryon channel ν.

In order to define other observables in terms of reaction amplitude Eq. (2.2), we first define a set of coordinated independent mutually orthogonal unit vectors $\hat{n}_i$ $(i = 1, 3)$

$$\hat{n}_3 \equiv \hat{k}\ , \quad \hat{n}_2 \equiv \frac{\hat{k}\times\hat{q}}{|\hat{k}\times\hat{q}|}\ , \quad \hat{n}_1 \equiv \hat{n}_2\times\hat{n}_3\ . \tag{E.2}$$

In the Center-of-Momentum (c.m.) frame where $\vec{k}+\vec{p}=\vec{q}+\vec{p}'=0$ the cartesian coordinate system $\{\hat{x},\hat{y},\hat{z}\}$ is given by

$$\{\hat{x},\hat{y},\hat{z}\} = \{\hat{n}_1,\hat{n}_2,\hat{n}_3\}_{(c.m.)}\ , \tag{E.3}$$

where the subscript $(c.m.)$ indicates that $\{\hat{n}_1,\hat{n}_2,\hat{n}_3\}$ is calculated in $c.m.$ frame. Similarly in the lab frame where $\vec{p}=0$ we have

$$\{\hat{x}_L,\hat{y}_L,\hat{z}_L\} = \{\hat{n}_1,\hat{n}_2,\hat{n}_3\}_{(lab)}\ . \tag{E.4}$$

Then using these coordinate independent unit vectors, the reaction plane is defined as $(\hat{n}_1\times\hat{n}_2)$-plane with $\hat{n}_2$ as its normal vector.

In photo-production reactions, the incoming real photon has two independent polarization states. We specify the two states of a linearly polarized photon by $\vec{\epsilon}_\parallel$ and $\vec{\epsilon}_\perp$ where $\vec{\epsilon}_\parallel$

($\vec{\epsilon}_\perp$) stands for the polarization vector parallel (perpendicular) to the reaction plane. More generally, the rotated linearly polarized photon states $\vec{\epsilon}_{\parallel'}$ and $\vec{\epsilon}_{\perp'}$ are obtained by rotating (counter clockwise) $\vec{\epsilon}_\parallel$ and $\vec{\epsilon}_\perp$ about $\hat{n}_3$-axis by an angle ϕ,

$$\vec{\epsilon}_{\parallel'} = \cos\phi\ \vec{\epsilon}_\parallel + \sin\phi\ \vec{\epsilon}_\perp\ ,$$
$$\vec{\epsilon}_{\perp'} = -\sin\phi\ \vec{\epsilon}_\parallel + \cos\phi\ \vec{\epsilon}_\perp\ . \tag{E.5}$$

The circularly polarized photon is specified by

$$\vec{\epsilon}_\pm \equiv \mp\frac{1}{\sqrt{2}}\left(\vec{\epsilon}_\parallel \pm i\vec{\epsilon}_\perp\right)\ . \tag{E.6}$$

Furthermore, for convince, we define projection operators $\hat{P}_\lambda$ which specify the polarization state of photons, $\hat{P}_\lambda\vec{\epsilon} \equiv \vec{\epsilon}_\lambda$. It should be noted that $\hat{P}_{\lambda'}\hat{P}_\lambda = \delta_{\lambda'\lambda}$ and $\sum_\lambda \hat{P}_\lambda = 1$. The projection operator $\hat{P}_\lambda$ is associated with the Stokes vector $\vec{P}^S$ (53) which specifies the direction and degree of polarization of the photon. For example, $\hat{P}_\perp$ and $\hat{P}_\parallel$ correspond to $P^S_{x=n_1} = +1$ and $P^S_{x=n_1} = -1$ respectively, while $\hat{P}_\pm$ corresponds to $P^S_{z=n_3} = \pm 1$. Also the difference between two appropriate projection operators can be expressed in terms of the Pauli spin matrices in photon helicity space, i.e., $\hat{P}_\perp - \hat{P}_\parallel = \sigma_{n_1}$ and $\hat{P}_+ - \hat{P}_- = \sigma_{n_3}$.

The Lorentz invariant reaction amplitude is related to the T-matrix amplitude defined in Eq. (2.3) by

$$\hat{\mathcal{M}}_{\nu'\nu}(\vec{q}', \vec{q}; E) = (2\pi)^{3/2}\sqrt{2E_{\nu'}}\sqrt{2w_{\nu'}}\ T_{\nu'\nu}(\vec{q}', \vec{q}; E)\ (2\pi)^{3/2}\sqrt{2E_\nu}\sqrt{2w_\nu} \tag{E.7}$$

where E_ν ($E_{\nu'}$) and w_ν ($w_{\nu'}$) are respectively on-shell baryon and meson energies of the initial (final) meson-baryon channel ν (ν').

Given the Lorentz invariant reaction amplitude, $\hat{\mathcal{M}}$, below we define coordinated-independent observables which are also Lorentz invariant. The cross section is defined as

$$\frac{d\sigma}{d\Omega} \equiv \frac{1}{4}Tr[\hat{\mathcal{M}}\hat{\mathcal{M}}^\dagger]\ , \tag{E.8}$$

where the trace is over both the nucleon spin and photon polarization. The $\frac{1}{4}$ in front is due to the averaging over target-nucleon spin and the photon beam polarization.

The single polarization observables, photon beam asymmetry, Σ, target nucleon asymmetry, T, and recoil nucleon asymmetry, P, are defined as

$$\begin{aligned}
\frac{d\sigma}{d\Omega}\Sigma &\equiv \frac{1}{4}Tr[\hat{\mathcal{M}}(\hat{P}_{\perp}-\hat{P}_{\parallel})\hat{\mathcal{M}}^{\dagger}] \ , \\
\frac{d\sigma}{d\Omega}T &\equiv \frac{1}{4}Tr[\hat{\mathcal{M}}\sigma_{n_2}\hat{\mathcal{M}}^{\dagger}] \ , \\
\frac{d\sigma}{d\Omega}P &\equiv \frac{1}{4}Tr[\hat{\mathcal{M}}\hat{\mathcal{M}}^{\dagger}\sigma_{n_2}] \ .
\end{aligned} \tag{E.9}$$

For double, beam-target, asymmetries, E, F, G, H, and P', we have

$$\begin{aligned}
\frac{d\sigma}{d\Omega}E &\equiv \frac{1}{4}Tr[\hat{\mathcal{M}}(\hat{P}_{+}-\hat{P}_{-})\sigma_{n_3}\hat{\mathcal{M}}^{\dagger}] \\
&= 2\frac{1}{4}Tr[\hat{\mathcal{M}}\hat{P}_{+}\sigma_{n_3}\hat{\mathcal{M}}^{\dagger}] \\
&= -2\frac{1}{4}Tr[\hat{\mathcal{M}}\hat{P}_{-}\sigma_{n_3}\hat{\mathcal{M}}^{\dagger}] \ , \\
\frac{d\sigma}{d\Omega}F &\equiv \frac{1}{4}Tr[\hat{\mathcal{M}}(\hat{P}_{+}-\hat{P}_{-})\sigma_{n_1}\hat{\mathcal{M}}^{\dagger}] \\
&= 2\frac{1}{4}Tr[\hat{\mathcal{M}}\hat{P}_{+}\sigma_{n_1}\hat{\mathcal{M}}^{\dagger}] \\
&= -2\frac{1}{4}Tr[\hat{\mathcal{M}}\hat{P}_{-}\sigma_{n_1}\hat{\mathcal{M}}^{\dagger}] \ , \\
\frac{d\sigma}{d\Omega}G &\equiv \frac{1}{4}Tr[\hat{\mathcal{M}}(\hat{P}_{\perp'}-\hat{P}_{\parallel'})\sigma_{n_3}\hat{\mathcal{M}}^{\dagger}] \\
&= 2\frac{1}{4}Tr[\hat{\mathcal{M}}\hat{P}_{\perp'}\sigma_{n_3}\hat{\mathcal{M}}^{\dagger}] \\
&= -2\frac{1}{4}Tr[\hat{\mathcal{M}}\hat{P}_{\parallel'}\sigma_{n_3}\hat{\mathcal{M}}^{\dagger}] \ , \\
\frac{d\sigma}{d\Omega}H &\equiv -\frac{1}{4}Tr[\hat{\mathcal{M}}(\hat{P}_{\perp'}-\hat{P}_{\parallel'})\sigma_{n_1}\hat{\mathcal{M}}^{\dagger}] \\
&= -2\frac{1}{4}Tr[\hat{\mathcal{M}}\hat{P}_{\perp'}\sigma_{n_1}\hat{\mathcal{M}}^{\dagger}] \\
&= 2\frac{1}{4}Tr[\hat{\mathcal{M}}\hat{P}_{\parallel'}\sigma_{n_1}\hat{\mathcal{M}}^{\dagger}] \ , \\
\frac{d\sigma}{d\Omega}P' &\equiv \frac{1}{4}Tr[\hat{\mathcal{M}}\sigma_{n_2}\sigma_{n_1}\hat{\mathcal{M}}^{\dagger}] \ .
\end{aligned} \tag{E.10}$$

In the above definition $\hat{P}_{\parallel'}$ and $\hat{P}_{\perp'}$ correspond to photon polarization given by Eq. (E.5) with $\phi = \pi/4$.

Lastly, the spin density matrix elements are defined as

$$\rho^{i}_{\lambda\lambda'} \equiv \frac{1}{4}\langle\lambda|\hat{\mathcal{M}}\sigma_{n_i}\hat{\mathcal{M}}^{\dagger}|\lambda'\rangle \tag{E.11}$$

for $i = 0, ..., 3$, where λ and λ' stand for the helicity of the produced meson or baryon and $\sigma_0 = 1$ is the unit matrix.

Bibliography

[1] Adair, R. K. High-energy maxima in the $\pi - p$ cross sections. *Phys. Rev. 113* (Jan 1959), 338–341.

[2] Afnan, I. R., and Stelbovics, A. T. Faddeev equations for the coupled $\mathrm{NN} - \pi\mathrm{NN}$ system. *Phys. Rev. C 23* (Apr 1981), 1384–1393.

[3] Ajaka, J., Assafiri, Y., Bouchigny, S., Didelez, J. P., Fichen, L., Guidal, M., Hourany, E., Kouznetsov, V., Kunne, R., Mushkarenkov, A. N., Nedorezov, V., Rudnev, N., Turinge, A., and Zhao, Q. Evidence for nucleon-resonance excitation in ω-meson photoproduction. *Phys. Rev. Lett. 96* (Apr 2006), 132003.

[4] Akbar, Z., Roy, P., Park, S., Crede, V., Anisovich, A. V., Denisenko, I., Klempt, E., Nikonov, V. A., Sarantsev, A. V., Adhikari, K. P., Adhikari, S., Amaryan, M. J., Anefalos Pereira, S., Avakian, H., Ball, J., Battaglieri, M., Batourine, V., Bedlinskiy, I., Boiarinov, S., Briscoe, W. J., Brock, J., Brooks, W. K., Burkert, V. D., Cao, F. T., Carlin, C., Carman, D. S., Celentano, A., Charles, G., Chetry, T., Ciullo, G., Clark, L., Cole, P. L., Contalbrigo, M., Cortes, O., D'Angelo, A., Dashyan, N., De Vita, R., De Sanctis, E., Deur, A., Djalali, C., Dugger, M., Dupre, R., Egiyan, H., El Fassi, L., Eugenio, P., Fedotov, G., Fersch, R., Filippi, A., Fradi, A., Garçon, M., Gevorgyan, N., Giovanetti, K. L., Girod, F. X., Gleason, C., Gohn, W., Golovatch, E., Gothe, R. W., Griffioen, K. A., Guidal, M., Guo, L., Hafidi, K., Hakobyan, H., Hanretty, C., Harrison, N., Hattawy, M., Heddle, D., Hicks, K., Hollis, G., Holtrop, M., Ireland, D. G., Ishkhanov, B. S., Isupov, E. L., Jenkins,

D., Joosten, S., Keith, C. D., Keller, D., Khachatryan, G., Khachatryan, M., Khandaker, M., Kim, A., Kim, W., Klein, A., Klein, F. J., Kubarovsky, V., Lanza, L., Livingston, K., MacGregor, I. J. D., Markov, N., McKinnon, B., Meekins, D. G., Mineeva, T., Mokeev, V., Movsisyan, A., Munoz Camacho, C., Nadel-Turonski, P., Niccolai, S., Osipenko, M., Ostrovidov, A. I., Paolone, M., Paremuzyan, R., Park, K., Pasyuk, E., Phelps, W., Pogorelko, O., Price, J. W., Prok, Y., Protopopescu, D., Raue, B. A., Ripani, M., Ritchie, B. G., Rizzo, A., Rosner, G., Sabatié, F., Salgado, C., Schumacher, R. A., Sharabian, Y. G., Skorodumina, I., Smith, G. D., Sober, D. I., Sokhan, D., Sparveris, N., Stepanyan, S., Strakovsky, I. I., Strauch, S., Taiuti, M., Ungaro, M., Voskanyan, H., Voutier, E., Wei, X., Wood, M. H., Zachariou, N., Zana, L., Zhang, J., and Zhao, Z. W. Measurement of the helicity asymmetry e in $\omega \to \pi^+\pi^-\pi^0$ photoproduction. *Phys. Rev. C 96* (Dec 2017), 065209.

[5] Anisovich, A. V., Beck, R., Klempt, E., Nikonov, V. A., Sarantsev, A. V., and Thoma, U. Pion- and photo-induced transition amplitudes to λk, σk and nη. *Eur. Phys. J. A 48*, 6 (Jun 2012), 88.

[6] Anisovich, A. V., Beck, R., Klempt, E., Nikonov, V. A., Sarantsev, A. V., and Thoma, U. Properties of baryon resonances from a multichannel partial wave analysis. *Eur. Phys. J. A 48*, 2 (Feb 2012), 15.

[7] Anisovich, A. V., Beck, R., Klempt, E., Nikonov, V. A., Sarantsev, A. V., Thoma, U., and Wunderlich, Y. Study of ambiguities in πp $\to \lambda$k0 scattering amplitudes. *The European Physical Journal A 49*, 10 (Oct 2013), 121.

[8] Anisovich, A. V., Burkert, V., Compton, N., Hicks, K., Klein, F. J., Klempt, E., Nikonov, V. A., Sandorfi, A. M., Sarantsev, A. V., and Thoma, U. Neutron helicity amplitudes. *Phys. Rev. C 96* (Nov 2017), 055202.

[9] Anisovich, A. V., Klempt, E., Nikonov, V. A., Matveev, M. A., Sarantsev,

A. V., and Thoma, U. Photoproduction of pions and properties of baryon resonances from a bonn-gatchina partial-wave analysis. *The European Physical Journal A 44*, 2 (May 2010), 203–220.

[10] Anisovich, A. V., Klempt, E., Nikonov, V. A., Sarantsev, A. V., and Thoma, U. Nucleon resonances in the fourth-resonance region. *Eur. Phys. J. A 47*, 12 (Dec 2011), 153.

[11] Arndt, R. A., Briscoe, W. J., Morrison, T. W., Strakovsky, I. I., Workman, R. L., and Gridnev, A. B. Low-energy ηn interactions: Scattering lengths and resonance parameters. *Phys. Rev. C 72* (Oct 2005), 045202.

[12] Arndt, R. A., Briscoe, W. J., Strakovsky, I. I., and Workman, R. L. Extended partial-wave analysis of πn scattering data. *Phys. Rev. C 74* (Oct 2006), 045205.

[13] Arndt, R. A., Briscoe, W. J., Strakovsky, I. I., Workman, R. L., and Pavan, M. M. Dispersion relation constrained partial wave analysis of πn elastic and $\pi n \to \eta n$ scattering data: The baryon spectrum. *Phys. Rev. C 69* (Mar 2004), 035213.

[14] Aznauryan, I. G. Multipole amplitudes of pion photoproduction on nucleons up to 2GeV using dispersion relations and the unitary isobar model. *Phys. Rev. C 67* (Jan 2003), 015209.

[15] Babacan, H., Babacan, T., Gokalp, A., and Yilmaz, O. ω-meson photoproduction on nucleons in the near-threshold region. *The European Physical Journal A - Hadrons and Nuclei 13*, 3 (Mar 2002), 355–362.

[16] Badalyan, A., Kok, L., Polikarpov, M., and Simonov, Y. Resonances in coupled channels in nuclear and particle physics. *Physics Reports 82*, 2 (1982), 31 – 177.

[17] Baenst-Vandenbrouke, A. D., and Baenst, P. D. *On the isobar model parameters of the first pion-nucleon resonance.* Mathematical Physics Department, University College Dublin, 1973.

[18] Baenst-Vandenbrouke, A. D., and Baenst, P. D. *On the isobar model parameters of the pion-nucleon resonance.* Mathematical Physics Department, University College Dublin, 1973.

[19] Barnes, V. E., Connolly, P. L., Crennell, D. J., Culwick, B. B., Delaney, W. C., Fowler, W. B., Hagerty, P. E., Hart, E. L., Horwitz, N., Hough, P. V. C., Jensen, J. E., Kopp, J. K., Lai, K. W., Leitner, J., Lloyd, J. L., London, G. W., Morris, T. W., Oren, Y., Palmer, R. B., Prodell, A. G., Radojičić, D., Rahm, D. C., Richardson, C. R., Samios, N. P., Sanford, J. R., Shutt, R. P., Smith, J. R., Stonehill, D. L., Strand, R. C., Thorndike, A. M., Webster, M. S., Willis, W. J., and Yamamoto, S. S. Observation of a hyperon with strangeness minus three. *Phys. Rev. Lett. 12* (Feb 1964), 204–206.

[20] Barth, J., Braun, W., Ernst, J., Glander, K.-H., Hannappel, J., Jöpen, N., Kalinowsky, H., Klein, F. J., Klein, F., Klempt, E., Lawall, R., Link, J., Menze, D., Neuerburg, W., Ostrick, M., Paul, E., Pee, H. v., Schulday, I., Schwille, W. J., Wiegers, B., Wieland, F. W., Wisskirchen, J., and Wu, C. Low-energy photoproduction of ω-mesons. *The European Physical Journal A - Hadrons and Nuclei 18*, 1 (Oct 2003), 117–127.

[21] Basdevant, J. L., and Berger, E. L. Unstable-particle scattering and an analytic quasi-unitary isobar model. *Phys. Rev. D 19* (Jan 1979), 239–245.

[22] Basdevant, J. L., and Berger, E. L. Unstable-particle scattering and an analytic quasi-unitary isobar model. *Phys. Rev. D 19* (Jan 1979), 239–245.

[23] Batinić, M., Ceci, S., Švarc, A., and Zauner, B. Poles of the zagreb analysis partial-wave t matrices. *Phys. Rev. C 82* (Sep 2010), 038203.

[24] Bayadilov, D. E., Beloglazov, Y. A., Gridnev, A. B., Kozlenko, N. G., Kruglov, S. P., Kulbardis, A. A., Lopatin, I. V., Novinsky, D. V., Radkov, A. K., Sumachev, V. V., and Filimonov, E. A. Study of η -production reaction

$\pi p \to \eta n$ in the near-threshold region. *The European Physical Journal A 35*, 3 (Mar 2008), 287–290.

[25] BERNARD, V., KAISER, N., AND MEINER, U.-G. Chiral dynamics in nucleons and nuclei. *International Journal of Modern Physics E 04*, 02 (1995), 193–344.

[26] BINNIE, D. M., CAMILLERI, L., DEBENHAM, N. C., DUANE, A., GARBUTT, D. A., HOLMES, J. R., JONES, W. G., KEYNE, J., LEWIS, M., SIOTIS, I., UPADHYAY, P. N., BURTON, I. F., AND MCEWEN, J. G. Study of narrow mesons near their thresholds. *Phys. Rev. D 8* (Nov 1973), 2789–2813.

[27] BROWN, R., CLARK, A., DUKE, P., EVANS, W., GRAY, R., GROVES, E., OTT, R., RENSHALL, H., SHAH, T., SHAVE, A., THRESHER, J., AND TYRRELL, M. Differential cross sections for the reaction pn between 724 and 2723 mev/c. *Nuclear Physics B 153* (1979), 89 – 111.

[28] BRUNS, P. C., MAI, M., AND MEINER, U.-G. Chiral dynamics of the s11(1535) and s11(1650) resonances revisited. *Physics Letters B 697*, 3 (2011), 254 – 259.

[29] BURKERT, V. D., AND ROBERTS, C. D. Colloquium: Roper resonance: Toward a solution to the fifty year puzzle. *Rev. Mod. Phys. 91* (Mar 2019), 011003.

[30] CAO, X., SHKLYAR, V., AND LENSKE, H. Coupled-channel analysis of $k\Sigma$ production on the nucleon up to 2.0 gev. *Phys. Rev. C 88* (Nov 2013), 055204.

[31] CAPSTICK, S. Photo- and electroproduction of nonstrange baryon resonances in the relativized quark model. *Phys. Rev. D 46* (Oct 1992), 2864–2881.

[32] CAPSTICK, S., AND ROBERTS, W. Quasi-two-body decays of nonstrange baryons. *Phys. Rev. D 49* (May 1994), 4570–4586.

[33] COLLINS, P., RITCHIE, B., DUGGER, M., KLEIN, F., ANISOVICH, A., KLEMPT, E., NIKONOV, V., SARANTSEV, A., ADHIKARI, K., ADHIKARI, S., ADIKARAM, D., AKBAR, Z., PEREIRA, S. A., AVAKIAN, H., BALL, J., BALTZELL, N., BASHKANOV, M., BATTAGLIERI, M., BATOURINE, V., BEDLINSKIY, I., BISELLI, A., BOIARINOV, S., BRISCOE, W., BROOKS, W., BURKERT, V., CAO, F. T., CAO, T., CARMAN,

D., Celentano, A., Charles, G., Chetry, T., Ciullo, G., Clark, L., Cole, P., Contalbrigo, M., Cortes, O., Crede, V., Dashyan, N., Vita, R. D., Sanctis, E. D., Defurne, M., Deur, A., Djalali, C., Dupre, R., Egiyan, H., Alaoui, A. E., Fassi, L. E., Eugenio, P., Fedotov, G., Filippi, A., Fleming, J., Ghandilyan, Y., Gilfoyle, G., Giovanetti, K., Girod, F., Glazier, D., Gleason, C., Golovatch, E., Gothe, R., Griffioen, K., Guidal, M., Hafidi, K., Hakobyan, H., Hanretty, C., Harrison, N., Hattawy, M., Heddle, D., Hicks, K., Hollis, G., Holtrop, M., Hughes, S., Ilieva, Y., Ireland, D., Ishkhanov, B., Isupov, E., Jenkins, D., Jiang, H., Jo, H., Joosten, S., Keller, D., Khachatryan, G., Khachatryan, M., Khandaker, M., Kim, A., Kim, W., Klein, A., Kubarovsky, V., Kuleshov, S., Lanza, L., Lenisa, P., Livingston, K., MacGregor, I., Markov, N., McKinnon, B., Meyer, C., Meziani, Z., Mineeva, T., Mokeev, V., Montgomery, R., Movsisyan, A., Munevar, E., Camacho, C. M., Nadel-Turonski, P., Net, L., Niccolai, S., Niculescu, G., Niculescu, I., Osipenko, M., Ostrovidov, A., Paolone, M., Paremuzyan, R., Park, K., Pasyuk, E., Phelps, W., Pisano, S., Pogorelko, O., Price, J., Procureur, S., Prok, Y., Protopopescu, D., Raue, B., Ripani, M., Rizzo, A., Rosner, G., Sabati, F., Salgado, C., Schumacher, R., Sharabian, Y., Simonyan, A., Skorodumina, I., Smith, G., Sober, D., Sokhan, D., Sparveris, N., Stankovic, I., Stepanyan, S., Strakovsky, I., Strauch, S., Taiuti, M., Ungaro, M., Voskanyan, H., Voutier, E., Walford, N., Watts, D., Wei, X., Wood, M., Zachariou, N., Zhang, J., and Zhao, Z. Photon beam asymmetry in the reaction pp for e=1.152 to 1.876gev. *Physics Letters B 773* (2017), 112 – 120.

[34] Cooper, E., and Jennings, B. Smooth relativistic two-body propagators. *Nuclear Physics A 483*, 3 (1988), 601 – 618.

[35] Dalitz, R. H. Strange-particle resonant states. *Annual Review of Nuclear Science*

13, 1 (1963), 339–430.

[36] Danburg, J. S., Abolins, M. A., Dahl, O. I., Davies, D. W., Hoch, P. L., Kirz, J., Miller, D. H., and Rader, R. K. Production and decay of η and ω mesons in the reaction $\pi^+ d \to (p)p\pi^+\pi^-\pi^0$ between 1.1 and 2.4 gev/c. *Phys. Rev. D 2* (Dec 1970), 2564–2588.

[37] Debenham, N. C., Binnie, D. M., Camilleri, L., Carr, J., Duane, A., Garbutt, D. A., Jones, W. G., Keyne, J., Siotis, I., and McEwen, J. G. Backward $\pi^- p$ reactions between 0.6 and 1.0 gev/c. *Phys. Rev. D 12* (Nov 1975), 2545–2556.

[38] Deinet, W., Mller, H., Schmitt, D., Staudenmaier, H.-M., Buniatov, S., and Zavattini, E. Differential and total cross sections for + p + n from 718 to 1050 mev/c. *Nuclear Physics B 11*, 2 (1969), 495 – 504.

[39] Denisenko, I., Anisovich, A., Crede, V., Eberhardt, H., Klempt, E., Nikonov, V., Sarantsev, A., Schmieden, H., Thoma, U., and Wilson, A. N decays to n from new data on pp. *Physics Letters B 755* (2016), 97 – 101.

[40] Donnachie, A., and Landshoff, P. Exclusive vector meson production at hera. *Physics Letters B 348*, 1 (1995), 213 – 218.

[41] Donnachie, A., and Landshoff, P. Exclusive vector photoproduction: confirmation of regge theory. *Physics Letters B 478*, 1 (2000), 146 – 150.

[42] Drechsel, D., Hanstein, O., Kamalov, S., and Tiator, L. A unitary isobar model for pion photo- and electroproduction on the proton up to 1 gev. *Nuclear Physics A 645*, 1 (1999), 145 – 174.

[43] Drechsel, D., Hanstein, O., Kamalov, S., and Tiator, L. A unitary isobar model for pion photo- and electroproduction on the proton up to 1 gev. *Nuclear Physics A 645*, 1 (1999), 145 – 174.

[44] Drechsel, D., Kamalov, S., and Tiator, L. Unitary isobar model –maid2007. *Eur. Phys. J. A* (2007), 34 – 69.

[45] Drechsel, D., Kamalov, S. S., and Tiator, L. Unitary isobar model –maid2007.

The European Physical Journal A 34, 1 (Oct 2007), 69.

[46] Drechsel, D., Knöchlein, G., Korchin, A. Y., Metz, A., and Scherer, S. Structure analysis of the virtual compton scattering amplitude at low energies. *Phys. Rev. C 57* (Feb 1998), 941–952.

[47] Dring, M., Hanhart, C., Huang, F., Krewald, S., and Meiner, U.-G. Analytic properties of the scattering amplitude and resonances parameters in a meson exchange model. *Nuclear Physics A 829*, 3 (2009), 170 – 209.

[48] Dring, M., Hanhart, C., Huang, F., Krewald, S., Meiner, U.-G., and Rnchen, D. The reaction +pk++ in a unitary coupled-channels model. *Nucl. Phys. A 851*, 1 (2011), 58 – 98.

[49] Eberhardt, H., Jude, T., Schmieden, H., Anisovich, A., Bantes, B., Bayadilov, D., Beck, R., Beloglazov, Y., Bichow, M., Bse, S., Brinkmann, K.-T., Challand, T., Crede, V., Diez, F., Drexler, P., Dutz, H., Elsner, D., Ewald, R., Fornet-Ponse, K., Friedrich, S., Frommberger, F., Funke, C., Gottschall, M., Gridnev, A., Grner, M., Gutz, E., Hammann, C., Hannappel, J., Hartmann, J., Hillert, W., Hoffmeister, P., Honisch, C., Jaegle, I., Kaiser, D., Kalinowsky, H., Kalischewski, F., Kammer, S., Keshelashvili, I., Kleber, V., Klein, F., Klempt, E., Koop, K., Krusche, B., Kube, M., Lang, M., Lopatin, I., Maghrbi, Y., Makonyi, K., Metag, V., Meyer, W., Mller, J., Nanova, M., Nikonov, V., Novotny, R., Piontek, D., Reeve, S., Reicherz, G., Rostomyan, T., Runkel, S., Sarantsev, A., Schaepe, S., Schmidt, C., Schmitz, R., Seifen, T., Sokhoyan, V., Sumachev, V., Thiel, A., Thoma, U., Urban, M., van Pee, H., Walther, D., Wendel, C., Wiedner, U., Wilson, A., and Winnebeck, A. Measurement of double polarisation asymmetries in -photoproduction. *Physics Letters B 750* (2015), 453 – 458.

[50] Edwards, R. G., Mathur, N., Richards, D. G., and Wallace, S. J. Flavor

structure of the excited baryon spectra from lattice qcd. *Phys. Rev. D 87* (Mar 2013), 054506.

[51] Engel, G. P., Lang, C. B., Limmer, M., Mohler, D., and Schäfer, A. Meson and baryon spectrum for qcd with two light dynamical quarks. *Phys. Rev. D 82* (Aug 2010), 034505.

[52] ENGEL, J., PITTEL, S., and VOGEL, P. Nuclear physics of dark matter detection. *International Journal of Modern Physics E 01*, 01 (1992), 1–37.

[53] Fasanoand, C. G., Tabakin, F., and Saghai, B. Spin observables at threshold for meson photoproduction. *Phys. Rev. C 46* (Dec 1992), 2430–2455.

[54] Feltesse, J., Ayed, R., Bareyre, P., Borgeaud, P., David, M., Ernwein, J., Lemoigne, Y., and Villet, G. The reaction p n up to p = 450 mev/c: experimental results and partial-wave analysis. *Nuclear Physics B 93*, 2 (1975), 242 – 260.

[55] Gell-Mann, M. Symmetries of baryons and mesons. *Phys. Rev. 125* (Feb 1962), 1067–1084.

[56] Goebel, C. J., and McVoy, K. W. Eigenphases and the generalized breit-wigner approximation. *Phys. Rev. 164* (Dec 1967), 1932–1936.

[57] Goebel, C. J., and McVoy, K. W. Eigenphases and the generalized breit-wigner approximation. *Phys. Rev. 164* (Dec 1967), 1932–1936.

[58] Gridnev, A. B., Horn, I., Briscoe, W. J., and Strakovsky, I. I. The k-matrix approach to the δ-resonance mass splitting and isospin violation in low-energy πn scattering. *Physics of Atomic Nuclei 69*, 9 (Sep 2006), 1542–1551.

[59] Gross, D. J., and Wilczek, F. Ultraviolet behavior of non-abelian gauge theories. *Phys. Rev. Lett. 30* (Jun 1973), 1343–1346.

[60] Haberzettl, H. private note.

[61] Haberzettl, H. Gauge-invariant theory of pion photoproduction with dressed hadrons. *Phys. Rev. C 56* (Oct 1997), 2041–2058.

[62] Haberzettl, H., Nakayama, K., and Krewald, S. Gauge-invariant approach

to meson photoproduction including the final-state interaction. *Phys. Rev. C 74* (Oct 2006), 045202.

[63] Hanhart, C., and Kudryavtsev, A. On momentum dependence of the reaction $\pi^- p \to \omega n$ near threshold. *The European Physical Journal A - Hadrons and Nuclei 6*, 3 (Nov 1999), 325–328.

[64] Hanhart, C., Sibirtsev, A., and Speth, J. The reaction $\pi N \to \omega N$ revisited: the $\omega - N$ scattering length. *arXiv e-prints* (Jul 2001), hep–ph/0107245.

[65] Höhler, H. *Landolt-Börnstein*, vol. 9. Springer, Berlin, 1983.

[66] Huang, F., Döring, M., Haberzettl, H., Haidenbauer, J., Hanhart, C., Krewald, S., Meissner, U.-G., and Nakayama, K. Pion photoproduction in a dynamical coupled-channels model. *Phys. Rev. C 85* (May 2012), 054003.

[67] Juliá-Díaz, B., Kamano, H., Lee, T.-S. H., Matsuyama, A., Sato, T., and Suzuki, N. Dynamical coupled-channels analysis of $^1\mathrm{H}(e, e'\pi)n$ reactions. *Phys. Rev. C 80* (Aug 2009), 025207.

[68] Juliá-Díaz, B., Lee, T.-S. H., Matsuyama, A., and Sato, T. Dynamical coupled-channels model of πn scattering in the $w \leqslant 2$ gev nucleon resonance region. *Phys. Rev. C 76* (Dec 2007), 065201.

[69] Juliá-Díaz, B., Lee, T.-S. H., Matsuyama, A., Sato, T., and Smith, L. C. Dynamical coupled-channels effects on pion photoproduction. *Phys. Rev. C 77* (Apr 2008), 045205.

[70] Kaiser, N., Siegel, P., and Weise, W. Chiral dynamics and the s11(1535) nucleon resonance. *Physics Letters B 362*, 1 (1995), 23 – 28.

[71] Kamano, H., Juliá-Díaz, B., Lee, T. S. H., Matsuyama, A., and Sato, T. Double and single pion photoproduction within a dynamical coupled-channels model. *Phys. Rev. C 80* (Dec 2009), 065203.

[72] Kamano, H., Nakamura, S. X., Lee, T.-S. H., and Sato, T. Nucleon resonances within a dynamical coupled-channels model of πn and γn reactions. *Phys. Rev. C 88*

(Sep 2013), 035209.

[73] Kamano, H., Nakamura, S. X., Lee, T.-S. H., and Sato, T. Dynamical coupled-channels model of K^-p reactions: Determination of partial-wave amplitudes. *Phys. Rev. C 90* (Dec 2014), 065204.

[74] Kamano, H., Nakamura, S. X., Lee, T.-S. H., and Sato, T. Dynamical coupled-channels model of K^-p reactions. ii. extraction of Λ^* and Σ^* hyperon resonances. *Phys. Rev. C 92* (Aug 2015), 025205.

[75] Karami, H., Carr, J., Debenham, N., Garbutt, D., Jones, W., Binnie, D., Keyne, J., Moissidis, P., Sarma, H., and Siotis, I. Elastic scattering and meson production near the threshold of p+n. *Nuclear Physics B 154*, 3 (1979), 503 – 518.

[76] Keyne, J., Binnie, D. M., Carr, J., Debenham, N. C., Duane, A., Garbutt, D. A., Jones, W. G., Siotis, I., and McEwen, J. G. Study of ω production near threshold in the reaction $\pi^-p \to \omega n$. *Phys. Rev. D 14* (Jul 1976), 28–41.

[77] Klein, F., Anisovich, A. V., Bacelar, J. C. S., Bantes, B., Bartholomy, O., Bayadilov, D., Beck, R., Beloglazov, Y. A., Castelijns, R., Crede, V., Dutz, H., Ehmanns, A., Elsner, D., Essig, K., Ewald, R., Fabry, I., Fuchs, M., Funke, C., Gregor, R., Gridnev, A. B., Gutz, E., Höffgen, S., Hoffmeister, P., Horn, I., Jaegle, I., Junkersfeld, J., Kalinowsky, H., Kammer, S., Kleber, V., Klein, F., Klempt, E., Konrad, M., Kotulla, M., Krusche, B., Lang, M., Löhner, H., Lopatin, I. V., Lotz, J., Lugert, S., Menze, D., Mertens, T., Messchendorp, J. G., Metag, V., Morales, C., Nanova, M., Nikonov, V. A., Novinski, D., Novotny, R., Ostrick, M., Pant, L. M., van Pee, H., Pfeiffer, M., Radkov, A., Roy, A., Sarantsev, A. V., Schmidt, C., Schmieden, H., Schoch, B., Shende, S. V., Sokhoyan, V., Süle, A., Sumachev, V. V., Szczepanek, T., Thoma, U., Trnka, D., Varma, R., Walther, D., Weinheimer, C., and Wendel, C. Beam asymmetries in near-threshold ω photoproduction off the proton. *Phys. Rev. D 78* (Dec 2008),

117101.

[78] Klingl, F. PhD thesis, University of Munich, 1998.

[79] Koniuk, R., and Isgur, N. Where have all the resonances gone? an analysis of baryon couplings in a quark model with chromodynamics. *Phys. Rev. Lett. 44* (Mar 1980), 845–848.

[80] Kozlenko, N. G., Abaev, V. V., Bekrenev, V. S., Kruglov, S. P., Koulbardis, A. A., Lopatin, I. V., Starostin, A. B., Draper, B., Hayden, S., Huddleston, J., Isenhower, D., Robinson, C., Sadler, M., Allgower, C., Cadman, R., Spinka, H., Comfort, J., Craig, K., Ramirez, A., Kycia, T., Clajus, M., Marusic, A., McDonald, S., Nefkens, B. M. K., Phaisangittisakul, N., Prakhov, S., Price, J. W., Tippens, W. B., Peterson, J., Briscoe, W. J., Shafi, A., Strakovsky, I. I., Staudenmaier, H., Manley, D. M., Olmsted, J., Peaslee, D., Knecht, N., Lolos, G., Papandreou, Z., Supek, I., Slaus, I., Gibson, A., Grosnic, D., Koetke, D., Manweiler, R., and Stanislaus, S. Measurement of the total and differential cross sections for the reaction $\pi p \to \eta n$ with the crystal ball detector. *Physics of Atomic Nuclei 66*, 1 (Jan 2003), 110–113.

[81] Krehl, O., Hanhart, C., Krewald, S., and Speth, J. What is the structure of the roper resonance? *Phys. Rev. C 62* (Jul 2000), 025207.

[82] Laget, J. On the longitudinal electromagnetic coupling of the . *Nuclear Physics A 481*, 4 (1988), 765 – 780.

[83] Laget, J. On the longitudinal electromagnetic coupling of the . *Nuclear Physics A 481*, 4 (1988), 765 – 780.

[84] Landay, J., Mai, M., Döring, M., Haberzettl, H., and Nakayama, K. Towards the minimal spectrum of excited baryons. *Phys. Rev. D 99* (Jan 2019), 016001.

[85] Landay, J., Mai, M., Döring, M., Haberzettl, H., and Nakayama, K.

Towards the minimal spectrum of excited baryons. *Phys. Rev. D 99* (Jan 2019), 016001.

[86] Lutz, M., Wolf, G., and Friman, B. From pion nucleon scattering to vector mesons in nuclear matter. *Nuclear Physics A 661*, 1 (1999), 526 – 529.

[87] Mai, M., Bruns, P. C., and Meissner, U.-G. Pion photoproduction off the proton in a gauge-invariant chiral unitary framework. *Phys. Rev. D 86* (Nov 2012), 094033.

[88] Manley, D. M. Baryon partial-wave analysis. *International Journal of Modern Physics A 18*, 03 (2003), 441–448.

[89] Mathur, N., and Padmanath, M. Lattice qcd study of doubly charmed strange baryons. *Phys. Rev. D 99* (Feb 2019), 031501.

[90] Matsuyama, A., Sato, T., and Lee, T.-S. Dynamical coupled-channel model of meson production reactions in the nucleon resonance region. *Physics Reports 439*, 5 (2007), 193 – 253.

[91] Michael, C. Resonances in the s11 pion nucleon amplitude. *Physics Letters 21*, 1 (1966), 93 – 95.

[92] Michael, C. Resonances in the s11 pion nucleon amplitude. *Physics Letters 21*, 1 (1966), 93 – 95.

[93] Morrison, T. W. PhD thesis, The George Washington University, 2000.

[94] Nozawa, S., Blankleider, B., and Lee, T. A dynamical model of pion photoproduction on the nucleon. *Nuclear Physics A 513*, 3 (1990), 459 – 510.

[95] Oh, Y., and Lee, T.-S. H. One-loop corrections to ω photoproduction near threshold. *Phys. Rev. C 66* (Oct 2002), 045201.

[96] Oh, Y., Titov, A. I., and Lee, T.-S. H. Nucleon resonances in ω photoproduction. *Phys. Rev. C 63* (Jan 2001), 025201.

[97] Olsson, M. Solutions of the multichannel unitarity equations describing the addition of a resonance and background: Application to a pole model of photoproduction. *Nuclear Physics B 78*, 1 (1974), 55 – 76.

[98] Olsson, M. Solutions of the multichannel unitarity equations describing the addition of a resonance and background: Application to a pole model of photoproduction. *Nuclear Physics B 78*, 1 (1974), 55 – 76.

[99] Oset, E., and Ramos, A. Dynamically generated resonances from the vector octet-baryon octet interaction. *The European Physical Journal A 44*, 3 (Jun 2010), 445–454.

[100] Oset, E., and Ramos, A. Dynamically generated resonances from the vector octet-baryon octet interaction. *The European Physical Journal A 44*, 3 (Jun 2010), 445–454.

[101] Paris, M. W. Dynamical coupled channels calculation of pion and omega meson production. *Phys. Rev. C 79* (Feb 2009), 025208.

[102] Penner, G., and Mosel, U. What is the Correct $\pi^- p \to \omega n$ Cross Section at Threshold? *arXiv e-prints* (Nov 2001), nucl–th/0111024.

[103] Penner, G., and Mosel, U. Vector meson production and nucleon resonance analysis in a coupled-channel approach for energies $m_N < \sqrt{s} < 2$GeV. ii. photon-induced results. *Phys. Rev. C 66* (Nov 2002), 055212.

[104] Petreczky, P., Izubuchi, T., Jin, L., Kallidonis, C., Karthik, N., Mukherjee, S., Shugert, C., and Syritsyn, S. Pion structure from lattice QCD. In *XIII Quark Confinement and the Hadron Spectrum. 31 July - 6 August 2018. Maynooth University (Confinement2018)* (Jul 2018), p. 88.

[105] Pichowsky, M., Şavkli, i. m. c., and Tabakin, F. Polarization observables in vector meson photoproduction. *Phys. Rev. C 53* (Feb 1996), 593–610.

[106] Politzer, H. D. Reliable perturbative results for strong interactions? *Phys. Rev. Lett. 30* (Jun 1973), 1346–1349.

[107] Post, M., and Mosel, U. Coupling of baryon resonances to the n channelwork supported by bmbf and dfg. *Nuclear Physics A 688*, 3 (2001), 808 – 822.

[108] Prakhov, S., Nefkens, B. M. K., Allgower, C. E., Arndt, R. A., Bekrenev, V., Briscoe, W. J., Clajus, M., Comfort, J. R., Craig, K., Grosnick, D., Isenhower, D., Knecht, N., Koetke, D., Koulbardis, A.,

Kozlenko, N., Kruglov, S., Lolos, G., Lopatin, I., Manley, D. M., Manweiler, R., Marušić, A., McDonald, S., Olmsted, J., Papandreou, Z., Peaslee, D., Phaisangittisakul, N., Price, J. W., Ramirez, A. F., Sadler, M., Shafi, A., Spinka, H., Stanislaus, T. D. S., Starostin, A., Staudenmaier, H. M., Strakovsky, I. I., Supek, I., Tippens, W. B., and Workman, R. L. Measurement of $\pi^- p \to \eta n$ from threshold to $p_{\pi^-} = 747\,\mathrm{MeV}/c$. *Phys. Rev. C 72* (Jul 2005), 015203.

[109] Richards, W. B., Chiu, C. B., Eandi, R. D., Helmholz, A. C., Kenney, R. W., Moyer, B. J., Poirier, J. A., Cence, R. J., Peterson, V. Z., Sehgal, N. K., and Stenger, V. J. Production and neutral decay of the η meson in $\pi^- p$ collisions. *Phys. Rev. D 1* (Jan 1970), 10–19.

[110] Rönchen, D., Döring, M., Haberzettl, H., Haidenbauer, J., Meissner, U. G., and Nakayama, K. Eta photoproduction in a combined analysis of pion- and photon-induced reactions. *Eur. Phys. J. A 51*, 6 (Jun 2015), 70.

[111] Rönchen, D., Döring, M., Huang, F., Haberzettl, H., Haidenbauer, J., Hanhart, C., Krewald, S., Meissner, U. G., and Nakayama, K. Coupled-channel dynamics in the reactions $\pi\mathrm{n} \to \pi\mathrm{n}, \eta\mathrm{n}, \mathrm{k}\lambda, \mathrm{k}\sigma$. *The European Physical Journal A 49*, 4 (Apr 2013), 44.

[112] Rönchen, D., Döring, M., Huang, F., Haberzettl, H., Haidenbauer, J., Hanhart, C., Krewald, S., Meissner, U. G., and Nakayama, K. Photocouplings at the pole from pion photoproduction. *Eur. Phys. J. A 50*, 6 (Jun 2014), 101.

[113] Rönchen, D., Döring, M., and Meissner, U. G. The impact of $k^+\lambda$ photoproduction on the resonance spectrum. *Eur. Phys. J. A 54*, 6 (Jun 2018), 110.

[114] Roy, P., Akbar, Z., Park, S., Crede, V., Anisovich, A. V., Denisenko, I., Klempt, E., Nikonov, V. A., Sarantsev, A. V., Adhikari, K. P., Adhikari, S., Anefalos Pereira, S., Ball, J., Balossino, I., Bashkanov,

M., Battaglieri, M., Batourine, V., Bedlinskiy, I., Biselli, A. S., Boiarinov, S., Briscoe, W. J., Brock, J., Brooks, W. K., Burkert, V. D., Carlin, C., Carman, D. S., Celentano, A., Charles, G., Chetry, T., Ciullo, G., Clary, B. A., Cole, P. L., Contalbrigo, M., D'Angelo, A., Dashyan, N., De Vita, R., Deur, A., Djalali, C., Dugger, M., Dupre, R., El Alaoui, A., El Fassi, L., Elouadrhiri, L., Eugenio, P., Fedotov, G., Fegan, S., Filippi, A., Fradi, A., Gavalian, G., Gevorgyan, N., Gilfoyle, G. P., Giovanetti, K. L., Girod, F. X., Gleason, C., Gohn, W., Golovatch, E., Gothe, R. W., Griffioen, K. A., Guidal, M., Guo, L., Hafidi, K., Hakobyan, H., Hanretty, C., Hattawy, M., Hicks, K., Holtrop, M., Ilieva, Y., Ireland, D. G., Ishkhanov, B. S., Isupov, E. L., Jenkins, D., Joo, K., Joosten, S., Keith, C. D., Keller, D., Khachatryan, G., Khandaker, M., Kim, A., Kim, W., Klein, A., Klein, F. J., Kubarovsky, V., Kuleshov, S. V., Lanza, L., Lenisa, P., Livingston, K., Lu, H. Y., MacGregor, I. J. D., Markov, N., Mayer, M., McCracken, M. E., McKinnon, B., Meekins, D. G., Meyer, C. A., Meziani, Z. E., Mineeva, T., Mokeev, V., Montgomery, R. A., Movsisyan, A., Munoz Camacho, C., Nadel-Turonski, P., Niccolai, S., Niculescu, G., Osipenko, M., Ostrovidov, A. I., Paremuzyan, R., Park, K., Pasyuk, E., Phelps, E., Phelps, W., Pierce, J. J., Pogorelko, O., Price, J. W., Procureur, S., Prok, Y., Protopopescu, D., Raue, B. A., Ripani, M., Riser, D., Ritchie, B. G., Rizzo, A., Rosner, G., Sabatié, F., Salgado, C., Schumacher, R. A., Sharabian, Y. G., Skorodumina, I., Smith, G. D., Sober, D. I., Sokhan, D., Sparveris, N., Stepanyan, S., Strakovsky, I. I., Strauch, S., Taiuti, M., Tan, J. A., Torayev, B., Ungaro, M., Voutier, E., Walford, N. K., Watts, D. P., Wei, X., Wood, M. H., Zachariou, N., Zhang, J., and Zhao, Z. W. Measurement of the beam asymmetry Σ and the target asymmetry t in the photoproduction of ω mesons off the

proton using clas at jefferson laboratory. *Phys. Rev. C 97* (May 2018), 055202.

[115] Roy, P., Park, S., Crede, V., Anisovich, A. V., Klempt, E., Nikonov, V. A., Sarantsev, A. V., Wei, N. C., Huang, F., Nakayama, K., Adhikari, K. P., Adhikari, S., Angelini, G., Avakian, H., Barion, L., Battaglieri, M., Bedlinskiy, I., Biselli, A. S., Boiarinov, S., Briscoe, W. J., Brock, J., Brooks, W. K., Burkert, V. D., Cao, F., Carlin, C., Carman, D. S., Celentano, A., Chatagnon, P., Chetry, T., Ciullo, G., Cole, P. L., Contalbrigo, M., Cortes, O., D'Angelo, A., Dashyan, N., De Vita, R., De Sanctis, E., Deur, A., Diehl, S., Djalali, C., Dugger, M., Dupre, R., Duran, B., Egiyan, H., Ehrhart, M., El Alaoui, A., El Fassi, L., Eugenio, P., Fegan, S., Filippi, A., Fradi, A., Gilfoyle, G. P., Girod, F. X., Golovatch, E., Gothe, R. W., Griffioen, K. A., Guidal, M., Guo, L., Hafidi, K., Hanretty, C., Harrison, N., Hattawy, M., Hayward, T. B., Heddle, D., Hicks, K., Holtrop, M., Ilieva, Y., Ireland, D. G., Ishkhanov, B. S., Isupov, E. L., Jenkins, D., Jo, H. S., Johnston, S., Joosten, S., Kabir, M. L., Keith, C. D., Keller, D., Khachatryan, G., Khachatryan, M., Khanal, A., Khandaker, M., Kim, A., Kim, W., Klein, F. J., Kubarovsky, V., Kuleshov, S. V., Kunkel, M. C., Lanza, L., Lenisa, P., Livingston, K., MacGregor, I. J. D., Marchand, D., McKinnon, B., Meekins, D. G., Meyer, C. A., Mineeva, T., Mokeev, V., Montgomery, R. A., Movsisyan, A., Munoz Camacho, C., Nadel-Turonski, P., Niccolai, S., Niculescu, G., Osipenko, M., Ostrovidov, A. I., Paolone, M., Pappalardo, L. L., Paremuzyan, R., Pasyuk, E., Payette, D., Phelps, W., Pierce, J., Pogorelko, O., Prok, Y., Protopopescu, D., Raue, B. A., Ripani, M., Riser, D., Ritchie, B. G., Rizzo, A., Rosner, G., Sabatié, F., Salgado, C., Schumacher, R. A., Seely, M. L., Sharabian, Y. G., Shrestha, U., Skorodumina, I., Sokhan, D., Soto, O., Sparveris, N., Strakovsky, I. I., Strauch,

S., Taiuti, M., Tan, J. A., Torayev, B., Tyler, N., Ungaro, M., Voskanyan, H., Voutier, E., Walford, N. K., Wang, R., Watts, D. P., Wei, X., Wood, M. H., Zachariou, N., Zhang, J., and Zhao, Z. W. First measurements of the double-polarization observables f, p, and h in ω photoproduction off transversely polarized protons in the N^* resonance region. *Phys. Rev. Lett. 122* (Apr 2019), 162301.

[116] Salpeter, E. E., and Bethe, H. A. A relativistic equation for bound-state problems. *Phys. Rev. 84* (Dec 1951), 1232–1242.

[117] Sarantsev, A. V., Anisovich, A. V., Nikonov, V. A., and Schmieden, H. Polarization degrees of freedom in near-threshold photoproduction of ω-mesons in the $\pi^0\gamma$ decay channel. *The European Physical Journal A 39*, 1 (Jan 2009), 61–70.

[118] Scholten, O. Coupled-Channels Partial-Wave Analysis of Kaon Photoproduction. *Progress of Theoretical Physics Supplement 186* (10 2010), 216–221.

[119] Sharp, D. H. Elementary particle physics. stephen gasiorowicz. wiley, new york, 1966. xxii + 613 pp., illus. $14.95. *Science 161*, 3836 (1968), 39–39.

[120] Shklyar, V., Lenske, H., and Mosel, U. Coupled-channel analysis of $k\Lambda$ production in the nucleon resonance region. *Phys. Rev. C 72* (Jul 2005), 015210.

[121] Shklyar, V., Lenske, H., and Mosel, U. 2π production in the giessen coupled-channels model. *Phys. Rev. C 93* (Apr 2016), 045206.

[122] Shklyar, V., Lenske, H., Mosel, U., and Penner, G. Coupled-channel analysis of ω-meson production in πn and γn reactions for c.m. energies up to 2 gev. *Phys. Rev. C 71* (May 2005), 055206.

[123] Shrestha, M., and Manley, D. M. Multichannel parametrization of πn scattering amplitudes and extraction of resonance parameters. *Phys. Rev. C 86* (Nov 2012), 055203.

[124] Sibirtsev, A., and Cassing, W. On the current status of ozi violation in πn and pp reactions. *The European Physical Journal A - Hadrons and Nuclei 7*, 3 (Mar 2000), 407–413.

[125] Sibirtsev, A., Schneider, S., Elster, C., Haidenbauer, J., Krewald, S., and Speth, J. ηn final state interaction in incoherent photoproduction of η mesons from the deuteron near threshold. *Phys. Rev. C 65* (Apr 2002), 044007.

[126] Sibirtsev, A., Tsushima, K., and Krewald, S. Systematic regge theory analysis of ω photoproduction. *Phys. Rev. C 67* (May 2003), 055201.

[127] Strakovsky, I. I., Prakhov, S., Azimov, Y. I., Aguar-Bartolomé, P., Annand, J. R. M., Arends, H. J., Bantawa, K., Beck, R., Bekrenev, V., Berghäuser, H., Braghieri, A., Briscoe, W. J., Brudvik, J., Cherepnya, S., Codling, R. F. B., Collicott, C., Costanza, S., Demissie, B. T., Downie, E. J., Drexler, P., Fil'kov, L. V., Glazier, D. I., Gregor, R., Hamilton, D. J., Heid, E., Hornidge, D., Jaegle, I., Jahn, O., Jude, T. C., Kashevarov, V. L., Keshelashvili, I., Kondratiev, R., Korolija, M., Kotulla, M., Koulbardis, A., Kruglov, S., Krusche, B., Lisin, V., Livingston, K., MacGregor, I. J. D., Maghrbi, Y., Manley, D. M., Marinides, Z., McGeorge, J. C., McNicoll, E. F., Mekterovic, D., Metag, V., Middleton, D. G., Mushkarenkov, A., Nefkens, B. M. K., Nikolaev, A., Novotny, R., Ortega, H., Ostrick, M., Otte, P. B., Oussena, B., Pedroni, P., Pheron, F., Polonski, A., Robinson, J., Rosner, G., Rostomyan, T., Schumann, S., Sikora, M. H., Starostin, A., Supek, I., Taragin, M. F., Tarbert, C. M., Thiel, M., Thomas, A., Unverzagt, M., Watts, D. P., Werthmüller, D., and Zehr, F. Photoproduction of the ω meson on the proton near threshold. *Phys. Rev. C 91* (Apr 2015), 045207.

[128] Švare, A. η physics and multi-resonance coupled-channel analysis. In *N* Physics and Nonperturbative Quantum Chromodynamics* (Vienna, 1999), S. Simula, B. Saghai, N. C. Mukhopadhyay, and V. D. Burkert, Eds., Springer Vienna, pp. 222–224.

[129] Thomas, C. E. Excited heavy mesons from lattice qcd. *AIP Conference Proceedings 1735*, 1 (2016), 030007.

[130] Tiator, L. The maid legacy and future. *Few-Body Systems 59*, 3 (Mar 2018), 21.

[131] Tiator, L., Drechsel, D., Kamalov, S. S., and Vanderhaeghen, M. Electromagnetic excitation of nucleon resonances. *The European Physical Journal Special Topics 198*, 1 (Sep 2011), 141.

[132] Tiator, L., Gorchtein, M., Kashevarov, V. L., Nikonov, K., Ostrick, M., Hadžimehmedović, M., Omerović, R., Osmanović, H., Stahov, J., and Švarc, A. Eta and etaprime photoproduction on the nucleon with the isobar model etamaid2018. *The European Physical Journal A 54*, 12 (Dec 2018), 210.

[133] Titov, A. I., Kämpfer, B., and Reznik, B. L. Production of ω and φ mesons in near-threshold πn reactions: Baryon resonances and the okubo-zweig-iizuka rule. *Phys. Rev. C 65* (May 2002), 065202.

[134] Titov, A. I., and Lee, T.-S. H. Effective lagrangian approach to the ω photoproduction near threshold. *Phys. Rev. C 66* (Jul 2002), 015204.

[135] Usov, A., and Scholten, O. $k\Lambda$ and $k\Sigma$ photoproduction in a coupled-channels framework. *Phys. Rev. C 72* (Aug 2005), 025205.

[136] Vegna, V., D'Angelo, A., Bartalini, O., Bellini, V., Bocquet, J.-P., Capogni, M., Casano, L. E., Castoldi, M., Curciarello, F., De Leo, V., Didelez, J.-P., Di Salvo, R., Fantini, A., Franco, D., Gervino, G., Ghio, F., Giardina, G., Girolami, B., Giusa, A., Lapik, A., Levi Sandri, P., Lleres, A., Mammoliti, F., Mandaglio, G., Manganaro, M., Moricciani, D., Mushkarenkov, A., Nedorezov, V., Randieri, C., Rebreyend, D., Rudnev, N., Russo, G., Schaerf, C., Sperduto, M.-L., Sutera, M.-C., Turinge, A., and Zonta, I. Measurement of the Σ beam asymmetry for the ω photoproduction off the proton and the neutron at the graal experiment. *Phys. Rev. C 91* (Jun 2015), 065207.

[137] Watson, K. M. Some general relations between the photoproduction and scattering of π mesons. *Phys. Rev. 95* (Jul 1954), 228–236.

[138] Weinberg, S. Phenomenological lagrangians. *Physica A: Statistical Mechanics and its Applications 96*, 1 (1979), 327 – 340.

[139] Williams, M., Applegate, D., Bellis, M., Meyer, C. A., Adhikari, K. P., Anghinolfi, M., Baghdasaryan, H., Ball, J., Battaglieri, M., Bedlinskiy, I., Berman, B. L., Biselli, A. S., Bookwalter, C., Briscoe, W. J., Brooks, W. K., Burkert, V. D., Careccia, S. L., Carman, D. S., Cole, P. L., Collins, P., Crede, V., D'Angelo, A., Daniel, A., Vita, R. D., Sanctis, E. D., Deur, A., Dey, B., Dhamija, S., Dickson, R., Djalali, C., Dodge, G. E., Doughty, D., Dugger, M., Dupre, R., Alaoui, A. E., Elouadrhiri, L., Eugenio, P., Fedotov, G., Fegan, S., Fradi, A., Gabrielyan, M. Y., Garçon, M., Gevorgyan, N., Gilfoyle, G. P., Giovanetti, K. L., Girod, F. X., Gohn, W., Golovatch, E., Gothe, R. W., Griffioen, K. A., Guidal, M., Guo, L., Hafidi, K., Hakobyan, H., Hanretty, C., Hassall, N., Hicks, K., Holtrop, M., Ilieva, Y., Ireland, D. G., Ishkhanov, B. S., Isupov, E. L., Jawalkar, S. S., Jo, H. S., Johnstone, J. R., Joo, K., Keller, D., Khandaker, M., Khetarpal, P., Kim, W., Klein, A., Klein, F. J., Krahn, Z., Kubarovsky, V., Kuleshov, S. V., Kuznetsov, V., Livingston, K., Lu, H. Y., Mayer, M., McAndrew, J., McCracken, M. E., McKinnon, B., Mikhailov, K., Mirazita, M., Mokeev, V., Moreno, B., Moriya, K., Morrison, B., Moutarde, H., Munevar, E., Nadel-Turonski, P., Nepali, C. S., Niccolai, S., Niculescu, G., Niculescu, I., Niroula, M. R., Niyazov, R. A., Osipenko, M., Ostrovidov, A. I., Paris, M., Park, K., Park, S., Pasyuk, E., Pereira, S. A., Perrin, Y., Pisano, S., Pogorelko, O., Pozdniakov, S., Price, J. W., Procureur, S., Protopopescu, D., Raue, B. A., Ricco, G., Ripani, M., Ritchie, B. G., Rosner, G., Rossi, P., Sabatié, F., Saini, M. S., Salamanca, J., Salgado, C., Schott, D., Schumacher, R. A., Seraydaryan, H., Sharabian, Y. G., Smith, E. S., Sober, D. I., Sokhan, D.,

Stepanyan, S. S., Stoler, P., Strakovsky, I. I., Strauch, S., Taiuti, M., Tedeschi, D. J., Tkachenko, S., Ungaro, M., Vineyard, M. F., Voutier, E., Watts, D. P., Weinstein, L. B., Weygand, D. P., Wood, M. H., Zhang, J., and Zhao, B. Differential cross sections and spin density matrix elements for the reaction $\gamma p \to p\omega$. *Phys. Rev. C 80* (Dec 2009), 065208.

[140] Williams, M., Applegate, D., Bellis, M., Meyer, C. A., Adhikari, K. P., Anghinolfi, M., Baghdasaryan, H., Ball, J., Battaglieri, M., Bedlinskiy, I., Berman, B. L., Biselli, A. S., Briscoe, W. J., Brooks, W. K., Burkert, V. D., Careccia, S. L., Carman, D. S., Cole, P. L., Collins, P., Crede, V., D'Angelo, A., Daniel, A., De Vita, R., De Sanctis, E., Deur, A., Dey, B., Dhamija, S., Dickson, R., Djalali, C., Dodge, G. E., Doughty, D., Dugger, M., Dupre, R., Alaoui, A. E., Elouadrhiri, L., Eugenio, P., Fedotov, G., Fegan, S., Fradi, A., Gabrielyan, M. Y., Garçon, M., Gilfoyle, G. P., Giovanetti, K. L., Girod, F. X., Gohn, W., Golovatch, E., Gothe, R. W., Griffioen, K. A., Guidal, M., Guler, N., Guo, L., Hafidi, K., Hakobyan, H., Hanretty, C., Hassall, N., Hicks, K., Holtrop, M., Ilieva, Y., Ireland, D. G., Ishkhanov, B. S., Isupov, E. L., Jawalkar, S. S., Jo, H. S., Johnstone, J. R., Joo, K., Keller, D., Khandaker, M., Khetarpal, P., Kim, W., Klein, A., Klein, F. J., Krahn, Z., Kubarovsky, V., Kuleshov, S. V., Kuznetsov, V., Livingston, K., Lu, H. Y., Mayer, M., McAndrew, J., McCracken, M. E., McKinnon, B., Mirazita, M., Mokeev, V., Moreno, B., Moriya, K., Morrison, B., Munevar, E., Nadel-Turonski, P., Nepali, C. S., Niccolai, S., Niculescu, G., Niculescu, I., Niroula, M. R., Niyazov, R. A., Osipenko, M., Ostrovidov, A. I., Paris, M., Park, K., Park, S., Pasyuk, E., Pereira, S. A., Perrin, Y., Pisano, S., Pogorelko, O., Pozdniakov, S., Price, J. W., Procureur, S., Protopopescu, D., Ricco, G., Ripani, M., Ritchie, B. G., Rosner, G., Rossi,

P., Sabatié, F., Saini, M. S., Salamanca, J., Salgado, C., Schott, D., Schumacher, R. A., Seraydaryan, H., Sharabian, Y. G., Smith, E. S., Sober, D. I., Sokhan, D., Stepanyan, S. S., Stoler, P., Strakovsky, I. I., Strauch, S., Taiuti, M., Tedeschi, D. J., Tkachenko, S., Ungaro, M., Vineyard, M. F., Voutier, E., Watts, D. P., Weygand, D. P., Wood, M. H., Zhang, J., and Zhao, B. Partial wave analysis of the reaction $\gamma p \to p\omega$ and the search for nucleon resonances. *Phys. Rev. C 80* (Dec 2009), 065209.

[141] Wilson, A., Crede, V., Anisovich, A., Bacelar, J., Bantes, B., Bartholomy, O., Bayadilov, D., Beck, R., Beloglazov, Y., Brinkmann, K., Castelijns, R., Dutz, H., Elsner, D., Ewald, R., Frommberger, F., Fuchs, M., Funke, C., Gregor, R., Gridnev, A., Gutz, E., Hannappel, J., Hillert, W., Hoffmeister, P., Horn, I., Jaegle, I., Jude, T., Junkersfeld, J., Kalinowsky, H., Kleber, V., Klein, F., Klein, F., Klempt, E., Kotulla, M., Krusche, B., Lang, M., Lhner, H., Lopatin, I., Lugert, S., Mertens, T., Messchendorp, J., Metag, V., Nanova, M., Nikonov, V., Novinski, D., Novotny, R., Ostrick, M., Pant, L., van Pee, H., Pfeiffer, M., Roy, A., Sarantsev, A., Schmidt, C., Schmieden, H., Shende, S., Sokhoyan, V., Sparks, N., Sle, A., Sumachev, V., Szczepanek, T., Thoma, U., Trnka, D., Varma, R., Walther, D., Wendel, C., and Wiedner, U. Photoproduction of mesons off the proton. *Physics Letters B 749* (2015), 407 – 413.

[142] Wilson, K. G. Confinement of quarks. *Phys. Rev. D 10* (Oct 1974), 2445–2459.

[143] Workman, R. L., Arndt, R. A., Briscoe, W. J., Paris, M. W., and Strakovsky, I. I. Parameterization dependence of t-matrix poles and eigenphases from a fit to πn elastic scattering data. *Phys. Rev. C 86* (Sep 2012), 035202.

[144] Zhang, H., Tulpan, J., Shrestha, M., and Manley, D. M. Multichannel parametrization of $\overline{K}n$ scattering amplitudes and extraction of resonance parameters. *Phys. Rev. C 88* (Sep 2013), 035205.

[145] Zhao, Q. Nucleonic resonance excitations with linearly polarized photons in $\gamma \vec{p}\, \omega p$. *Phys. Rev. C 63* (Jan 2001), 025203.

[146] Zhao, Q. *VECTOR MESON PHOTOPRODUCTION IN THE QUARK MODEL.* 2001, pp. 237–240.

[147] Zhao, Q., Li, Z., and Bennhold, C. Vector meson photoproduction with an effective lagrangian in the quark model. *Phys. Rev. C 58* (Oct 1998), 2393–2413.

[148] Zhao, Q., Li, Z., and Bennhold, C. and photoproduction with an effective quark model lagrangian. *Physics Letters B 436*, 1 (1998), 42 – 48.

[149] Zweig, G. An SU_3 model for strong interaction symmetry and its breaking; Version 2. 80 p. Version 1 is CERN preprint 8182/TH.401, Jan. 17, 1964.